A fracture mechanics approach to failure analyses of concrete materials

Modéer, Matz

1979

DIVISION OF BUILDING MATERIALS
UNIVERSITY OF LUND

A FRACTURE MECHANICS APPROACH TO FAILURE ANALYSES OF CONCRETE MATERIALS

MATZ MODÉER

REPORT TVBM-1001
LUND SWEDEN 1979

CODEN: LUTVDG/(TVBM-1001)/1-102/(1979)

A FRACTURE MECHANICS APPROACH TO FAILURE ANALYSES OF CONCRETE MATERIALS

MATZ MODÉER

ISSN 0348-7911

REPORT TVBM-1001
LUND SWEDEN 1979 (3:e upplagan, tryckt 1985)

PREFACE

How does concrete fail?

This thesis is an attempt to add some answers to this question.

The work has been carried out at the Division of Building Materials, the Lund Institute of Technology, the University of Lund and has been financially supported by the Swedish Board for Technical Development.

It began in 1974 when Professor Arne Hillerborg, head of the Division of Building Materials presented the idea that later became "The Fictitious Crack Model". The author would therefore like to express his gratitude to Professor Arne Hillerborg whose encouragement has been invaluable.

The author would also like to thank the technical staff of the Division of Building Materials for their assistance in carrying out the experimental work and the staff of the Department of Solid Mechanics at the Lund Institute of Technology for their assistance in carrying out the computational work.

There are a tremendous accumulation of practical things to take care of when preparing a report of this kind. Almost all these problems have been taken care of in the most efficient way by Miss Mona Hammar. The author would like to express his acknowledgements.

Lund, March 1979

Matz Modéer

PREFACE TO THE SECOND EDITION

Almost nothing is out of misstakes.
This report is no exception.

Some of the misstakes from the first edition are corrected in this second edition. The corrections are not that severe that the first edition is out of value.

The second edition is prepared by Miss Mona Hammar and Mr Leif Erlandsson. The author would like to express his thanks.

Trondheim, June 1979

Matz Modéer

DISPOSITION OF THE THESIS

The disposition of the thesis is primarily shown below.

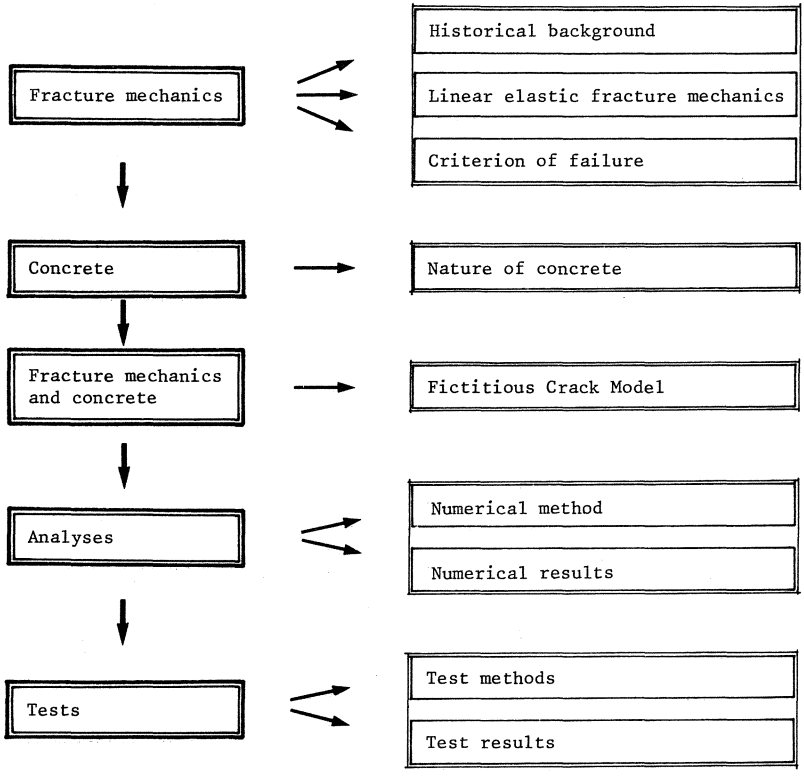

CONTENTS

SUMMARY

The aim of most people in deducing strength theories is to explain why materials are as weak as they are. A valuable tool in these efforts is the fracture mechanics approach as it does not necessarily consider a structural material to be homogeneous and continuously distributed over its volume. Fracture mechanics introduces new but important concepts such as dislocations and stress concentrations, which are realities within most structural materials.

C. E. Inglis' solution of the notch problem provides the first step in explaining the background of internal cracking of concrete materials under load. He shows that existing irregularities in the structure can act as stress concentrators. Thus internal stresses of concrete materials can be much higher than the applied load divided by the area of the specimen.
Griffith proposed that strain energy is transformed to surface energy when a crack is opened, i.e. he recognized that the driving force of crack extension is the difference between the energy which can be released if the crack is extended and that needed to create new surfaces. But, does this agree with the fracture of concrete materials?

If no material restrictions are introduced, the elastic tensile stress normal to a crack surface in a tension field tends towards infinity at the crack tip.
The ability of structural materials to resist stresses and strains is of course limited. This limitation is expressed as a local yielding at a crack tip.
In a cement paste, the matrix of the composite concrete, this local ductility must also be a reality. One possible yield mechanism of the gel is described below.

The gel is built up of a framework of crystallized calcium silicate hydrates or tobermorite crystals. These needle-shaped crystals, with a length on the order of 0.001 mm, overlap and are thus able to slide along each other to some extent.
If now some part of the framework is stressed up to a sufficiently high stress, this crystal slide occurs and the stress is thus limited. If the slide is so big that the crystals separate, that part of the framework is cracked and another part cracks in the same manner; i.e. if the energy provided is greater than that needed for the actual separation.

The tip region of a macrocrack, in the following called a crack, is highly stressed. Within this region there are many non-uniform holes, some more slender and crack-like than others.
In this variety of holes, the maximum stress is reached in front of several of them. Now many small cracks, in the following called microcracks, develop within the actual tip-region. Close to the crack tip the formal stress is higher than at a more distant point and the number of microcracks is therefore larger. Some of them are also connected and form even bigger microcracks.

Usually concrete materials are considered to be cracked when the uniaxial tensile strength f_t is reached. But the tip-region of this "crack" is actually a fictitious crack as it is still able to carry some load due to the formation of microcracks.
Thus the microcracked zone may be illustrated as a fictitious crack able to transfer a tensile stress σ which is a function of the fictitious crack width w according to a σ-w curve.

In this way two curves are needed to describe the deformation characteristics of a material, one ordinary stress-strain or σ-ε curve when $\varepsilon \leq \varepsilon(f_t)$, and one σ-w curve when $\varepsilon > \varepsilon(f_t)$.
The fictitious crack tip is a limit between the zone where σ depends on ε and the zone where σ depends on w. As the load increases, the fictitious crack increases in length and width. When the width reaches a limiting value w_ℓ, the stress at the point disappears and an actual crack propagates.
The development of the microcracked zone may thus be traced from the first application of a stress until final rupture.

This fracture model is called the "Fictitious Crack Model" or briefly the FCM. The model is a general purpose fracture model which is related to the well-known Barenblatt cohesive force model and the Dugdale yield model, the latter being a special case of the FCM.

In fracture mechanics the energy absorbed in forming one unit area of a crack is called G_c. With the same notation as before, G_c is the total energy absorption when w passes from zero to w_ℓ.
Thus, the area between the σ-w curve and the coordinate axes equals G_c.

In the thesis a method for measuring this fracture energy for concrete materials is presented. The method is experimentally verified and seems to be a convenient way to measure G_c of concrete and its different compounds.

A convenient method of fracture analysis is the Finite Element Method, briefly the FEM. In very general terms it is a numerical method by which continuous media can be represented approximately by equivalent discrete elements.

The elements are given properties as a limited number of force-deformation relationships at the nodal points connecting the elements.

In the FCM the σ-ε curve and the σ-w curve thus may be represented as shown in Fig 1.

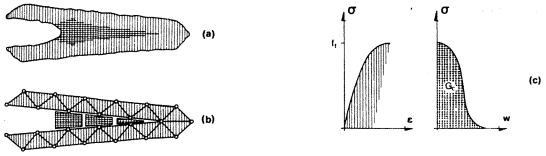

Fig 1. Crack representation in the FCM.
(a) actual tensile crack (b) FEM representation and (c) material properties.

The greatest advantage of this method is its simplicity. The analyses are easy to grasp and inexpensive to perform.

Analyses using the FCM on concrete materials show that bending strength f_b, splitting strength f_s, and apparent fracture toughness K'_{Ic} vary with the specimen depth as in Fig 2.

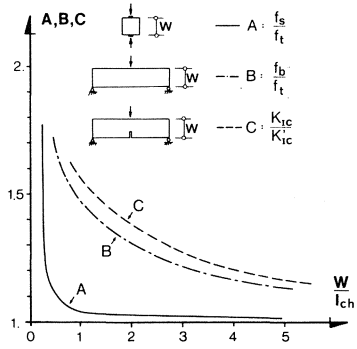

Fig 2. Properties for concrete materials versus specimen depth W over a characteristic length ℓ_{ch}.

The characteristic length ℓ_{ch} is a parameter G_cE/f_t^2 where G_c is the fracture energy, E the Young's modulus, and f_t the uniaxial tensile strength.

In the thesis it is shown that ℓ_{ch} (concrete) = 200-300 mm, ℓ_{ch} (mortar) = 100-200 mm, and ℓ_{ch} (paste) = 5-10 mm. These values, as shown in Fig 2, give variations with specimen depth of f_b, f_s, and K'_{Ic} which are in accordance with different experimental results.

The present design rules and standard specifications are often based on laboratory tests in which the specimen dimensions are relatively small. The effects of the absolute dimensions of structures, considered by the FCM, may therefore indicate that the actual safety margin is lower than intended.
The big challenge with the FCM at present, however, is to adapt the method to fracture analyses of reinforced structures. Some test analysis show very interesting results and there are many indications that the FCM is also a powerful tool for these purposes.

A better and more economical use of concrete and reinforcement may be the ultimate goal of the FCM within concrete structure technology.

1. FRACTURE MECHANICS

1.1 HISTORICAL BACKGROUND

1.1.1 Theory of elasticity

Elasticity is a fundamental property of structural materials. Man has used this elasticity of bodies since prehistoric times but it was not until Galileo Galilei 1638 described the property in his famous "Discourses" that the theory of elasticity, as we know it, was founded.

The fundamental law of elasticity was given by Robert Hooke forty years later, in 1676, in his anagram "ceiiinosssttuv", i.e. UT TENSIO SIC VIS.

After another 170 years, between 1680 and 1850, scientists like Bernoulli, Euler, Navier, Cauchy, Poisson and Clapeyron had developed the theory of elasticity. Then, in 1852, Lamé published a treatise on the matter under the title "Lecons sur la théorie mathématique de l'élasticité des corps solides" which became a classic and has not lost its significance even today.

This mathematical theory has sometimes been used in deducing strength theories of structural materials, i.e. to explain why materials are as weak as they are. In spite of these efforts, engineers have not always been able to predict the behaviour of complicated structures, which has sometimes led to terrible accidents. Thus there is a predictability gap between theory and practise.

The reason for the discrepancies found is that the theory of elasticity considers a structural material to be homogeneous and continuously distributed over its entire volume, while no materials fulfil this consideration. They are all full of grooves, fillets, holes, threads, dislocations and other irregularities. It is therefore logical that the actual predictability gap exists.

1.1.2 Fracture mechanics

The solution of the notch problem by Kolosov and Inglis, provided the first step in explaining the background of internal cracking of structural materials under load. They showed that existing irregularities within the structure can act as stress raisers or points of stress concentration. The maximum stress at such a point is customarily determined by first calculating the nominal stress, i.e. as if the stress raiser did not exist, and then multiplying this value by a stress concentration factor. These factors thus indicate the increased stresses due to an irregularity in a hypothetical ideal material as predicted by the theory of elasticity.

The most valuable single contribution to the theory of internal stresses and their role in structural engineering is, maybe, that made by A. A. Griffith. He stated in 1921, "The driving force for crack extension is the difference between the strain energy which is

released if the crack is extended and that needed to create new fracture surfaces". In other words, he proposed that strain energy is transformed to surface energy when a crack is opened.

In the late 1940's, however, E. Orowan and G. R. Irwin pointed out that the surface energy of most structural materials is only a negligible quantity within the total energy absorption. Most of the energy is expended in producing plastic strains in front of crack tips.

In this way the linear elastic fracture mechanics was formulated. This theory is valid if the plastic zone at the crack tip is small compared with the crack length and the dimensions of the structural body.

A general yielding fracture mechanics theory was not born until 1968, when J. R. Rice recognized a parameter, known as the J-integral, which is derived from non-linear elastic material behaviour and which bears the same function as the energy absorption in the linear elastic theory by Orowan and Irwin. The exact formulation of this general theory, however, still remains to be done.

A general failure law for structural materials has not yet been formulated. The statement by M. Bosch in 1940 is still relevant, "Zusammenfassend ist festzustellen, das zur Zeit leider noch keine allgemein gültige Erklärung der Bruchgefahr bekannt ist und in absehbarer Zeit auch nicht zu erwarten ist".

1.2. LINEAR ELASTIC FRACTURE MECHANICS

1.2.1 Stresses in front of a hole

Consider a circular hole, with radius a, in an infinite plate under a uniform tensile stress σ, Fig 1.

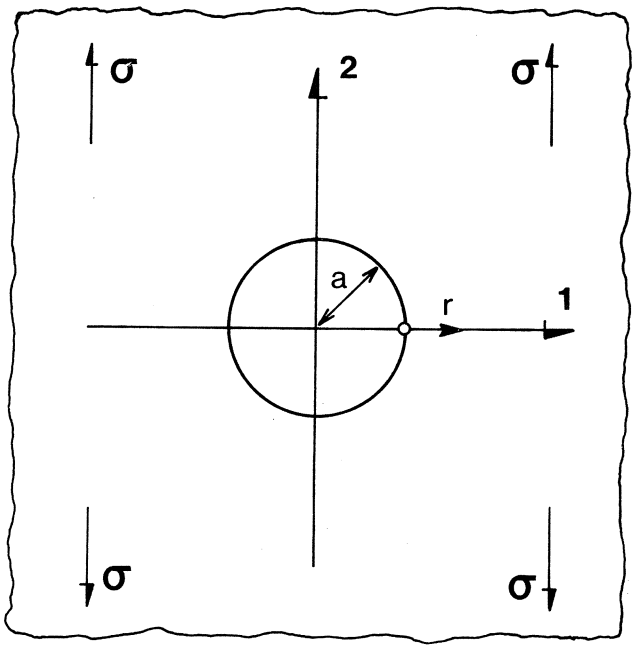

Fig 1. A circular hole in an infinite plate

The stress normal to the 1-axis, a distance r from the edge of the hole, is given in the well-known solution by Leon (1908),

$$\sigma_2 = \sigma \left[1 + \frac{1}{2}\left(\frac{a}{a+r}\right)^2 + \frac{3}{2}\left(\frac{a}{a+r}\right)^4 \right] \qquad \ldots.(1)$$

When $r \to \infty$, σ_2 tends towards the uniform applied tensile stress σ; when $r = 0$, σ_2 equals $3\,\sigma$.

If the circular hole becomes elliptical, with semi-major axis a and semi-minor axis b and with its major axis normal to the uniform tensile stress σ, σ_2 for r = 0 is given in Inglis' solution from 1913,

$$\sigma_2 = \sigma(1 + 2\frac{a}{b}) \qquad \ldots.(2)$$

This increases without limit as the ellipse becomes longer and more slender and becomes identical to Eq (1) when a = b, i.e. $\sigma_2 = 3\sigma$.

If the minor axis is much shorter than the major axis, i.e. if b<<a, the ellipse becomes what is known as a crack, fig 2.

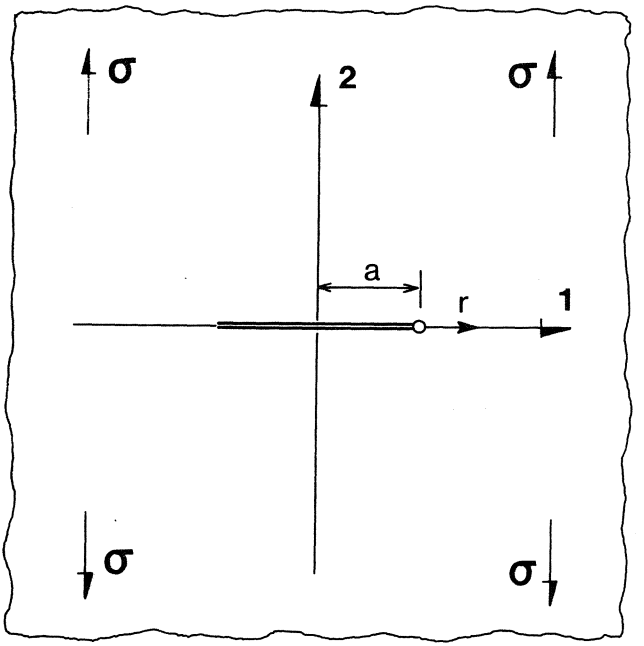

Fig 2. A crack in an infinite plate

The stress normal to the crack plane along the 1-axis a distance r from the crack tip was given in 1939 by Westergaard,

$$\sigma_2 = \frac{\sigma}{\sqrt{1 - (\frac{a}{a+r})^2}} \qquad \ldots.(3)$$

When $r \to \infty$, σ_2 tends towards the uniform applied tensile stress σ; when $r \to 0$, σ_2 tends towards infinity.

If Eq (3) is expressed as a binominal series (see Appendix A), the relation between the two extremes of the elliptical hole, the circular hole and the crack, is seen in,

$$\sigma_2 = \sigma \left[1 + \frac{1}{2}\left(\frac{a}{a+r}\right)^2 + \frac{3}{2}\left(\frac{a}{a+r}\right)^4 \right] \quad \text{...circular hole}$$

$$\sigma_2 = \sigma \left[1 + \frac{1}{2}\left(\frac{a}{a+r}\right)^2 + \frac{3}{8}\left(\frac{a}{a+r}\right)^4 + \frac{5}{16}\left(\frac{a}{a+r}\right)^6 + .. \right] \quad \text{...crack}$$

The two extremes are also compared in Fig 3,

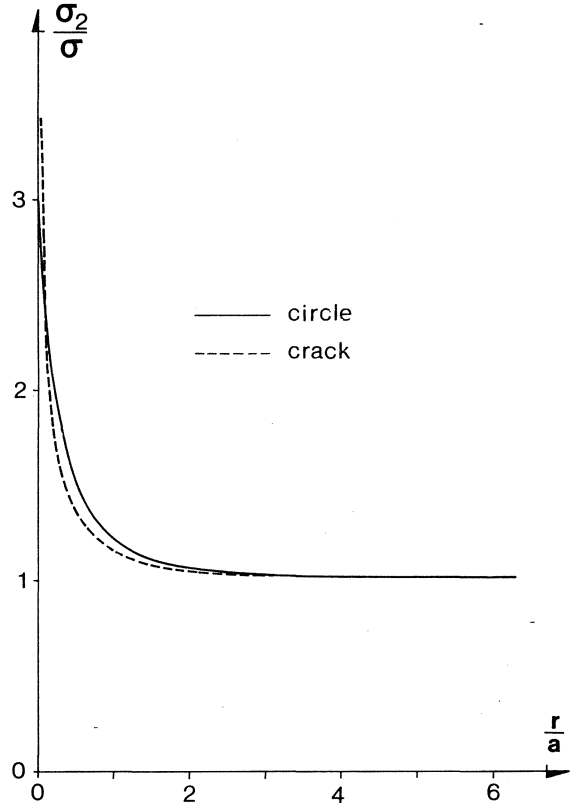

Fig 3. Stress distributions in front of a circular hole and a crack in an infinite plate under a uniform tensile stress σ.

Thus, for σ-values close to the fracture stress, a circular hole may be as dangerous as a crack. In brittle materials it is not the shape of a hole that is critical, it is the presence of it.

1.2.2 Crack modes

When a crack is under an applied uniform tension, the crack surfaces tend to part from each other so that the crack is opened. This configuration is therefore called the opening mode I or briefly mode I. Mode II and mode III are both shear modes, one in each direction of the crack plane. The three configurations are shown in Fig 1.

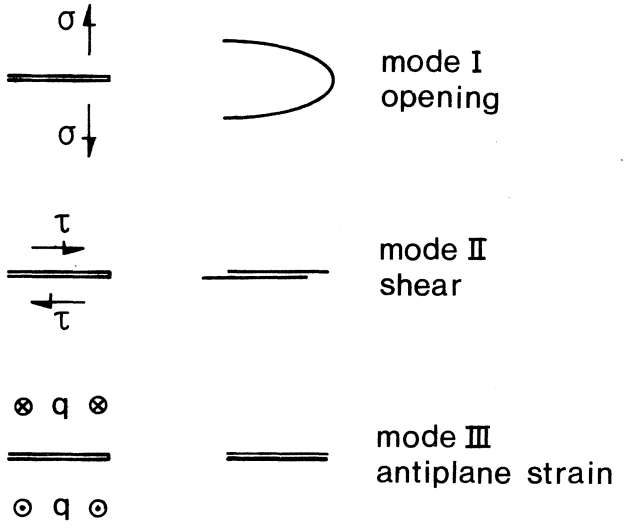

Fig 1. The different crack modes.

1.2.3 Stress intensity factor

The stress close to a crack tip is often written in terms of a single parameter K, the "stress intensity factor", which is defined by Eq 1.

$$K = \text{stress } \sqrt{\pi a} \qquad \ldots.(1)$$

For mode I the stress in front of a crack tip in an infinite plane is given by Eq 1.2.1(3). Close to the crack tip, when r<<a, this equation becomes approximately,

$$\sigma_2 = \sigma\sqrt{\frac{a}{2r}} \qquad \ldots.(2)$$

By combining Eq:s (1) and (2) we get,

$$\sigma_2 = \frac{K_I}{\sqrt{2\pi r}} \qquad \ldots.(3)$$

where K_I is the stress intensity for the actual mode I. The advantage of writing the stress close to the crack tip in this way arises from the point that the $1/\sqrt{2\pi r}$ dependency is followed for any applied stress system. Different combinations of applied loads give each their own contribution to the resultant stress in a specific mode and may simply be calculated by adding the individual stress intensities.

The forms for K have been calculated for a number of loading configurations, the most common found in any modern engineering handbook. They are all of the type,

$$K = \text{stress } \sqrt{a}\ F \qquad \ldots.(4)$$

where F is a calibration function which defines K of the specific body under consideration. In many cases F becomes on the order of 2, for a crack in an infinite plate F is $\sqrt{\pi} \sim 1.8$.

1.2.4 Brittle fracture

In 1921 Griffith proposed that the driving force for crack extension is the difference between the energy which is released if the crack is extended and that needed to create new fracture surfaces.

To elucidate this it is convenient to consider a crack of the length 2a in an infinite plate as shown in Fig 1.2.1(2). The strain energy Q per unit thickness of this plate is,

$$Q = Q_o - Q_c \qquad \ldots.(1)$$

where Q_o is the strain energy if no crack is present and Q_c the strain energy that is released if the crack is present.

According to Griffith, for the case of plane stress, the value of Q_c is

$$Q_c = \frac{\sigma^2 \pi a^2}{E} \qquad \ldots.(2)$$

where E is the Young´s modulus. This can be used to find the change ΔQ in the strain energy when the crack is extended a virtual length $2\Delta a$ simply as:

$$\Delta Q = \frac{\partial Q}{\partial a} \Delta a = - \frac{2\sigma^2 \pi a}{E} \Delta a \qquad \ldots.(3)$$

The energy ΔS needed to create new fracture surfaces of the length $4\Delta a$ is,

$$\Delta S = \gamma\ 4\Delta a \qquad \ldots.(4)$$

where γ is the surface energy, i.e. the energy that is needed to create one unit crack surface of the actual material.

The Griffith driving force for crack extension can now be expressed as:

$$\Delta Q + \Delta S \qquad \ldots.(5)$$

When this expression equals zero, the critical stage is reached. For this condition Eq:s (3) and (4) yield,

$$\frac{\sigma^2 \pi a}{E} = 2\gamma \qquad \ldots.(6)$$

The stress in Eq (6) is actually the fracture stress σ_F. Thus,

$$\sigma_F = \sqrt{\frac{E\ 2\gamma}{\pi a}} \qquad \ldots.(7)$$

1.2.5 Fracture energy

The strain energy release rate $-\partial Q/\partial a$ from Eq 1.2.4(3) is often called 2G as in Griffith. Thus,

$$-\frac{\partial Q}{\partial a} = 2G \qquad \ldots.(1)$$

When $G = 2\gamma$, as in Eq 1.2.4(6), it is critical and thus called G_c or the fracture energy.

By combining Eq:s 1.2.3(1), 1.2.4(3), and (1) we get:

$$G = \frac{K_I^2}{E} \qquad \ldots.(2)$$

When $G \to G_c$, so $K_I \to K_{Ic}$, yielding,

$$G_c = \frac{K_{Ic}^2}{E} \qquad \ldots.(3)$$

This value is valid for plane stress conditions which means that at crack propagation no yield in shear takes place and the G_c originates from a pure cleavage work. At plane strain conditions this yield takes place and participate in the work of fracture.

As concrete materials not yield in shear, the difference between plane stress and plane strain is negligible. Equation (3) is therefore approximately true for both plane stress and plane strain conditions.

1.2.6 Quasi-brittle fracture

No structural materials are truly brittle. In spite of that, experiments have shown that for many materials the fracture stress is of the form:

$$\sigma_F = \sqrt{\frac{E\ \text{constant}}{\pi a}} \qquad \ldots.(1)$$

The constants, however, are found to be very much greater than the surface energies γ of the materials. In the late 1940´s this led E. Orowan and G. R. Irwin, independently of each other, to suggest that the surface energy of many structural materials is only a negligible quantity within the total energy absorption at crack extension. Most of the energy is expended in producing plastic strains in the highly strained zones in front of crack tips.

Thus Orowan wrote the Griffith fracture stress σ_F as,

$$\sigma_F = \sqrt{\frac{E(2\gamma + \gamma_p)}{\pi a}} \qquad \ldots.(2)$$

where γ_p represents the energy plastically dissipated in producing unstable crack propagation.

Irwin´s approach is similar. He denoted the constant of Eq (1) as G_c, thus yielding,

$$\sigma_F = \sqrt{\frac{E\ G_c}{\pi a}} \qquad \ldots.(3)$$

The advantage of these solutions is that linear elastic solutions can be used in fracture analyses, provided that the plastic zone is small compared with the crack length and the specimen dimensions.

To describe the meaning of "small plastic zone", it is convenient to consider a case such as that in Fig 1,

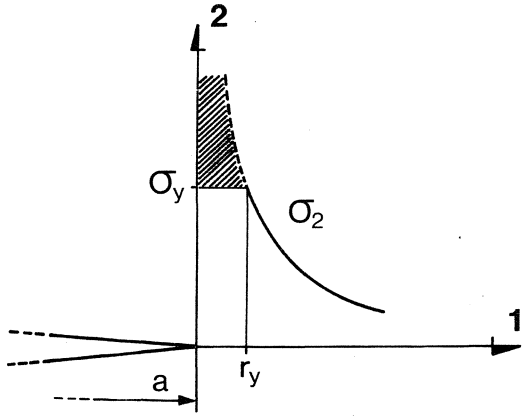

Fig 1. A crack under tension.

Within a distance r_y ahead of the crack tip the stress σ_2 reaches the limiting uniaxial yield stress σ_y. By this, however, a force equal to the shaded area in Fig 1, is released and is thus able to extend the plastic zone a further Δr_y.

A concept of a "notional elastic crack" has sometimes been arrived at in this manner. The notional crack tip is supposed to be located at the point Δr_y as seen in Fig 2. The tip-region of this notional crack is thus only a fictitious crack.

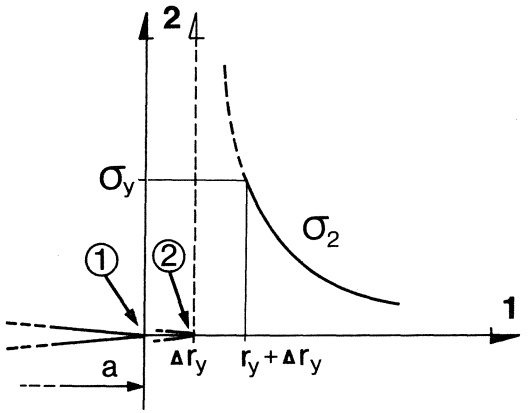

Fig 2. A notional crack under tension
1) real crack tip
2) notional crack tip

The fracture stress for the notional crack can be written as:

$$\sigma_F = \sqrt{\frac{E\,G_c}{\pi(a+\Delta r_y)}} \qquad \ldots.(4)$$

If Eq (4) is to tend towards Eq (3), two conditions must be fulfilled at the same time:

1. The material extension in the crack direction must be large compared with Δr_y or the stress distribution of Fig 2 is distorted in a substantial manner.

2. $a \gg \Delta r_y$.

1.3 CRITERION OF FAILURE

1.3.1 Fracture criterias

An equation which defines all those combinations of stress components which will cause fracture, defines a fracture criterion. Different criterias are treated in [28].

The linear envelope of the Coulomb-Mohr theory of failure provides an sufficient criterion for the fracture of many brittle materials. The basic equation for this straight line envelope is

$$|\tau| = c - \sigma_N \tan \varphi \qquad \ldots.(1)$$

where τ = shear stress acting on the plane of failure
c = cohesion intercept
σ_N = normal stress acting on the plane of failure
φ = angle of friction

The relation between the major and the minor principal stresses for the Coulomb-Mohr theory is elucidated in Fig 1. In the figure, σ_I is the major and σ_{III} the minor principal stress.

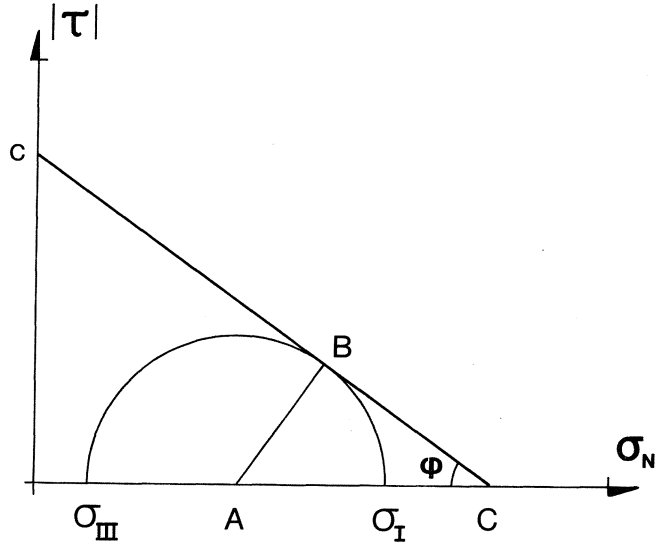

Fig 1. Relationship between principal stresses for the Coulomb-Mohr criterion of failure.

From the triangle ABC in Fig 1 it is seen that

$$\sin \phi = \frac{\frac{1}{2}(\sigma_I - \sigma_{III})}{c\cot\varphi - \frac{1}{2}(\sigma_I + \sigma_{III})} \qquad \ldots.(2)$$

After simplification this equation may be written

$$\sigma_I \frac{1+\sin \varphi}{2c \cos \varphi} - \sigma_{III} \frac{1-\sin \varphi}{2c \cos \varphi} = 1 \qquad \ldots.(3)$$

or

$$\frac{\sigma_I}{f_t} - \frac{\sigma_{III}}{f_c} = 1 \qquad \ldots.(4)$$

where

$$f_t = \frac{2c \cos \varphi}{1 + \sin \varphi}$$

$$f_c = \frac{2c \cos \varphi}{1 - \sin \varphi} \qquad \ldots.(5)$$

f_t is the uniaxial tensile strength and f_c the uniaxial compression strength. These quantities are illustrated in Fig 2.

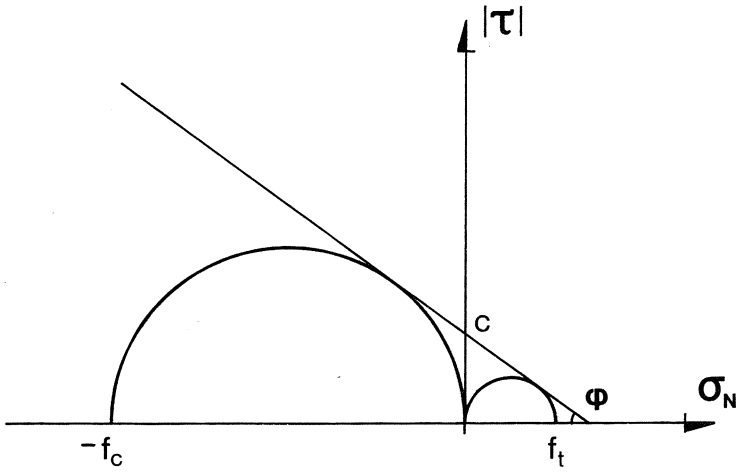

Fig 2. Geometric significance of f_t and f_c.

For a state of plane stress, Eq (4) is an expression for two straight lines as shown in Fig 3. In the figure these two lines are drawn between f_t and $-f_c$.

For many brittle materials Eq (4) is no accurate criterium when σ_1 and σ_2 have the same sign. A better criterium is reached if attention and a compression cut-off is used in this case, see Fig 3.

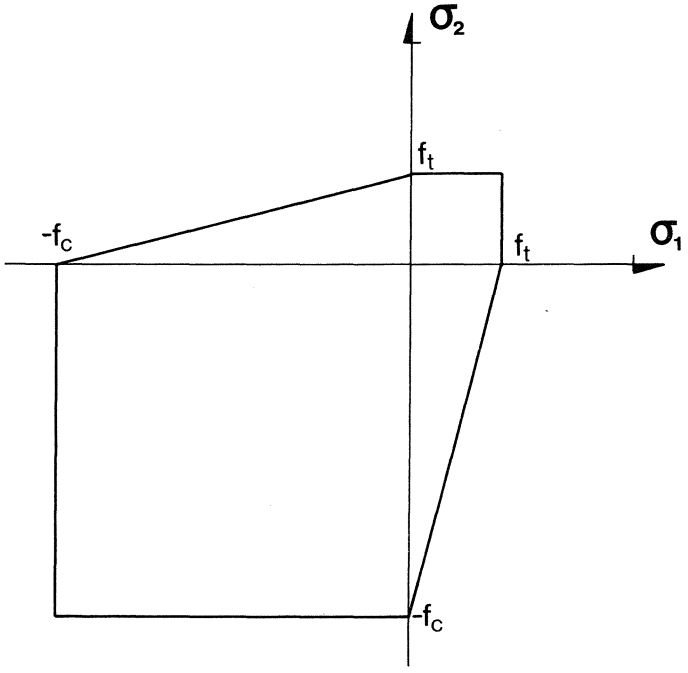

Fig 3. Coulomb-Mohr criterion for plane stress.

Many analyses presented in this thesis, however, is performed by means of the major principle stress criterion, Fig 4. If the Coulomb-Mohr criterion is used, it is discussed under the actual heading.

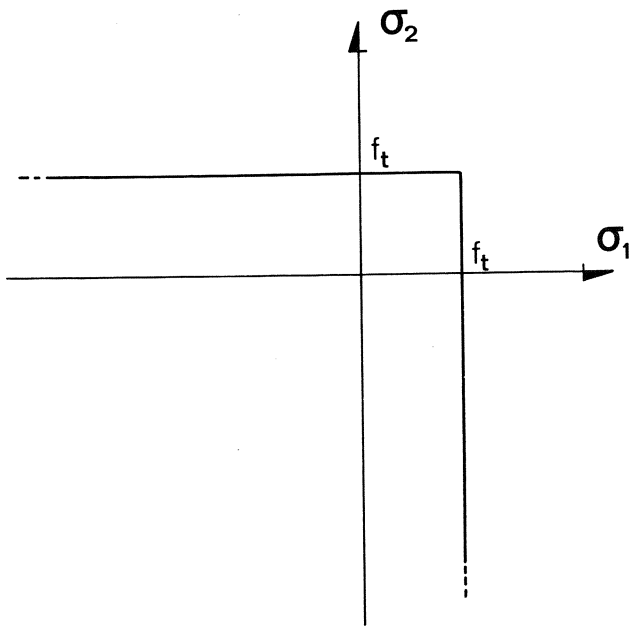

Fig 4. Major principle stress criterion for plane stress.

This is a simple and often sufficient failure criterion for brittle materials. One advantage is that this criterion does not introduce skew crackplanes even for very small values $\sigma_{minor}/\sigma_{major}$, see under "1.3.2 Failure angle hypothesis". This advantage may, however, turn to a disadvantage if $\sigma_{minor}/\sigma_{major}$ is big.

1.3.2 Failure angle hypothesis

The failure is often supposed to occur on the plane where Coulomb-Mohr´s criterion is satisfied; it may be seen that the point B in Fig 1.3.1(1) is the image of the physical plane of fracture. The angle Φ between the major principal axis and the normal to the plane of failure is

$$\Phi = \frac{1}{2} \Delta CAB = \frac{1}{2}(90 - \varphi) = 45 - \varphi/2 \qquad \ldots.(1)$$

In Fig 1.3.1(1) only half of the Mohr´s circle is shown. The reflection of point B in the σ-axis therefore also represents a possible plane of failure. The normal to this second failure plane makes an angle of $-\Phi$ with the major principal axis. These two equally probable planes of failure are shown in Fig 1.

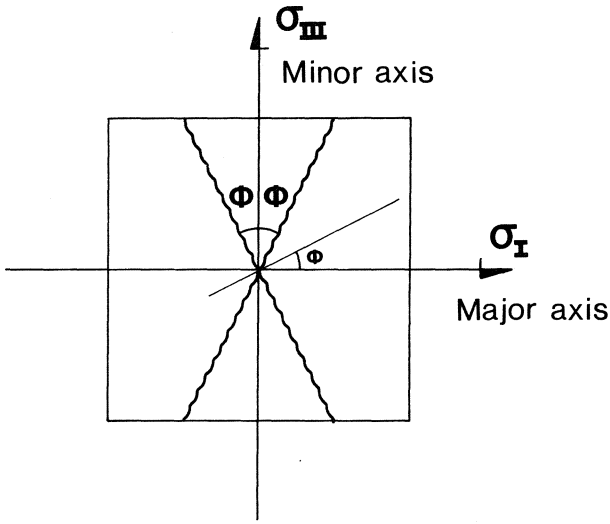

Fig 1. Equally probable planes of failure.

2. NATURE OF CONCRETE

2.1 DEFINITION

"Concrete" originates from *concretus* which is the past participle of the latin verb *concrescere*, meaning "to join together" or "to unite in growth". Thus the word concrete is a verb form that defines a process rather than a material. This is a good description as the term concrete can be constructed to include a considerable variety of products.

The usual engineering definition of concrete is expressed in the Encyclopedia Britannica, 1963 edition, that says, "Concrete is a building material consisting of a mixture in which a paste of Portland cement and water binds inert aggregates into a rock-like mass as the paste hardens through chemical reaction of cement with water ".

2.2 CEMENTITIOUS MATRIX

"Cement" originates from the latin word *cementus*, meaning "cut stone". The hardened cement is thus an artificial stone, usually made by a mixture of Portland cement and water. This Portland cement was invented in 1824 by I. Aspdin, and named Portland simply because the colour of the cement is the same as that of a natural rock from the island Portland.

A freshly mixed cement paste is a dispersion of cement particles in water which has a certain structure owing to the forces of attraction and repulsion among these particles. When the components of the cement and the water react, the reaction products develop a structure that originates from this dispersion structure and that is called hydrated cement.

The structure of the hydrated cement comprises a hierarchy of aggregations or gel particles, the latter being a term for particles in the submicroscopic range of size called colloidal, i.e. from 0.001 μm to 0.1 μm. These colloids are special in so far as one of the three dimensions is often greater than the upper limit 0.1 μm; they are thus needle-shaped.

The most important collodial particle of hydrated cement is an impure calcium silicate hydrate with properties like those of a natural mineral called tobermorite. Although hydrated Portland cement contains up to 25% of hydrated compounds other than the calcium silicate, the hardened paste has properties that justify its classification as a "tobermorite gel".

Along with the colloidal particles in the paste there is crystalline calcium hydroxide. The amount of calcium hydroxide is usually about 15% per volume of the hardened paste, a considerable proportion that must influence the behaviour of the paste in a significant manner. Calcium hydroxide crystals are usually surrounded by and intergrown with colloidal material, and thus they constitute an integral part of the solid structure. In concrete and mortar, according to Idorn et . al. [16] , calcium hydroxide is precipitated in the following locations, (a) as large or small crystal aggregates and in banded formations in the cement paste;

(b) on the surfaces of aggregate particles; (c) in cavities under aggregate particles; (d) in narrow spaces between aggregate particles; (e) around air bubbles; and (f) inside originally air-filled bubbles.

The collodial matter, together with calcium hydroxide appears as a solid structure. But this structure is porous to a large extent, how porous depending on (1) the original water to cement ratio by weight, (2) the rate of hydration, and (3) if any air entraining agent is added. The pores occur in a wide variety of sizes and shapes but different types are still recognized.

Between the needle-shaped tobermorite crystals the smallest pores are located. They have a mean diameter of between 0.002 µm and 0.004 µm and are called gel pores [30].

That part of the originally water-filled space which has not become filled with hydration products constitutes the capillary poresystem of the paste. The mean diameter of the capillary pores is very much larger than that of the gel pores, except in pastes where the gel nearly fills the available space. They may perhaps be considered to vary between 0.01 and 1.0 µm in diameter [40].

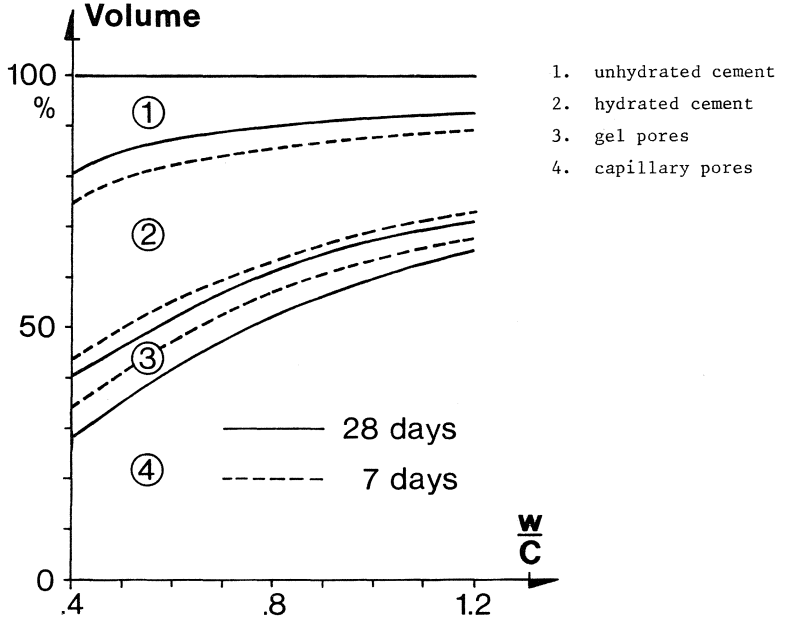

Fig 1. Volume distribution of the main constituents of standard Portland cement paste for different original water-cement ratios after 7 days hardening and after 28 days hardening.

The action of the air entraining agents is that they introduce pores that are embedded in the capillary pore system and increase the diameter of the capillaries up to between 20 and 100 μm [40]. The shape of these pores is more ore less spherical.

The main constituents of hardened Portland cement paste are thus unhydrated cement particles, tobermorite gel, calcium hydroxide, gel pores and entrapped air-voids.

If we limit the constituents to unhydrated cement, hydrated cement, gelpores, and capillary pores, we get a volume distribution of these after 7 and 28 days as shown in Fig 1, Hillerborg [19] . The curves are valid at 20 °C.

2.3 AGGREGATE PARTICLES

Concrete is not only characterized by the cementitious matrix but also to a great extent by the aggregate particles. As these particles comprise about 50 per cent of the volume of mortar and about 75 per cent of the volume of concrete, it is not surprising that the aggregate gradation, shape and surface texture strongly influence the properties of the composite.

The volume distribution of the main constituents of a concrete with 70 per cent aggregate is shown in Fig 1. The figure shows the distribution for a concrete after 7 and 28 days and which has hardened at 20 °C (the figure is an extension of Fig 2.2(1)).

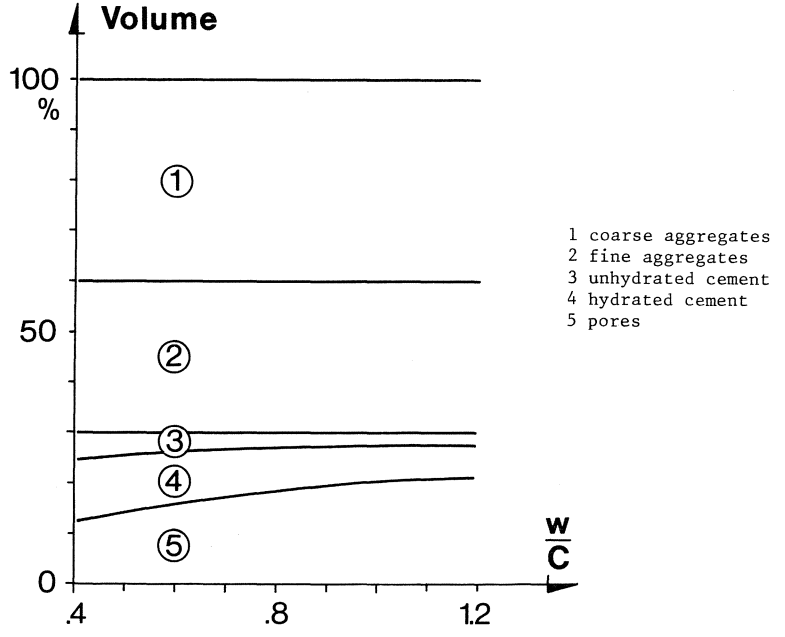

Fig 1. Volume distribution of the main constituents of a standard concrete, with 70 per cent aggregates of the volume for different original water-cement ratio. The figure is an extension of the 28 day curve from Fig 1.

The most aggregates are chemical stable rock materials. These can be natural as regards its shape, such as river gravel, or manufactured, such as crushed material, both types giving the concrete different properties. The differences are not so much in the shape of the aggregates as in the texture of their surfaces. A smoother shape, such as that of river aggregates, does not raise such stress gradients as the angular shape of crushed materials. However, these effects are not decisive and may often be more or less neglected. More important is the surface texture, as the bond between the aggregates and the paste is mainly mechanical in its nature. Thus, river aggregates bond to the paste in a weaker way than crushed aggregates, a matter discussed more in detail further on in the text.

The influence of the aggregate grading on the properties of concrete materials has been extensively studied since the invention of Portland cement and many methods have been proposed for arriving at an ideal grading. None of these have been universally successful, but grading specifications have been developed which on the average will give a concrete of a satisfactory kind.

The gradation is determined by separation of the aggregate with sieves; a convenient system is to double the consecutive sieve-openings, e.g. 1, 2, 3, 4 and 8 mm. Under such a system, with a logaritmic scale, lines can be spaced at constant intervals to represent the successive sizes. An example of a chart drawn on this basis is that in Fig 2.

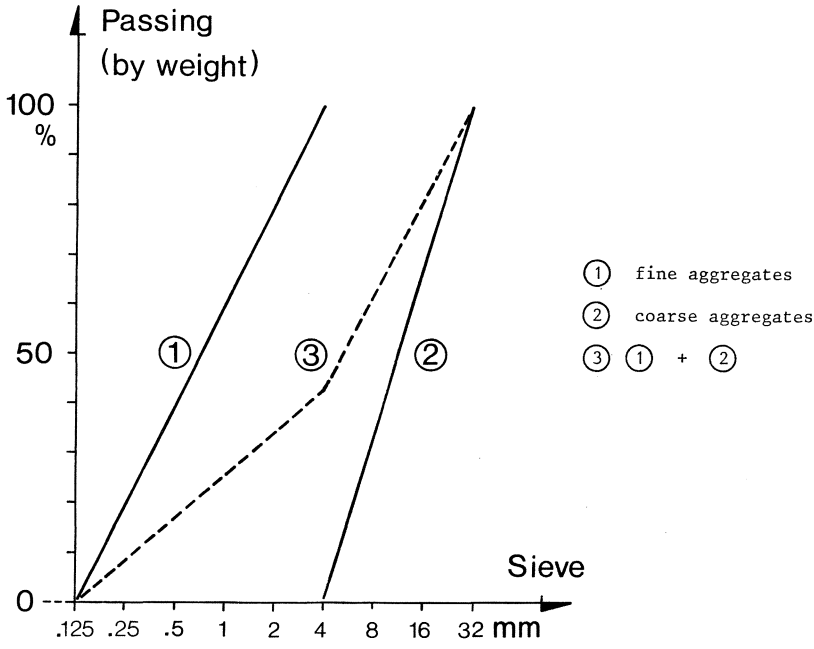

Fig 2. Example of size distribution for concrete aggregates.

The gradings in Fig 2 are expressed as the total percentage by weight passing each sieve. The total percentage retained on each sieve or the percentage retained between consecutive sieves could naturally also be chosen.

2.4 ENTIRE COMPOSITE

The complex behaviour of a material can be understood only by studies of its interior structure. These structural studies can be done on different levels, from the atomic scale up to a scale where the material can be considered continuous and homogeneous.

On the smallest scale a material consists of a great number of discrete particles. This particle structure may, on a bigger scale, be replaced by a continuous media composed of a group of particles which have properties that are an average of the included particles and their bounds the term average having no distinct definition.

It is in this way possible to build up any material, even a complex composite such as concrete. The different particle groups can be chosen so that, on a scale where the mechanical behaviour considered is large compared with the size of the particles of the composite, an average behaviour of a material which is homogeneous and continuously distributed over its volume is an acceptable approximation.

By means of this grouping, concretes may be considered as two-phase materials with one homogeneous and one particle phase. In cement paste the particle phase is unhydrated cement particles and the homogeneous phase is cement gel, in mortar the two phases are fine aggregates with a diameter equal to or less than 4 mm and cement paste, and in concrete they are coarse aggregates with a diameter bigger than 4 mm and mortar.

In these two-phase materials the particles have free mean distances to each other that are about 10 times the mean diameter of the particle considered (see Appendix B). It is thus apparent that, at their respektive dimensional levels, the two-phase division is fair. This also imply that a concrete specimen bigger than 10* the mean diameter of the stones within it can be considered as a one-phase material.

The properties of paste, mortar and concrete can accordingly be considered as averages of the properties of the included phases and bonds between phases.

3. FRACTURE MECHANICS AND CONCRETE

3.1 FRACTURE OF HOMOGENEOUS BRITTLE MATERIALS

If no material restrictions are introduced, the elastic tensile stress normal to a crack surface in a tension field tends towards infinity at the crack tip, Fig 1.

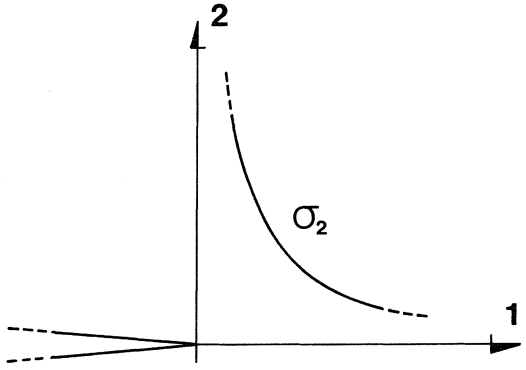

Fig 1. Elastic stress distribution normal to a crack in an infinite plate in a tension field.

The ability of structural materials to resist stresses and strains is of course limited. In a ductile material this limitation is expressed as a local yielding at a crack tip, Fig 2.

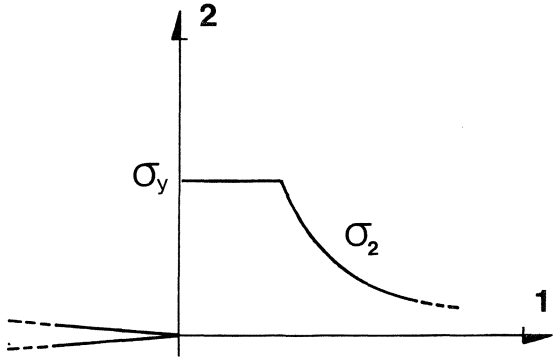

Fig 2. Elasto-plastic stress distribution normal to a crack in an infinite plate in a tension field.

A brittle material is usually not associated with any stress-resisting limit of this kind. It is often considered perfectly elastic, as in Fig 1, or unable to carry any load after a certain stress level is reached.

3.2 FRACTURE OF CONCRETE

Concrete materials are normally considered unable to carry any load at crack tips after a certain stress is reached. The material is said to be cracked.

This criterion, however, is not reliable because it predicts that the material behaviour is discontinuous. A better criterion is reached if the cement paste is considered to behave in a ductile manner, a consideration which is probable, for the following reason,

The gel is built up of a framework of crystallized calcium silicate hydrates (see Appendix B) or tobermorite crystals. These needle-shaped crystals with a length on the order of 0.001 mm, overlap and are thus able to slide along each other to some extent.

If now some part of the framework is stressed up to a sufficiently high stress, this crystal slide occurs and the stress is thus limited. If the slide is so big that the crystals separate, that part of the framework is cracked and another part cracks in the same manner, i.e. if the energy provided is greater than that needed for the actual separation.

The tip-region of a macrocrack, in the following called a crack, is highly stressed. Within this region there are many non-uniform holes, some more slender and crack-like than others.

In this variety of holes, the maximum stress is reached in front of several of them. Now many small cracks, in the following called microcracks, develop within the actual tip-region. Close to the crack tip the formal stress is higher than at a more distant point and the number of microcracks is therefore larger. Some of them are also connected and form even bigger microcracks.

The stress distribution in front of a mode I crack in a paste may for these reasons, look like that in Fig 1.

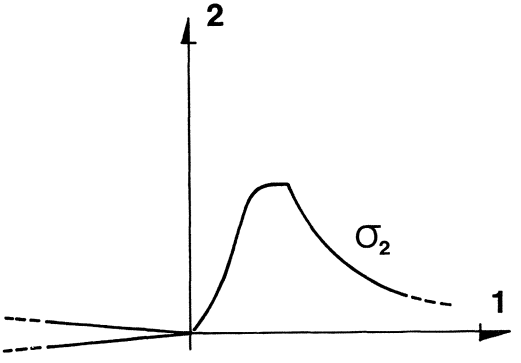

Fig 1. Stress distribution in front of a mode I crack in a cement paste specimen.

3.3 FORMATION OF MICROCRACKS

The formation of microcracks is a physical reality, a statement supported by the photos in Fig 2 below.

Under some specified conditions (discussed later in the text), a precracked specimen, later called a notched specimen, in a three-point bend test breaks in a stable manner, i.e. by stable crack growth through the specimen. Such a test was photographed using an arrangement as shown in Fig 1.

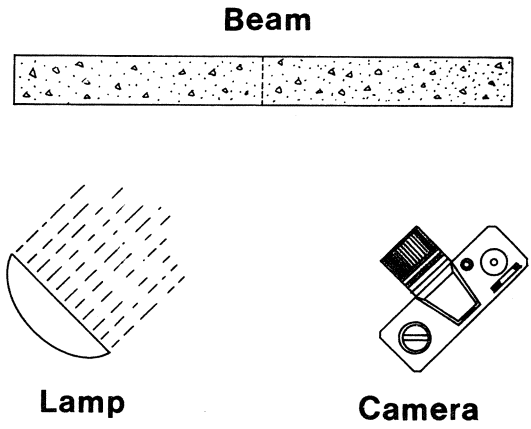

Fig 1. Arrangement for photographing a stable crack growth through a three-point bend specimen.

To prevent drying shrinkage and the connected microcrack formation, the specimens are always hardened under water and kept wet during the entire test. This results in a water-saturated specimen surface that reflects the light from the lamp, as shown in Fig 1.

Now, when the microcracked zone is developing through the specimen, the water at the surface is transported into the specimen by capillary suction and the surface loses its light-reflecting ability. Thus, the microcracked zone is visualized as a grey band through the specimen, Fig 2. The main crack is visible in photo number 2 as a black line.

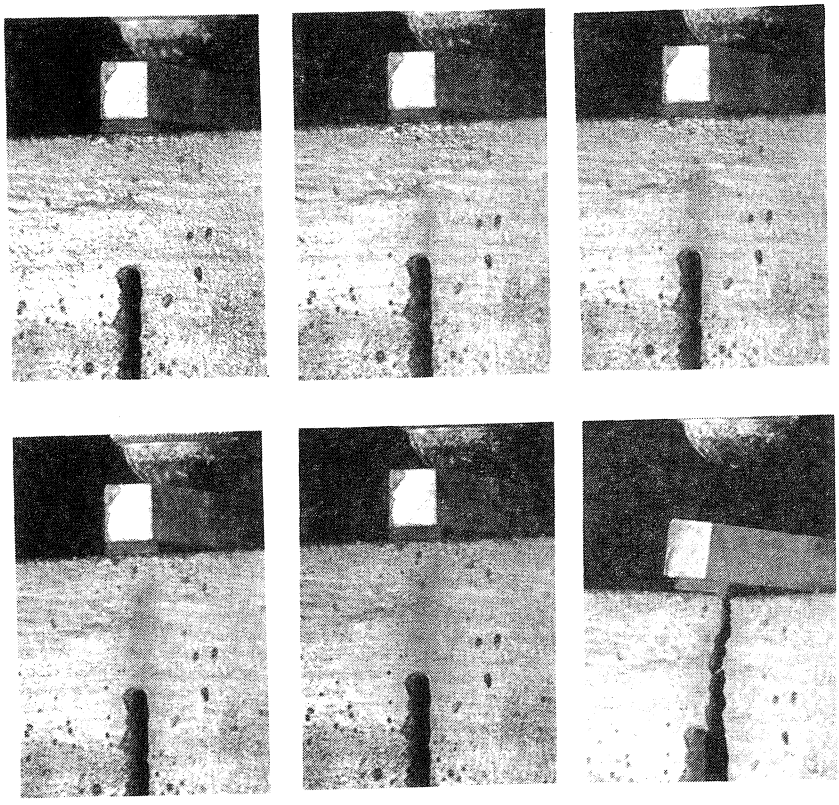

Fig 2. Photos showing the microcracked zone in front of a crack in a mortar specimen. The scale is approximately 1:1.

The specimen in Fig 2 is a mortar specimen. If it had been a paste specimen, the microcracked zone would not have been so pronounced. This is because the aggregates in the mortar stop and distribute the microcracks far more than the unhydrated cement particles of the cement paste.

3.4 FICTITIOUS CRACK MODEL

The "Fictitious Crack Model" or briefly the "FCM", is a general purpose fracture model [18] . In this thesis the application of the model to crack propagation is demonstrated for mode I mainly.

Usually concrete materials are considered to be cracked when the uniaxial tensile strength f_t is reached. But the tip-region of this "crack" is actually a fictitious crack as it is still able to carry some load due to the formation of microcracks, Fig 1.

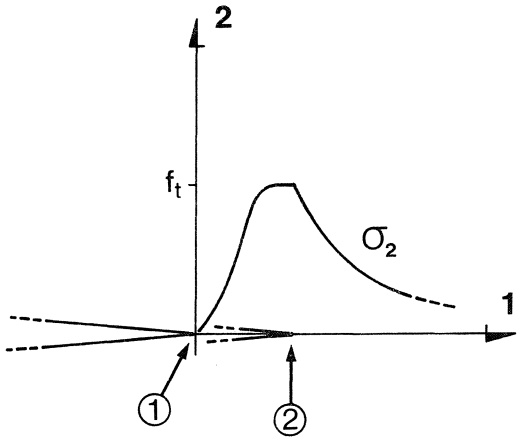

Fig 1. Stress distribution normal to a mode I crack in a concrete material
1) real crack tip
2) fictitious crack tip

Thus the microcracked zone may be illustrated as a fictitious crack able to transfer a tensile stress σ which is a function of the fictitious crack width w according to a σ-w curve.

In this way two curves are needed to describe the deformation characteristics of a material, one ordinary stress strain or σ-ε curve when $\varepsilon \leq \varepsilon(f_t)$, and one σ-w curve when $\varepsilon > \varepsilon(f_t)$, Fig 2.

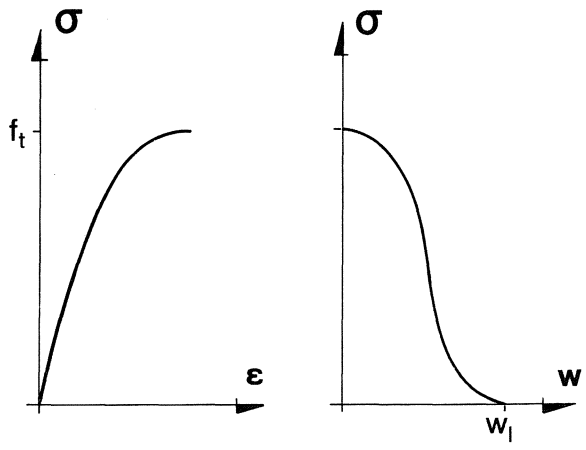

Fig 2. Main characteristics of the fictitious crack model.

The fictitious crack tip is a limit between the zone where σ depends on ε and the zone where σ depends on w. As the load increases, the fictitious crack increases in length and width. When the width reaches a limiting value w_ℓ, the stress at that point disappears and an actual crack propagates.

The development of the microcracked zone may thus be traced from the first application of a stress until final rupture.

3.5 THE σ-w CURVE

In fracture mechanics the energy absorbed in forming one unit area of a crack is called G_c. With the same notation as before, G_c is the total energy absorption when w passes from zero to w_ℓ as expressed in Eq (1) (see Appendix C),

$$G_c = \int_0^{w_\ell} \sigma(w)\, dw \qquad \ldots.(1)$$

Thus, the area between the σ-w curve and the coordinate axes equals G_c, Fig 1.

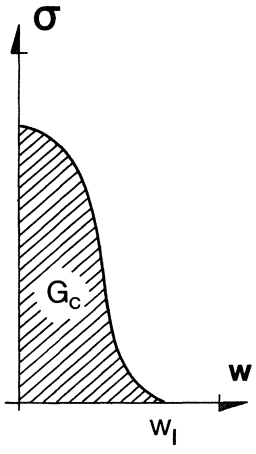

Fig 1. Relationship between G_c and the σ-w curve.

4. ANALYSES

4.1 NUMERICAL METHOD

4.1.1 The Finite Element Method

A convenient method of fracture analysis is the Finite Element Method, or briefly the FEM. In very general terms it is a numerical method by which continuous media can be represented approximately by equivalent discrete elements. The standard work in the field seems to be that by Zienkiewicz [44].

Cracks can be simulated in the FEM by relaxation of element nodes as in Fig 1.

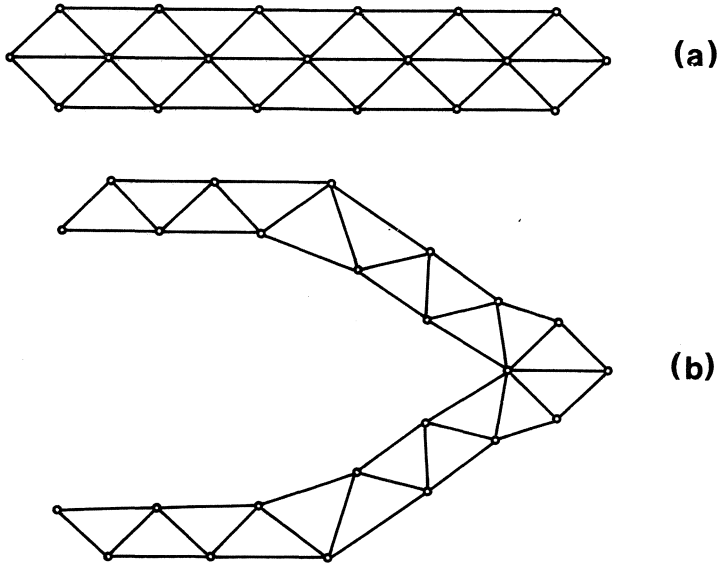

Fig 1. Mode I crack representation in the FEM
(a) uncracked geometry
(b) cracked geometry

The elements are given properties as a limited number of force-deformation relationships at the nodal points connecting the elements. In the FCM (Fictitious Crack Model) the σ-ε and the σ-w curves thus may be represented as shown in Fig 2.

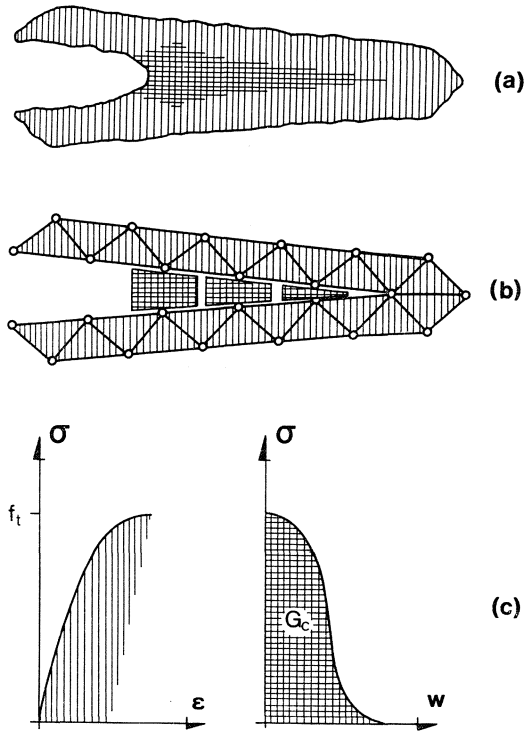

Fig 2. Mode I crack representation in the FCM
(a) actual tensile crack
(b) FEM representation
(c) material properties

Because of the analytical complexities associated with the curved σ-ε and σ-w curves, it is logical to explore some simplifications. If the material behaviour of Fig 2 (c) is approximated by a set of piecewise linear curves, it is still possible to get any degree of accuracy desired while the computational efforts are diminished in a substantial manner.

Examples of different approximate linear curves are shown in Fig 3. Notice that the area between the σ-w curve and the coordinate axes always equals G_c.

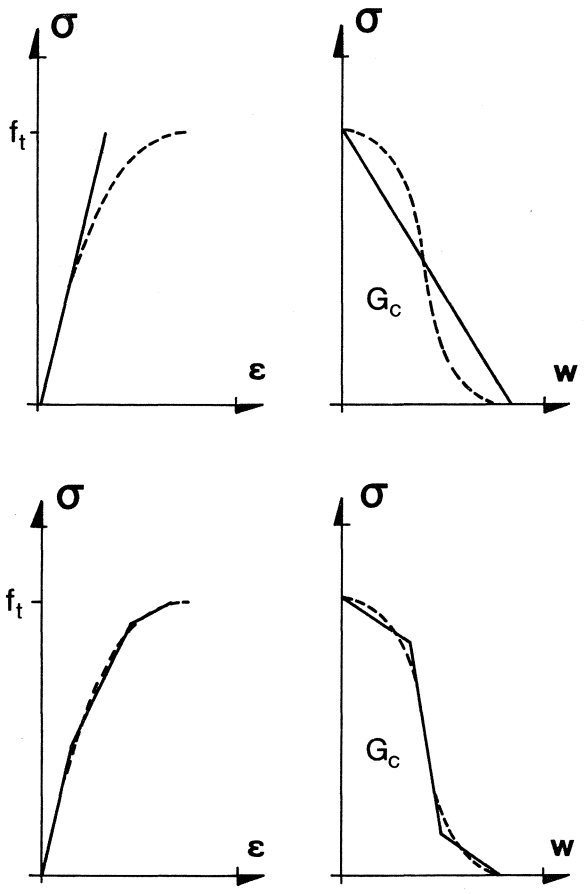

Fig 3. Approximations of the material properties.

The simplest linear approximation, one straight line, is used in most of the analyses presented in the thesis. If not, it is discussed under the actual heading (the σ-ε and the σ-w curves separately).

4.1.2 The Fictitious Crack

The fictitious crack, i.e. the tip-region of the actual crack, is represented in FEM-analyses in a way similar to the Barenblatt cohesive force method [4]. The σ-w curve is thus represented by forces acting at the surface of the fictitious crack.

These forces can be represented in two ways in FEM, directly as forces or as elements at the nodal points within the fictitious crack. Here the representations will be called the force method and the element method (it is not two *different* methods, actually; the difference is the way of representing the forces within the fictitious crack).

In the force method the basic equation is

$$[w]=[w]_e+[w]_i \qquad \ldots.(1)$$

where $[w]$ = fictitious crack width matrix
e = external forces
i = forces between the fictitious crack surface

Equation (1) is of the same type as the basic equation in the well-known flexibility method. The difference is the term $[w]_i$ which is a bridge between the classical theory of elasticity and the fracture mechanics.

In solving Eq (1), two conditions must be added,

1. Equilibrium between restraining stress and fictitious crack width according to a σ-w curve.
2. A fracture criterion, i.e. the fracture stress at the fictitious crack tip dependent on external forces and forces between the fictitious crack surfaces.

A sometimes decisive advantage of the force method (the method is exemplified in Appendix D) is that it is easy to change dimensions and properties of the specimen. Once the flexibility of the structure is found, no further FEM-analyses are required when these changes are made. It is only the system of equations, see Appendix D, that are changed.

In the element method the forces acting at the surfaces of the fictitious crack are represented by special elements (see 4.1.4 and Appendix E), here called FCM-elements.

The properties of these FCM-elements are chosen according to a decreasing σ-w curve; their modulus M is thus negative. This does not cause any trouble in the FEM-analyses if a proper method of finding the inverse of the global stiffness matrix is used, e.g. the well-known Crout-method.

The greatest advantage of the element method is its simplicity. The analyses are easy to grasp and, if no changes in the properties are to be done, inexpensive to perform.

The element method is used in most calculations presented in this thesis. It is therefore discussed more extensively later on.

4.1.3 A test analysis

The very first analysis by means of the element method was carried out to test the method and to elucidate its possibilities; the structure of Fig 1 was analyzed.

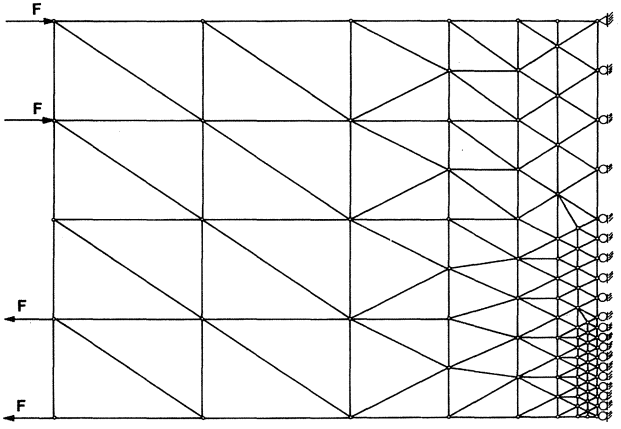

Fig 1. Element mesh, boundary conditions and load for test example.

The material properties chosen were E = 30 000 MN/m^2, f_t = 3 MN/m^2, ν = 0.2, and G_c = 30 N/m. The beam depth was 0.040 m, the width 0.001 m and the lenght 0.110 m. The low value for the beam width was chosen because it simplifies the area calculation of the FCM elements.

The elements were three-point plane elements and four-point isoparametric plane elements. The choise of elements and element mesh was based on experiences reported in the literature.

If the analysis is performed by means of ordinary methods, i.e. with no FCM-elements involved, the maximum value of F is 523 N. An analysis including FCM-elements yields an F value of 830 N, an increase of 59 per cent of the value 523 N. This increase is on the same order as that found under the heading of bending strength.

In figures 2, 3, 4, and 5 some of the results of the analysis are shown. Fig 2 shows the stress at the midsection of the beam for different loads.

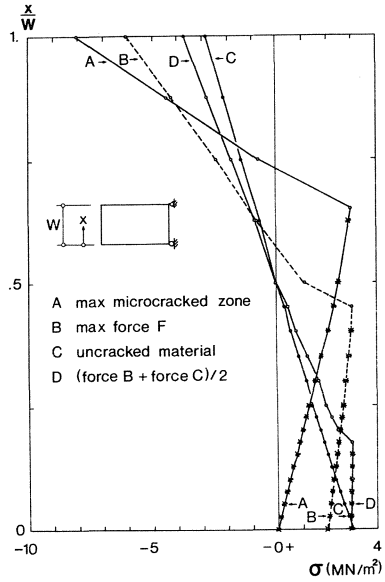

Fig 2. Stress distribution at the midsection of the beam versus crack length.

The stars represent stresses in FCM-elements, the circles average stresses in nodal points. As the beam depth is only 0.040 m, the relative length of the microcracked zone, or the fictitious crack, is considerable.

The restraining stress in the microcracked zone decreases in a very smooth and uniform manner. This is an important result as it confirms the continuous, and thereby natural material behaviour described by the FCM. For reasons of equilibrium, the areas on the tension and compression side at each position of the fictitious crack tip are equal.

The smoothness of the FCM is also verified in Fig 3. In this figure the fictitious crack width for the different steps is shown, i.e. each time a new node reaches the maximal tensile strength. The dotted lines represent the fictitious crack and the continuous lines the actual crack, x/W is the same as in Fig 2. Observe that the different Fig:s overlap.

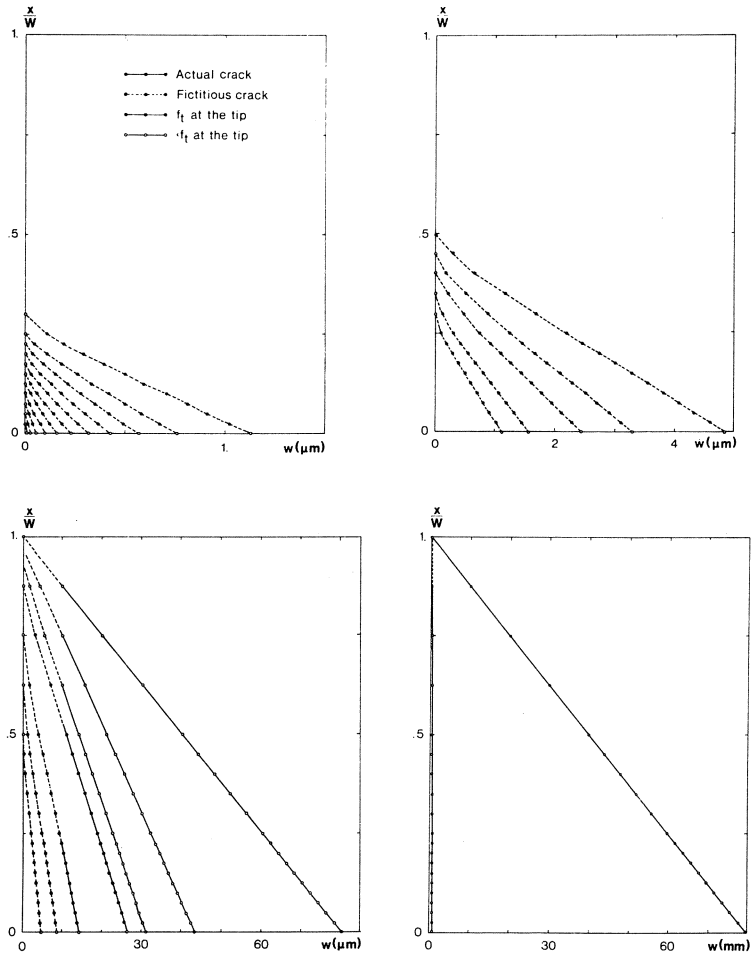

Fig 3. Fictitious and actual crackwidth versus cracklength.

As seen in this figure, the crack expands smoothly and continuously; at the tip-region of the fictitious crack even a tendency to open up in gradually increasing manner is obvious. This tendency is natural and would probably have been even more obvious if the element mesh had been finer.

The length of the microcracked zone and the real crack versus the external force F are shown in Fig 4.

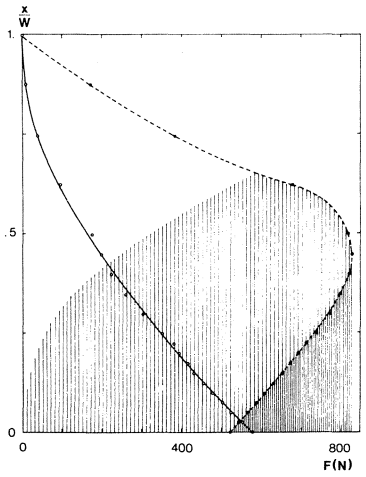

Fig 4. Length of microcracked zone and real crack versus the external force F.

The location of the fictitious crack tip is shown as a dotted line and the actual crack tip as a continuous line. The difference between these two lines, i.e. the length of the microcracked zone versus the external force, is shown as a shaded area.

From Fig 4, it is obvious that the ability of a specimen to resist greater external forces than predicted by the theory of elasticity is dependent on the formation of the microcracked zone. The extension of the microcracked zone is almost linear until the maximum external force is reached; this supports the important hypothesis that the microcracked zone does not change its shape when it is extended in a stable manner.

If the beam depth had been twice that actually used, the length of the microcracked zone at the point of maximum external force would have been almost the same as in the actual case. This explains the dependency of the specimen dimensions upon the maximum force, a theme which is discussed throughout the thesis and which is one of its main results.

Finally, Fig 5 shows the deformation at and between two points at each side of the midsection versus the external force.

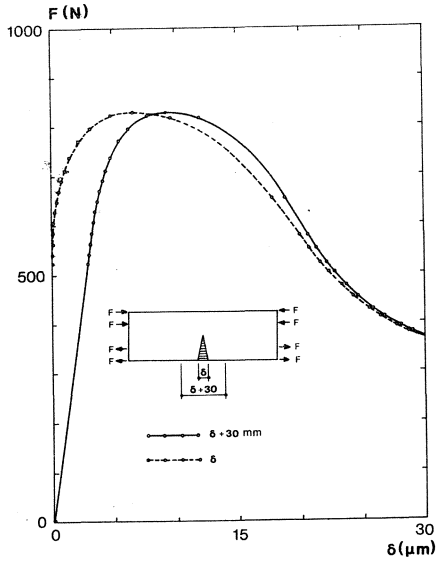

Fig 5. Deformations versus external force F.

The elastic deformations do of course increase up to the point where the microcracked zone starts developing; they are then almost constant until the external force reaches its maximum value. After that, the elastic deformation reverts.

Fig 5 is also important because it tells how a curved σ-ε curve in the macroscale is formed. In the microscale the curved σ-ε curve is due to some yield mechanism, e.g. the previous discussed crystal slide, while it in the macroscale is due to the microcrack formation.

4.1.4 Choise of elements

The elements used in most analysis in this thesis are isoparametric plane elements with four nodes. These uncomplicated elements simplify changes of material properties and boundary conditions when the FCM is used.

The FCM-elements are plane elements with two nodes, i.e. beam elements, and they are only able to resist axial forces. Thus they emphasize the big advantage of the FCM, its simplicity.

It would of course, be possible to use only one size of the four-node elements. But as this is uneconomical, often small elements with a fine mesh are used at points of big stress gradients and bigger elements with a rather coarse mesh elsewhere. When changing element sizes, plane elements with three nodes, i.e. constant strain elements, have been used. An example of this change is shown in Fig 1.

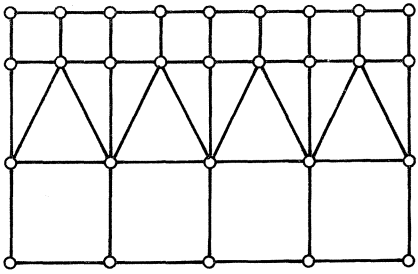

Fig 1. Change of element size.

As the FCM represents a natural material behaviour, there are no stress gradients at the extremes within the structure. The small element demand therefore disappears.

However, two conditions of the element mesh must be fulfilled if the analyses are to be succesful.

The first condition is that the change-over from one element size to another, as shown in Fig 1, does not influence the final result too much. As the introduction of the plane three-node elements represents a stiff band in the structure, the distance, i.e. the number of elements, to this band from a point of interest therefore must be questioned. To check this, the structure of Fig 2 was analyzed.

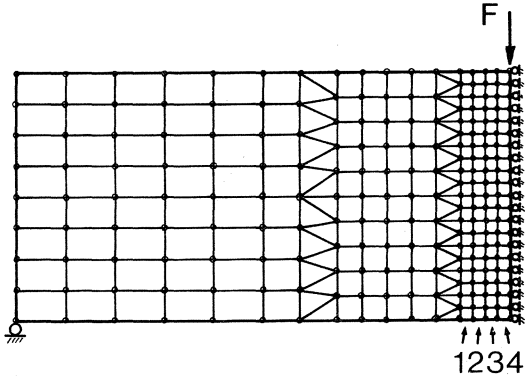

Fig 2. Element mesh for test of sufficient number of elements to a stiff band, i.e. a band of constant strain elements.

The element rows, denoted 1, 2, 3 and 4 in Fig 2, were incorporated one by one into the element structure. For each structure the elastic stress distribution at the midsection of the beam was compared, see Fig 3.

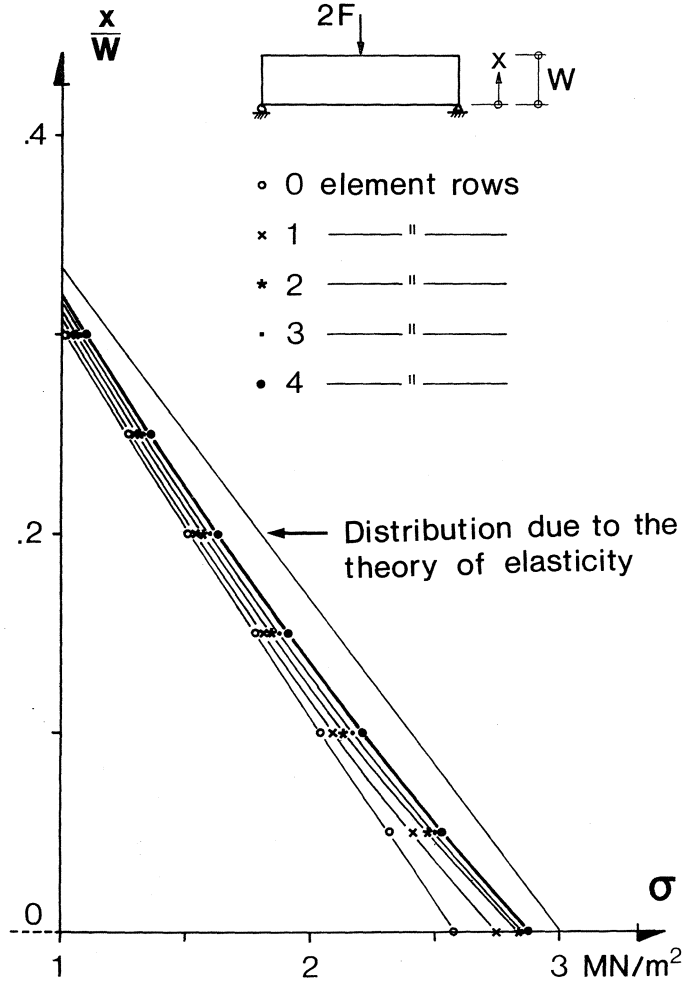

Fig 3. Elastic stress distribution at the midsection of the beam in Fig 2.

There are no big differences between the compared results at the supposed crack area, i.e. the lower regions of the beam below the point load. Thus, four rows are sufficient and this number is regularly used.

The second condition is that the number of elements within each element row must be enough, from both the pure elastic and the microcracked viewpoint.

The elastic condition is simply checked out by the reasonableness of the pure elastic stress distribution within the actual section. Results from such an estimation are shown in Fig 4; the load case is the same as that in Fig 2.

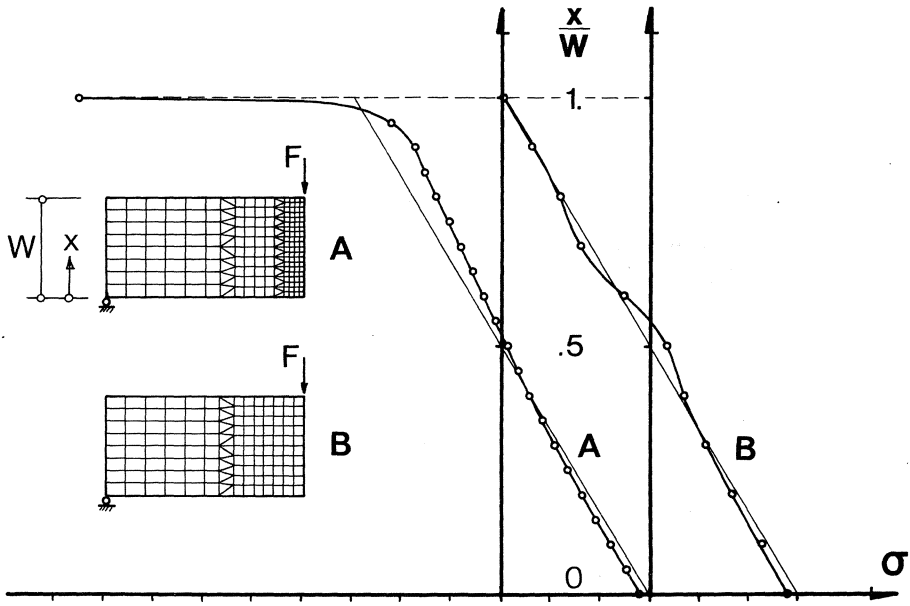

Fig 4. Estimation of sufficient number of elements in one row.

The number of elements at the midsection ought to exceed ten; a proper value may be twenty as the number of elements behaving elastically must be sufficient even when a crack is propagating through the section.

A microcracked zone in front of a crack-tip is represented by FCM-elements between nodes at each side of a fictitious crack. As the zone has limited dimensions, the element mesh must be so fine that the fictitious crack may be represented properly. One way to characterize the dimensions of the microcracked zone is by means of the characteristic length ℓ_{ch} (see 5.2.6).

The general rule has been chosen that the distance between two nodes along the same side of a fictitious crack does not exceed ten to twenty per cent of the characteristic length of the actual material. This is also shown in Fig 5.

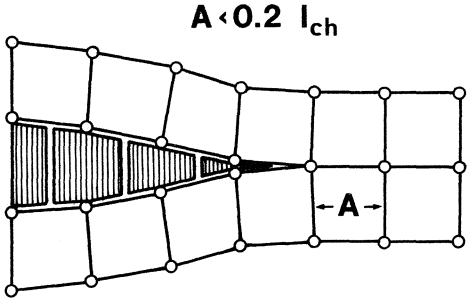

Fig 5. Maximum size of a four-node element near a microcracked zone.

4.1.5 Choise of σ-w curve

For brittle materials, like concretes, it is reasonable that the restraining stress versus the fictitious crack width can be approximated as any of the curves in Fig 1. In all three cases G_c, the area between the curves and the coordinate axes or the fracture energy, is equal.

Here, as well as everywhere else in the thesis, the σ-ε curve is approximated as one single straight line. Most likely does this not influence the numerical results in a substantial manner.

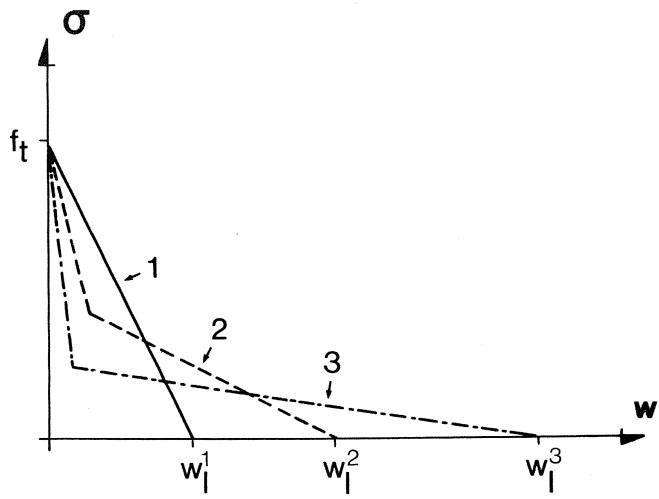

Fig 1. Different choises for σ(w).

For a beam under bending, as shown in Fig 2, these three σ-w curves were used in analyses by means of the FCM. The chosen element mesh is the same as that in Fig 4.1.4(2).

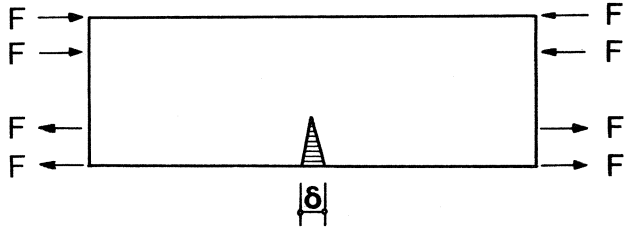

Fig 2. Beam under bending.

Let F be the external force, F_0 the external force of fracture in the pure brittle case (i.e. when $G_c = 0$), w the fictitious crack width, and w_ℓ^i the the maximum fictitious crack width of curve i. F/F_0 versus w_i/w_ℓ^1 for i = 1, 2 and 3 then yields the result shown in Fig 3.

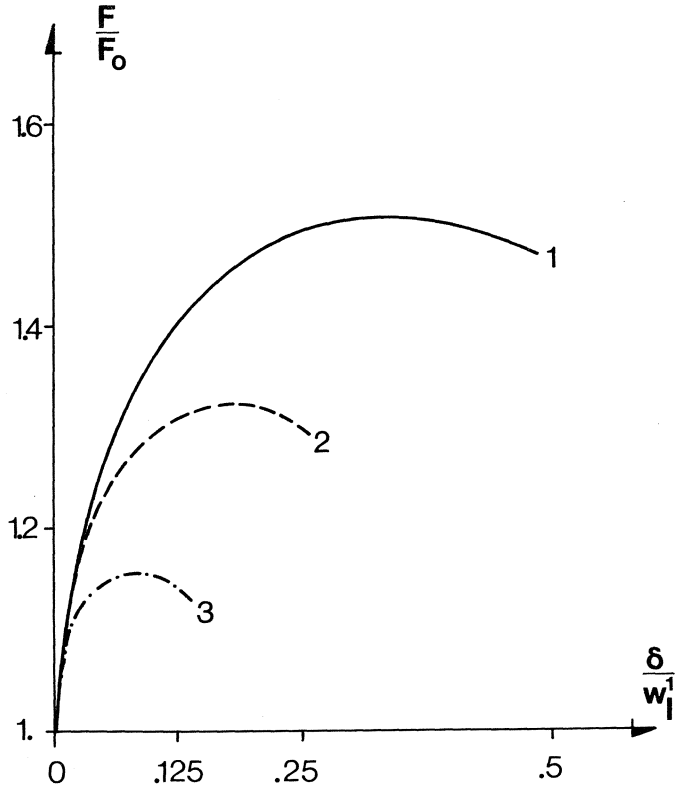

Fig 3. F/F_0 versus δ/w_1^1 for the three different $\sigma(w)$ in Fig 1.

One interesting point is that the (F/F_0) maxima are reached long before the breakpoints in Fig 1 are reached. Thus, it is the initial gradient of the σ-w curve that determines the maximum of moment capacity for the actual beam. This must be remembered when the approximation of the σ-w curve is done.

Of note is also that curve 3 in Fig 2 in principle may be the same as that of a fiber-reinforced concrete, Fig 4. This curve is valid if the fibers have a low modulus of elasticity and/or a bad bond to the concrete.

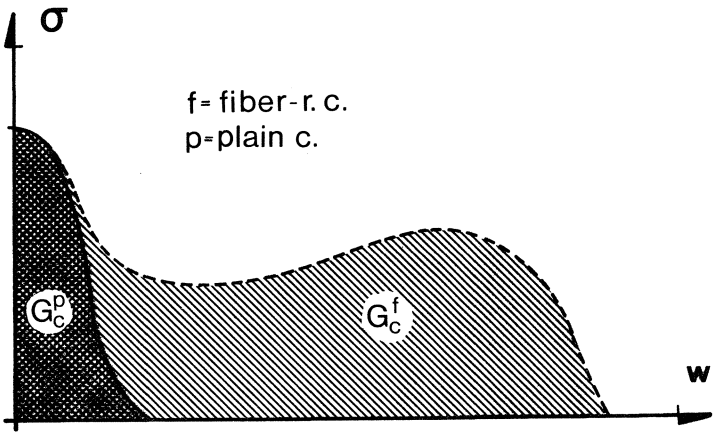

Fig 4. σ-w curve for fiber-reinforced concrete.

The fiber admixture may thus, according to the results above, in spite of the high G_c-value not influence the material strength in a marked way but only the elongation at fracture. If the material strength is to be increased by a fiber admixture, the σ-w curve must have a small gradient in its upper half.

4.1.6 Element mesh chosen arbitrarily

If the crack path is known, e.g. for a beam under three-point bending, the element mesh is chosen to fit this path, Fig 1.

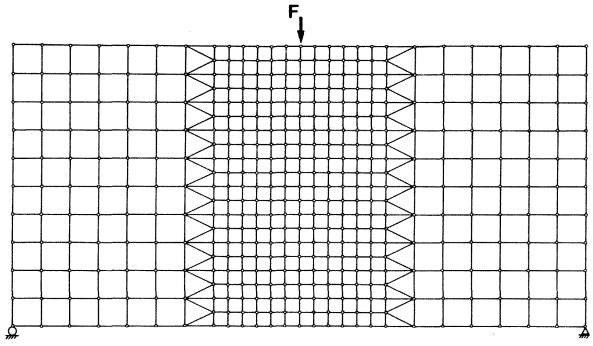

Fig 1. Beam under three-point bending; element mesh chosen to fit the supposed crack path.

The crack path, however, is not always known, in which case the element mesh must be chosen in an arbitrarily way.

Suppose that the crack path of the beam in Fig 1 is not known. The element mesh is therefore of the arbitrarily chosen type, Fig 2.

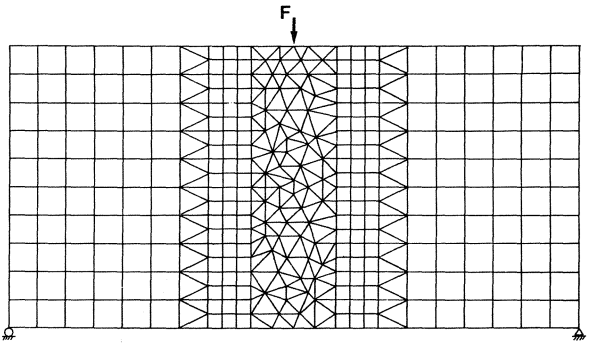

Fig 2. Beam under three point bending; element mesh chosen arbitrarily.

To analyze this problem a crack path criterion must be introduced. Consider therefore an element mesh such as that in Fig 3.

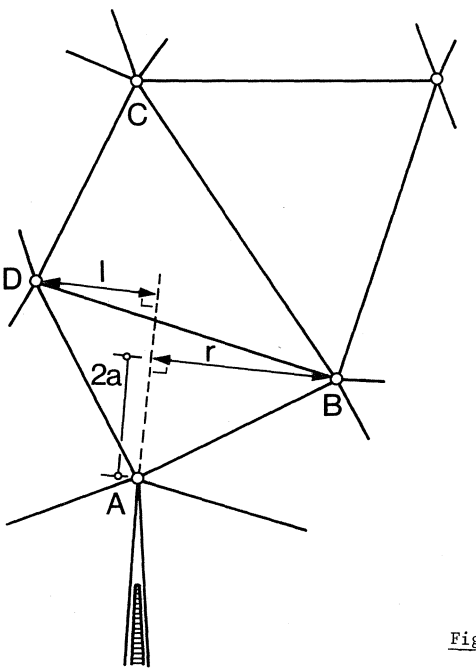

Fig 3. Choise of crack path.

A fictitious crack has reached the node A. When now the external load increases, the major principle stress reaches the uniaxial tensile strength at a new node, here assumed to be node A. The direction of this major principle stress is perpendicular to the dotted line in Fig 3.

Thus the real crack from A is opened along the dotted line, at least near node A. If the element size is not big, this direction is also a fair path through the entire element. But there are only two possible crack paths in the FEM-mesh, either from node A to node B or from node A to node D.

If the crack follows the line A - B, it has been moved away from the proper way a distance r perpendicular to the actual direction. The distance r is called an error to the right. In the same way an error ℓ to the left is obtained from A to D. These two errors are shown in Fig 3.

The analytical crack is thus accomplished with an error, either to the right or to the left, at each node. As the crack propagates, these errors are added and a total error R or L is reached, i.e. a total error to the Right or to the Left.

This total error is, of course, to be minimized and the proper direction may thus be found.

In the example in Fig 3, suppose that node A is subject to an error L approximately equal to half the distance r. The minimum error after node A is then $R \approx r - r/2 = r/2$, which is smaller than $L \approx \ell + r/2$. The analytical crack path from A is thus A - B.

The direction of the FCM-element introduced at node A is perpendicular to the real crack path, i.e. the dotted line in Fig 3. The area of the FCM-element is half the distance 2a in Fig 3 multiplied by the width of the elements (a convenient width is 1, yielding an area of a) and then added to a similar contribution from below node A. This contribution is explained later on.

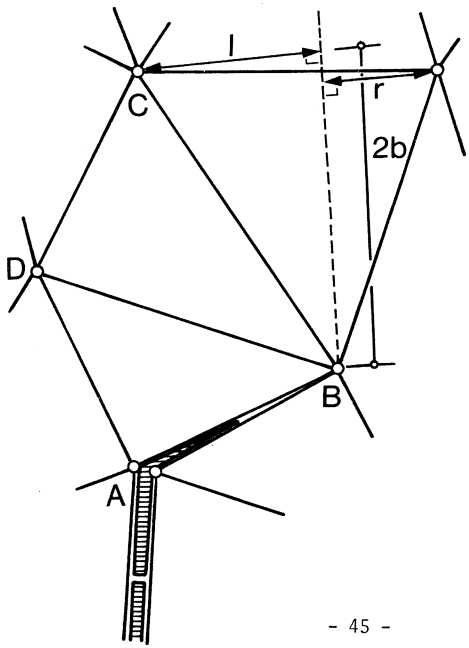

Fig 4. Choise of crack path.

The new situation is shown in Fig 4. The analytical fictitious crack tip is here located at node B.

The external load is increased until the major principle stress at a new node, here assumed to be node B, reaches the uniaxial tensile strength f_t. The perpendicular direction to this major principle stress is shown as a dotted line in Fig 4.

The minimum total error is now L, approximately of the same size as R of node A. This yields an analytical crack direction from B to C. The direction of the FCM-element at node B is perpendicular to the dotted line in Fig 4, its area is a + b. The new situation is shown in Fig 5.

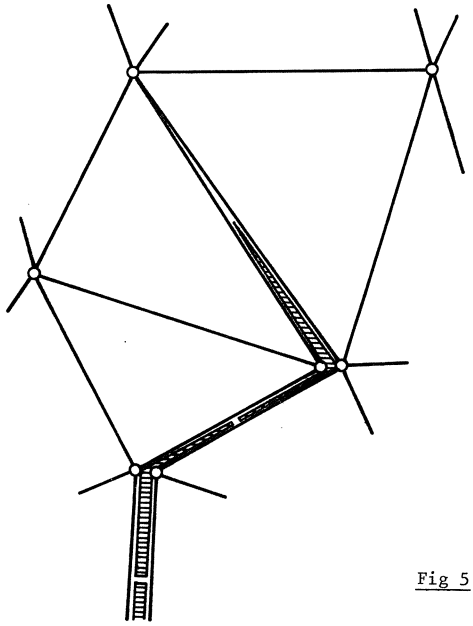

Fig 5. Choise of crack path.

In this way an analytical crack path may be found, a path which is an average of the real crack path. The directions and areas of the FCM-elements are almost correct. All this yields a simple, convenient, and fair approximation of the exact solution.

The element structure of Fig 2 was analysed in this manner.
The material properties of the beam were E = 30 000 MN/m^2, f_t = 3 MN/m^2, ν = 0.2, and G_c = 75 N/m. The beam depth was 0.1 m.

The analytical crack path of these analyses is shown in Fig 6. In the figure the real crack path is drawn as a dotted line.

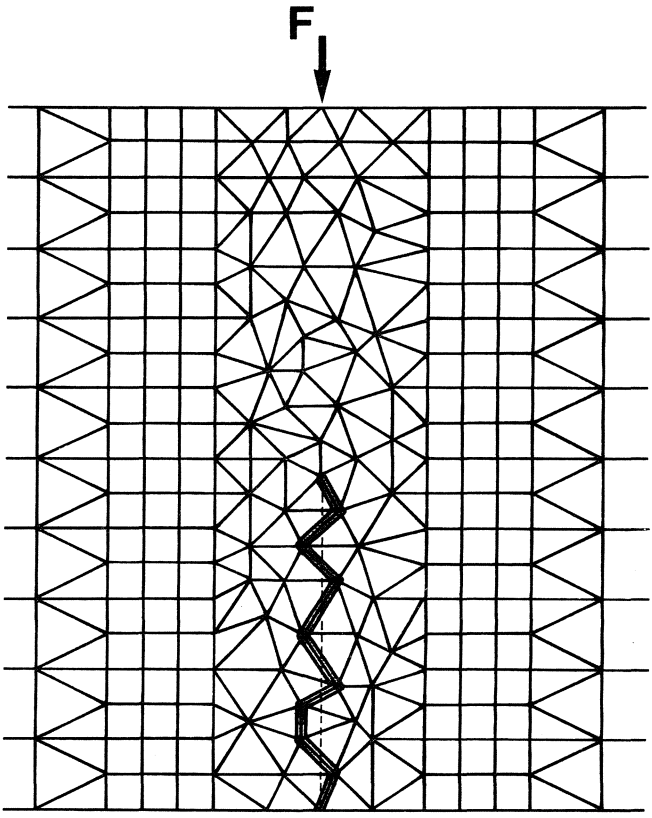

Fig 6. Analytical crackpath for the loadcase and element mesh in Fig 2. The correct crack path is drawn as a dotted line.

The result of these analyses is that F_0, the pure elastic fracture load, is 114 N and the maximum fracture load is 207 N. The increase of the value 114 N is thus 82 per cent, a proper increase according to the results discussed under the heading "Bending strength" (W/ℓ_{ch} for the beam in Fig 2 is 0.4).

4.1.7 Elastic recovery

Near a microcracked zone the elastic stress is decreased. The extension of this recovered area was partly analysed by means of the case and FEM mesh in Fig 1.

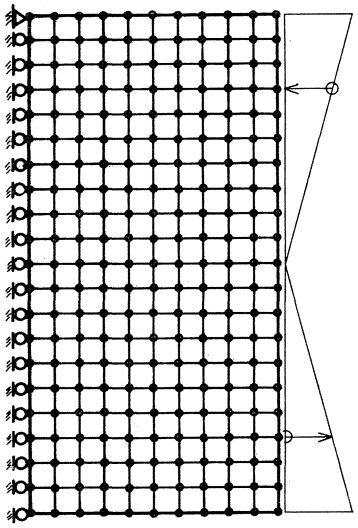

Fig 1. Load case and FEM mesh.

The elastic recovery for a fictitious crack, i.e. a microcracked zone, with a length of 0.25 * (the beam depth) is shown in Fig 2.

The stress at different sections of the beam is represented as different kinds of lines. The wavy line represents the pure elastic fracture stress, the other lines are decoded in the small figure between the different lines and the coordinate axes.

The stress is smaller than the pure elastic fracture stress approximately as far from the midsection, i.e. the section of the main crack, as the length of the cracked zone. More distant from the midsection the stress is higher than the pure elastic fracture stress and a new crack is therefore opened. This new crack does of course affect the main crack, but, on the safe side, the analytical result of Fig 2 suggests that the elastic recovery is extended as far from a crack as the crack length itself. In the case of multiple cracks this is an important suggestion, Fig 3.

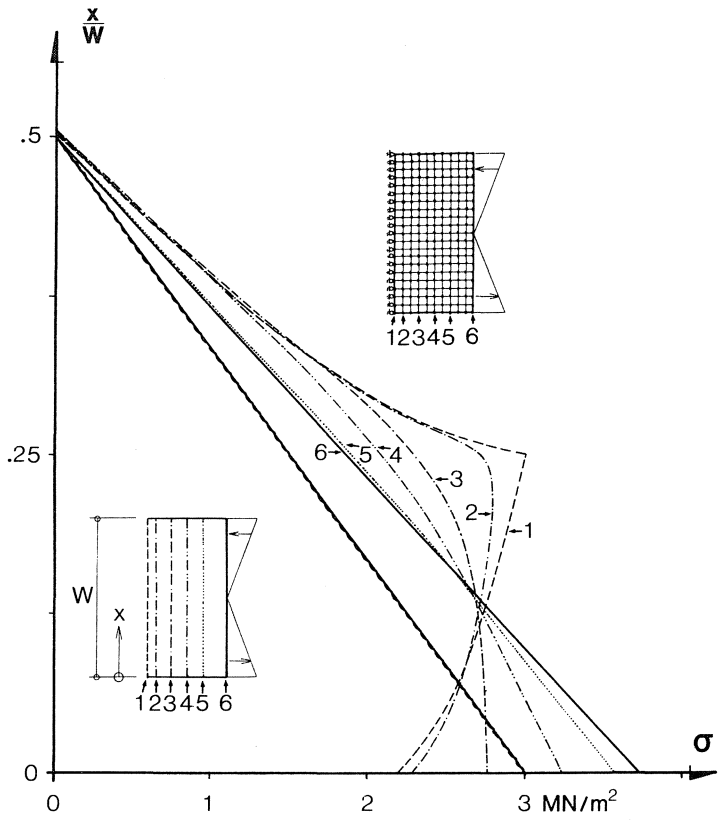

Fig 2. Elastic recovery near a microcracked zone.

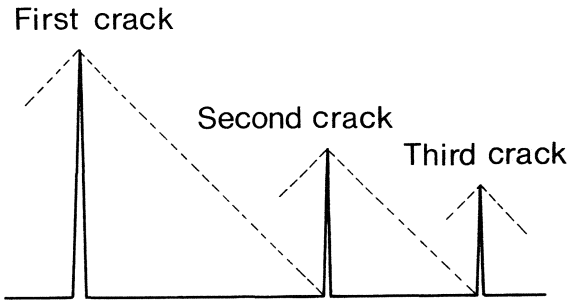

Fig 3. Multiple crack formation.

4.1.8 Shrinkage

It is easy to represent shrinkage stresses in the analyses, but it is difficult to represent them in a proper way. These shrinkage stresses are approximately proportional to the rate of drying of the specimen as shown in Fig 1. They also interact with the elastic stresses and are therefore an important factor in cracking.

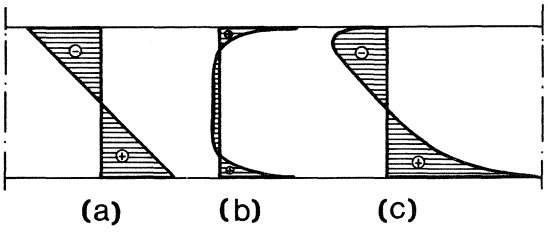

Fig 1. Stress distribution in a beam
(a) stress caused by external load. Moisture equilibrium.
(b) unloaded. Internal stresses caused by drying.
(c) resultant stress distribution (a) + (b).

For a concrete specimen with the water-to-cement ratio 0.65, the cement content 350 kg/m^3, and the aggregate content 1700 kg /m^3, the relative humidity versus the distance to the surface is shown in Fig 2. The figure shows the rate of drying for different times at a surrounding temperature and relative humidity of 20 ^{o}C and 40% respectively (from Nilsson [27]).

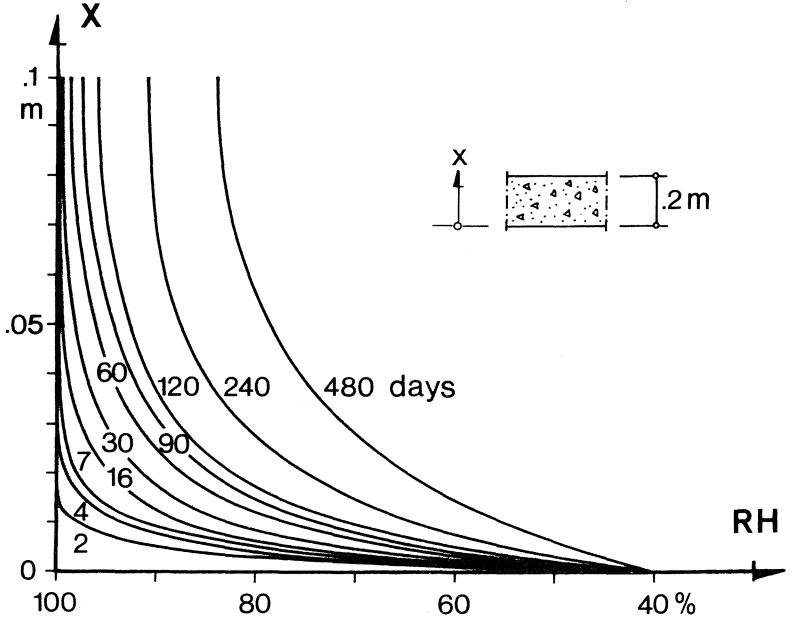

Fig 2. Moisture distribution in normal concrete after different times.

The shrinkage stresses due to these different moisture conditions may now e.g. be represented by different temperatures and accurat coefficients of thermal expansion (many standard FEM program are adjusted to thermal analyses).

The temperature distribution is directly proportional to the moisture content. If a relative humidity of 100% is represented by a temperature of 0 °C, i.e. no shrinkage stress, and 40% by -1.0 °C, the temperature distribution at 30 days is shown in Fig 3.

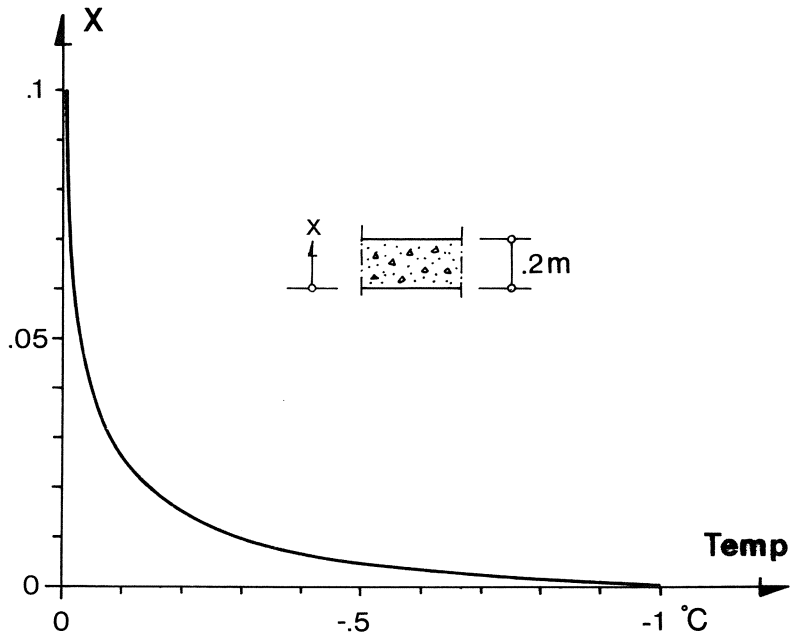

Fig 3. Example of temperature, i.e. moisture (i.e. shrinkage), distribution in a normal concrete.

In the FEM analyses the nodal points are now given temperatures like those in Fig 3. A nodal point at the surface of a beam is given a temperature of -1.0 °C, at the midsection 0°C, and so on.

4.1.9 Multiphase materials

If the material consists of two or more phases, the analytical treatment is considerably more laborious compared with the one-phase case. In order to elucidate some of these difficulties and to solve some of the analytical problems involved, the structure in Fig 1 was analysed.

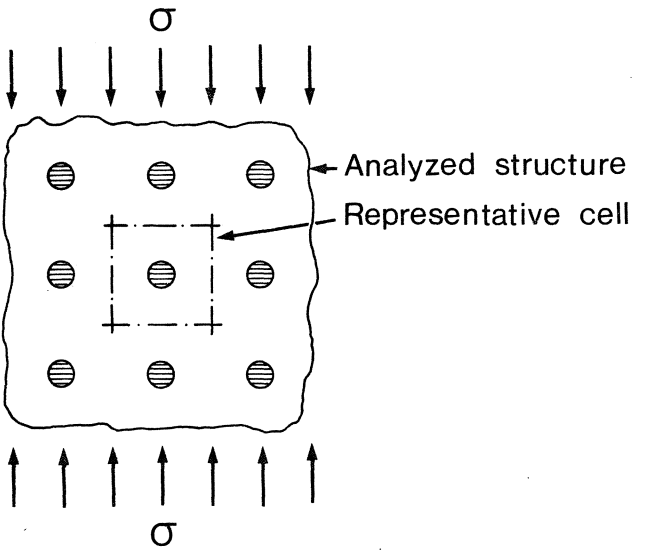

Fig 1. Analyzed structure and representative cell.

The representative cell thus is a part of an infinite matrix with regularly arranged circular aggregates. The matrix chosen was a cement paste and the aggregate a rock aggregate; the side length of the cell was 0.048 m and the aggregate diameter 0.012 m.

The first problem was to choose an element mesh. If the purpose had been a more or less exact solution, the element mesh would have been chosen as described before. As this is not the case a coarser and more economical mesh was chosen, and as it is a symmetrical problem only one fourth of the structure was studied, Fig 2.

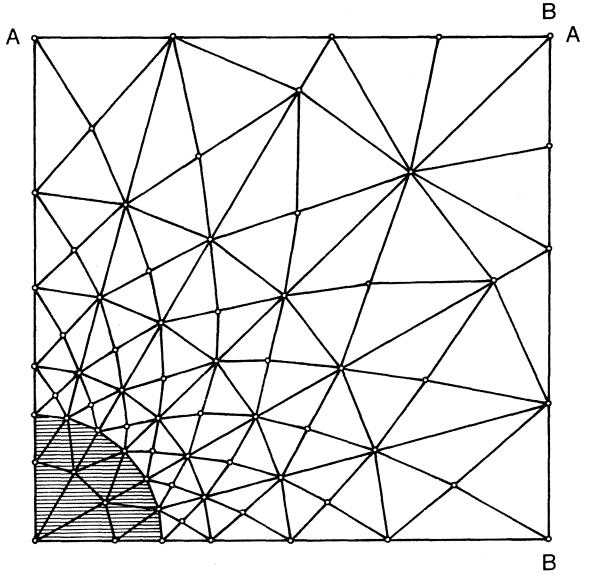

Fig 2. Element mesh of one fourth of a representative cell in an infinite matrix as shown in Fig 1.

The FCM is related to nodal stresses. These stresses in the FEM are calculated as an average of the stresses at the separate element nodes connected in a nodal point of the mesh.

This way of calculating stress raises some problems as the elements connected at the interface all have different properties.

One way to simplify the problems is to assume that the contact zone and the matrix have the same elastic properties except, of course, the strength. The mesh in Fig 2 may also be changed at the interface as shown in Fig 3.

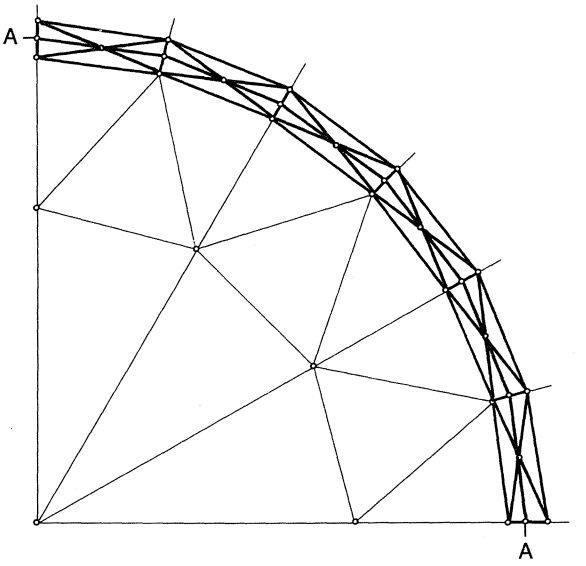

Fig 3. Element mesh at the interface between an aggregate particle and the matrix.

The contact zone is supposed to be located within the element band surrounding the aggregate particle, i.e. along the line A - A in Fig 3. If so, no discontinuities are obtained when the nodal stresses of the mesh are calculated.

Another problem is to simulate the infinity of the structure. The boundaries A - A and B - B seen in Fig 2 must not change their initial directions, for reasons of symmetry. They must also be able to move freely simultaneously in the vertical and the horizontal directions. These conditions were accomplished by adding very stiff elements as shown in Fig 4.

These stiff elements may give rise to a sort of ill-conditioned system. However, the method of matrix inversion used, i.e. the Crout method, is not sensitive to this kind of disturbance (some cautiousness must of course be used when using the Crout method).

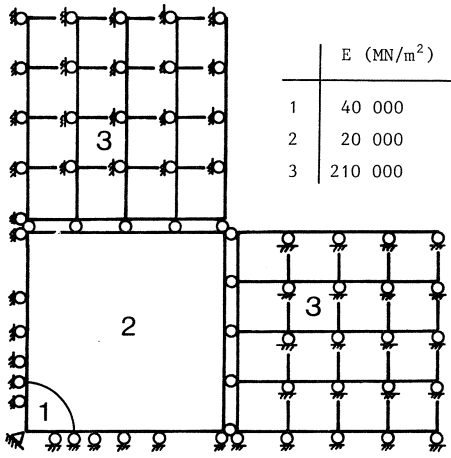

	E (MN/m^2)	ν	Width*10^{-3} (m)
1	40 000	.25	1
2	20 000	.25	1
3	210 000	.3	10

Fig 4. Simulation of the structural infinity.

A crucial problem is the fracture criterion and how the fracture mechanical behaviour should be dealt with in analyses.

A natural fracture criterion for concrete materials on any level is the Coulomb-Mohr criterion (see under the heading "1.3.1 Fracture criterias". This criterion is illustrated by Fig 5, which shows the shear stress as a function of the normal stress at the following sites in plain and reinforced concrete (the figure originates from Alexander [2]),

a) at the interface between paste bonded to aggregate
b) at the interface between paste bonded to steel
c) within the paste matrix
d) at the interface between paste which is in contact with, but is not bonded to, aggregate, steel or hydrated cement.

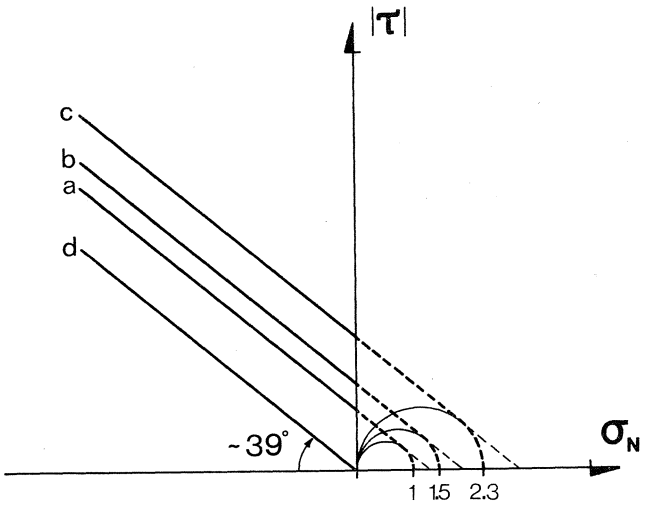

Fig 5. Shear stress at which sliding failure initiates, from ("1.3.1 Fracture criterias").

As seen, the angle of friction is the same in all cases a, b, c and d, i.e. approximately 39°. This is partly consistent with other measurements, e.g. that of Taylor and Broms [38] , an often quoted paper. They point out an angle of friction between aggregate and paste of about 30 - 40°. In the analyses presented in the end of this heading, an angle of friction of 36° is used.

The figure is also enlarged compared with that of Alexander who pointed out the values for negative σ_N-values. If these lines are extrapolated, as in Fig 5, one gets the supposed tensile strengths and may estimate their relations. As seen, the paste tensile strength is more than twice the bond strength between aggregate and paste, a value in accordance with experimental results (see under the heading "5.2.3 Tensile strength"). The value for the interface between paste and steel may be useful when analyzing reinforced structures by means of the FCM.

The FEM-analyses, however, are not altogether simple. One problem is to prevent the matrix elements from being pushed into the aggregate elements when the matrix is sliding along the matrix.

The method used to solve this problem is illustrated in Fig 6.

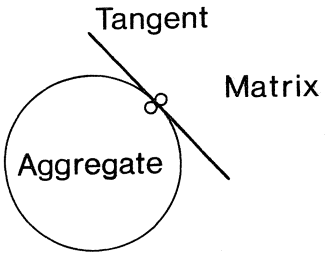

Fig 6. Coupling between aggregate and matrix nodes.

The aggregate node and the matrix node are coupled so that they move independently along the tangent but follow each other perpendicular to the tangent. This is a good approximation as long as the deformations are small.

Another problem is how to represent different stress modes at the interface, i.e. tension, compression and shear. The tension mode is taken care of by the FCM as described before. The pure compression mode is not critical, of course on a sufficient level, because before the material is broken in compression, the tensile or shear strength is obtained somewhere in the material and the compressive stress is thus decreased.

The shear mode is the most questionable. For this mode some sort of a G_{IIc}-value is needed, but as these values are not yet available, the G_{Ic}, i.e. the same as the previous G_c, is used.

Consider the case in Fig 7.

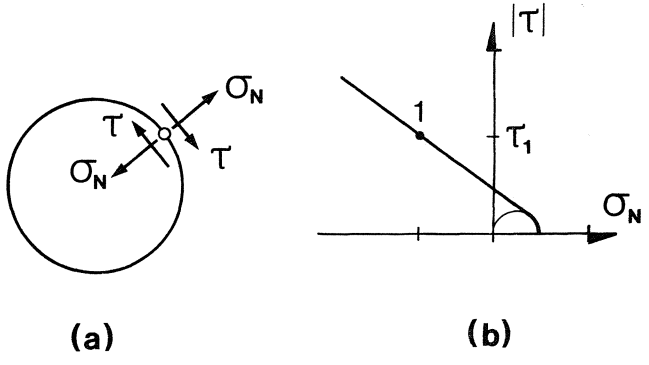

Fig 7. (a) Studied case (b) Point of failure

Fig 7 a) shows an interface node and how it is sheared; suppose that the point 1 of Fig 7 b) is reached. A FCM-element must be involved.

For that reason a new node is introduced, situated very close to the old node and along the tangent to the aggregate surface at the old node and also in the direction of the shear stress.

We get a node configuration as shown in Fig 8.

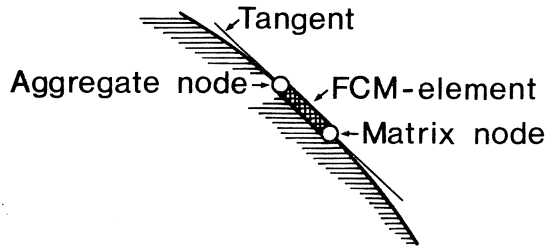

Fig 8. Introduction of a new node along the interface when a FCM element is involved.

Between these nodes an FCM element is placed, the nodes are also coupled as described before. The properties of this element may after each computatitional step be estimated as shown in Fig 9.

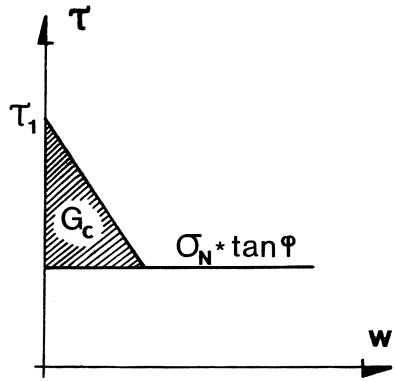

Fig 9. Approximative properties of an FCM element in shear.

If the fracture energy G_c is consumed and the normal stress is still negative, the friction $\sigma_N * \tan\varphi$ is left. This friction is represented in the analyses as a force at the matrix node equal to the friction * (the actual area) and directed as shown in Fig 10.

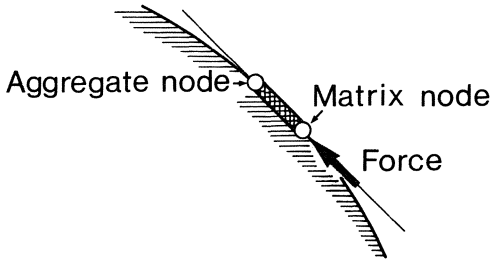

Fig 10. Analytical representation of the residual frictional force.

If the normal stress becomes positive before all the energy G_c is used, the remaining energy G_c' is consumed by an ordinary mode I FCM element as described in Fig 11. The nodes in this case are free from their earlier coupling.

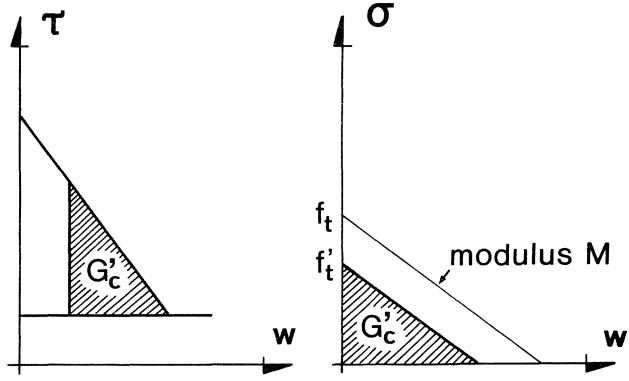

Fig 11. How the restraining energy is consumed when the mode II is turned to mode I.

The remaining fracture energy G_c' and the modulus M yields the remaining tensile capacity f_t' and the problem may be solved.

In the matrix, away from the aggregate particles, the material can be cracked in tension and shear. The tension case is the same as before, the shear case is once again questionable.

Very close to the node that is fractured in shear another node is introduced. It is placed in any of the directions predicted by the failure angle hypothesis (see 1.3.2) and in the direction of the shear stress as in Fig 8. If the failure angle direction is not obvious, both directions must be tried; then the most critical, i.e. the one that permits the smallest external load-change, is chosen.

To represent a mode II crack, i.e. a shear crack, in a proper way a rather fine element mesh is needed. This type of crack does not always propagate in its own plane and therefore a fine element mesh does not disturb the sliding that must occur.

When analysing the structure of Fig 1, all these hypotheses were used except that which stated a fine matrix-element mesh. This exeption was only made for economical reasons and did not affect the analyses, nor their purposes, in any substantial manner. The properties of the cement paste and the interface were chosen as seen in Table 1.

	f_t (MN/m^2)	E (MN/m^2)	G_c (N/m)
Cementpaste	5	20 000	8
Interface	1.5	20 000	15

Table 1. Material properties of the studied case.

Some of the results are seen in Fig:s 12, 13, 14, 15, and 16. In the figures are a shear failure denoted S and a tensile failure denoted T.

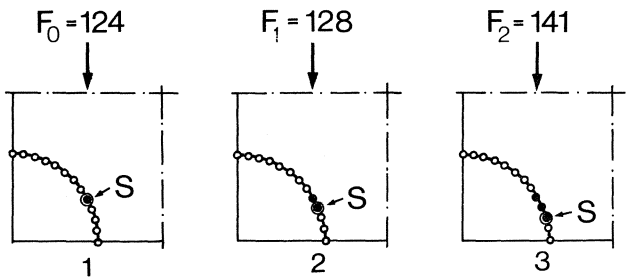

Fig 12. Failure of the structure in Fig 1.

As seen from Fig 12.1, the first node fails in shear. The node is situated at an angle of 30^{o} from the horizontal plane, an angle which is predicted by the failure angle hypothesis as the angle of friction was chosen as 36^{o}. The external force is 124 N.

The second and third nodes have also failed in shear, the second at an external force of 128 N and the third of 141 N.

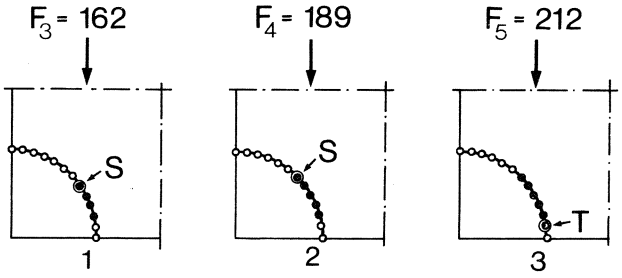

Fig 13. Failure of the structure in Fig 1.

The fourth node has failed in shear on the opposite side of the first node. The fictitious crack has now propagated in both directions of the initial slip. The external force is 162 N.

Also the fifth node has failed in shear, but the sixth node has failed in tension. The external force F_4 is 189 N and F_5 is 212 N. The tension failure at the equator of the aggregate particle thus does not occur until the external force is 171 per cent bigger than the pure elastic value F_0.

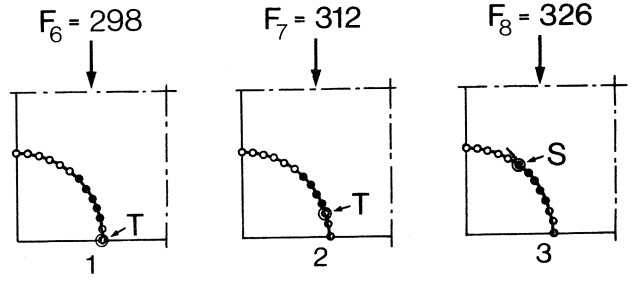

Fig 14. Failure of the structure in Fig 1.

Also the seventh node has failed in shear for a force of 298 N. The fictitious crack of the upper half of the aggregate particle is now connected with that of the lower half. The external force is 240 per cent bigger than the pure elastic value F_1.

The eigth node to crack is not a new node; the third node, see Fig 12.3 is now converted from shear to tension, still using a FCM-element. The external force is 312 N.

The ninth node has failed in shear, not only along the interface but also out in the matrix; the external force is 326 N. The situation is now that shown in Fig 15.

At this important moment the external force is 263 per cent bigger than the pure elastic value F_0 and the matrix crack develops at an angle of 53^o from the horizontal plane. Observe that all cracks are still fictitious, owing to the fineness of the analyzed aggregate.

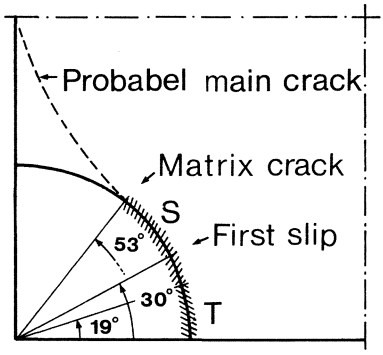

Fig 15. Failure of the structure in Fig 1.

The next node to fail is situated out in the matrix, away from the interface, see Fig 16.1. This may indicate that a matrix crack starts in the matrix and not at the interface of an aggregate!

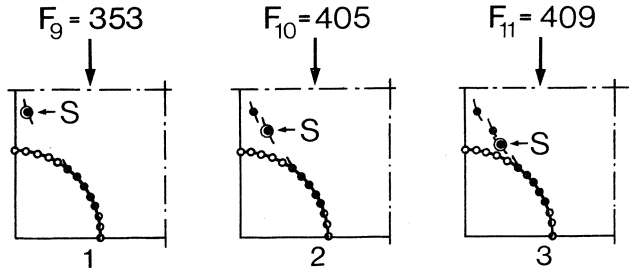

Fig 16. Failure of the structure in Fig 1.

The next two nodes to fail do so for almost the same external force, 405 N, and 409 N. The three nodes in Fig 16 fail along the planes inclined. The paste thus has a tendency to crack in a vertical way. The other nodes round about have almost failed too; the stress field above the particle is very uniform.

This stress uniformity indicates that a dominant irregularity in a real specimen may decide how the crack extension will be. As an average, however, the crack exterior in Fig 15 is probable. This is also consistent with experimental studies, e.g. those by Sidenbladh [35] .

As the element mesh of the matrix is coarse and as the purpose of the analyses is fulfilled, no further loads have been examined.

The true maximum value of the external load may be around 500 N. If so, the pure elastic value F_0 is 25 per cent and the matrix-crack value F_9 is 71 per cent of the maximum value. This is consistent with values given in the literature.

An important matter is that these cracks are fictitious. The real cracks may thus be opened at different points from these, a matter which would have been more clear if the analyzes had been continued.

Too many and important conclusions, however, should not be drawn from this single analysed case. The important thing is that these analyses are possible.

4.1.10 Reinforced concrete

Concrete systems may be looked upon as two-phase materials, see "2.4 Entire composite". This is also valid if the concrete is reinforced, the two phases now being concrete and steel. The only difference from the plain case is that the particle-phase, i.e. the steel, is not randomly distributed over the entire matrix but is concentrated to specific areas. From the fracture mechanics point of wiew, no insurmountable obstacles are raised by this division.

A simple way to represent the reinforcement is to overlap the concrete elements with steel elements. This overlapping may go from node to node or over several nodes. An illustrative example of the latter is shown below.

Consider a slab on a wall as in Fig 1. The studied area is shaded and the reinforcement is represented as a bar, fixed only at its ends. The crack path is supposed to follow the dotted line.

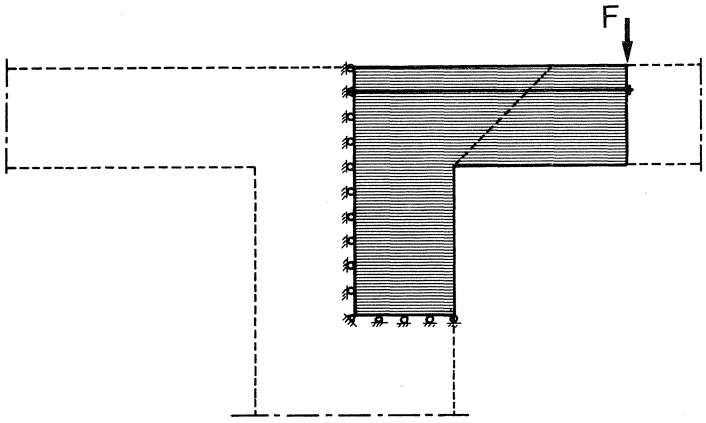

Fig 1. Studied case and reinforcement idealization.

The element mesh of this structure is shown in Fig 2. The mesh is rather coarse as the only reason for the analysis is to demonstrate the method.

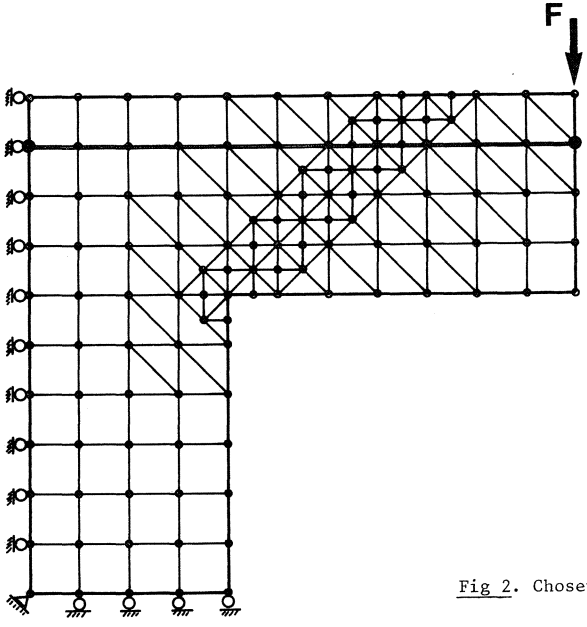

Fig 2. Chosen element mesh.

The material properties were

Concrete: $E = 30\ 000$ MN/m^2
$f_t = 3$ MN/m^2
$G_c = 100$ N/m

Steel: $E = 210\ 000$ MN/m^2
Area = 0.5 per cent of the concrete area

Two different slab depths were analysed, 0.16 m and 0.80 m. The smaller is a typical laboratory specimen, the bigger a full scale structure. The results of the analyses are shown in Fig 3.

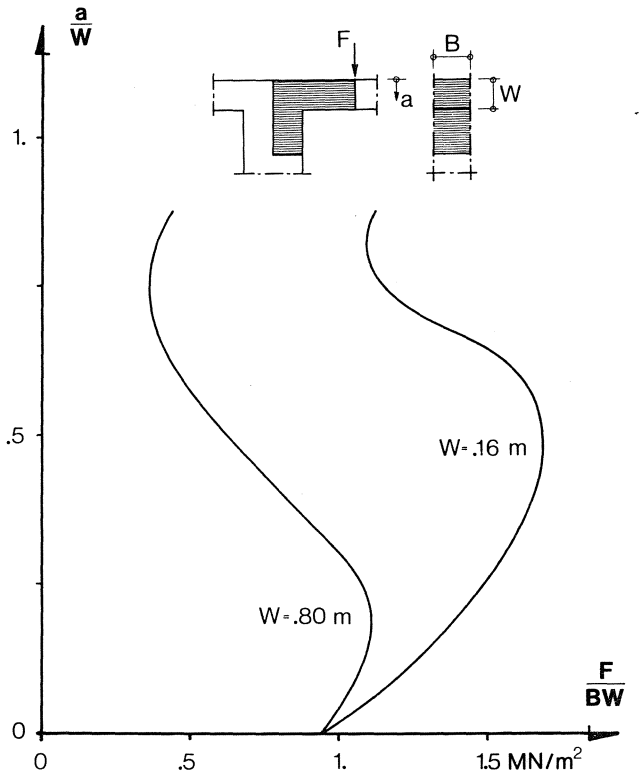

Fig 3. Shear stress for slab depths 0.16 m and 0.80 m.
a denotes the position of the fictitious crack tip.

The figure shows the relative location of the fictitious crack tip versus the maximum shear stress F/(B*W). If the fracture criterion of the structure is that fracture occurs when the crack becomes unstable, the carrying capacity of the 0.80 m slab relative to the 0.16 m slab is 1.10/1.60 = 0.65.

Note that F/(B*W) is not specified when a/W > 0.88, a position when the reinforcement has begun to play a dominant role (which is seen from the S-shaped curves in Fig 3). If this is to be possible, a finer element mesh must be used. If so, another fracture criterion may be formulated, e.g. when the lower part of the slab is broken in compression.

However, the reduction of the extrapolated elastic carrying capacity by a factor of 0.65 is most interesting and is, as a matter of fact, very close to similar laboratory experiments, Nylander et. al. [24].

Another, and probably better, way to represent the reinforcement is the same as that of "4.1.9 Multiphase materials". An example with an element mesh is shown in Fig 4.

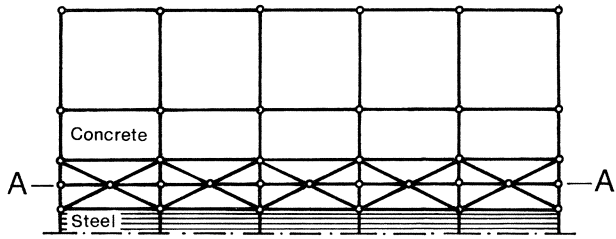

Fig 4. Interfacial representation between reinforcement and concrete.

The interface is represented by the lines A - A within the element band close to the steel elements. No analyses with this representation have yet been performed.

4.2 NUMERICAL RESULTS

4.2.1 Fracture toughness

One of the strength-determining properties of structural materials is the fracture energy G_c. The usual way to obtain G_c is by means of the fracture toughness K_{Ic}. The relation between G_c and K_{Ic} is in the case of plane stress (see 1.2.5),

$$G_c = \frac{K_{Ic}^2}{E} \qquad \ldots.(1)$$

where E is the Young´s modulus.

Values of K_{Ic} are experimentally found by means of an ordinary three-point bend test of a precracked specimen, see Srawley [36] . The manufactured crack length is a, the depth is W, the thickness is B and the length is S, together yielding a specimen such as that in Fig 1.

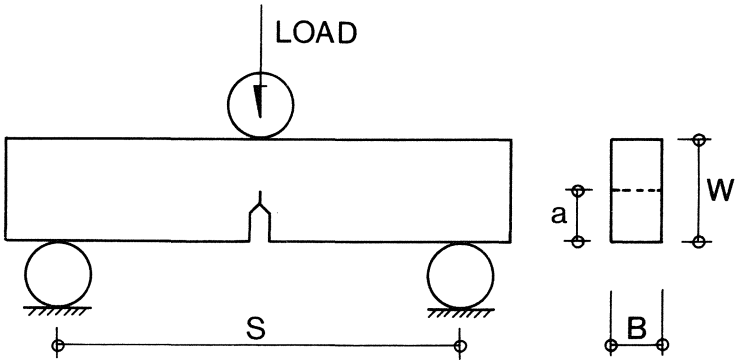

Fig 1. Essentials of bend specimen for K_{Ic}-test.

The stress intensity factor K_I can now be calculated by means of Eq (2) where M is the applied bending moment and F(a/W) a calibration function which defines K_I of the specific body under consideration, see 1.2.3,

$$K_I = \frac{6\,M}{BW^2}\sqrt{a}\,F\left(\frac{a}{W}\right) \qquad \ldots.(2)$$

where $F\left(\frac{a}{W}\right)$ is a polynom of the type:

$$F\left(\frac{a}{W}\right) = \Sigma \text{constant}_i \left(\frac{a}{W}\right)^i \qquad (i = 0,1,\ldots,4) \qquad \ldots.(3)$$

K_I increases with the load until it reaches a critical value, i.e. the fracture toughness K_{Ic}. If B = W/2, S = 4W, and P is the load at fracture, Eq (2) becomes,

$$K_{Ic} = \frac{12\ P\sqrt{a}}{W^2}\ F(\frac{a}{W}) \qquad ....(4)$$

where the value of F(a/W) is:

$$F(\frac{a}{W}) = 1.93 - 3.07(\frac{a}{W}) + 14.53(\frac{a}{W})^2 - 25.11(\frac{a}{W})^3 + 25.80(\frac{a}{W})^4 \qquad ....(5)$$

When using Eq (4), it is understood that the material is approximately linear elastic. If this assumption is to be valid, the dimensions of the specimen must fulfil certain demands, see 1.2.6.

For metals these demands are expressed by means of Eq (6),

$$\text{Dimension} > \alpha\left[\frac{K_{Ic}}{\sigma_y}\right]^2 \qquad ....(6)$$

where α is a factor > 1 and σ_y is the yielding stress of the metal.

Such demands, however, do not exist for concrete materials; why do they not ?

The fracture toughness, calculated from Eq (4), will never agree with the true value from Eq (1). To examine this difference between the apparent fracture toughness from Eq (4) and the true fracture toughness, a FEM analysis was carried out. The element mesh modelling the three-point bend specimen of Fig 1 is shown in Fig 2.

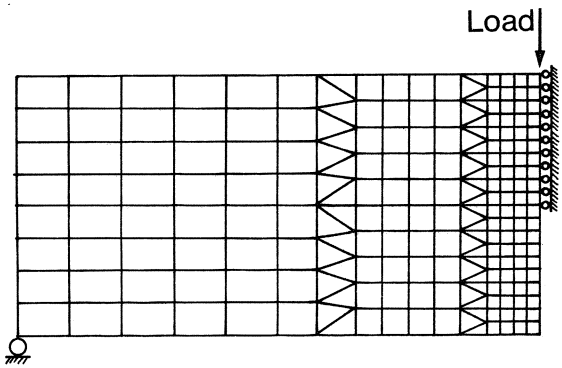

Fig 2. FEM mesh of the studied body.

The σ-ε and σ-w curves were approximated as straight lines. Better approximations of the curves would have given a more correct result, but this analysis was performed to indicate the necessity of considering the specimen dimensions also for concrete materials, not for an exact result.

Three different a/W ratios were examined; a/W = 0.1, a/W = 0.2 and a/W = = 0.3. The fracture toughness was obtained in plane stress which for concrete materials is a value as good as the plain strain value, see 1.2.5. The fracture criterion chosen was the major principle stress criterion, i.e. a crack starts developing when the stress reaches the uniaxial tensile strength f_t.

The results of the analyses are demonstrated in Fig 3.

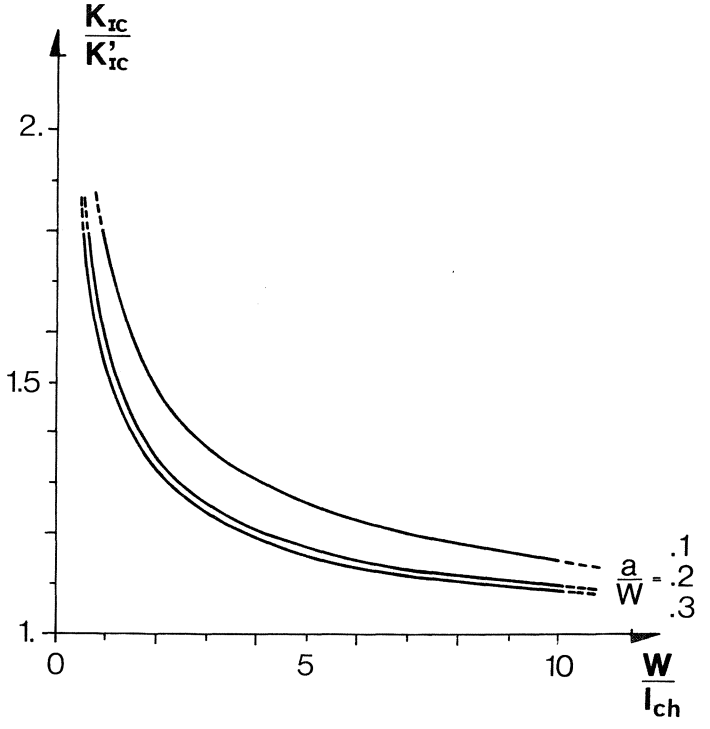

Fig 3. Fracture toughness over apparent fracture toughness versus specimen depth over the characteristic length. The figure is valid for apparent fracture toughness values calculated by means of a three-point bend test.

The fracture toughness K_{Ic} is calculated from Eq (1) and the apparent fracture toughness K_{Ic}^{i} from Eq (4). The characteristic length ℓ_{ch} is a material parameter:

$$\ell_{ch} = \left(\frac{K_{Ic}}{f_t}\right)^2 \qquad \ldots.(7)$$

This characteristic length is synonymous with the term of demand from Eq (6); the limiting stress for concrete materials is not a yield stress but the tensile strength f_t.

As seen in Fig 3 it is very reasonable to demand specific dimensions for concrete materials. The value W/ℓ_{ch} ought to exceed 10 if Eq (4) is to be considered faultless.

ℓ_{ch} for concrete is 0.2 - 0.3 m, for mortar 0.1 - 0.2 m, and for paste 0.005 - 0.010 m, see 5.2.6 Characteristic length. Many measured values of fracture toughness and fracture energies calculated by means of these values may thus differ a great deal from the real values because the specimen sizes are too small.

4.2.2 Bending strength

It is difficult to measure the tensile strength of concrete materials in a direct tension test. Several indirect methods have therefore been adopted, the most common being the bending test and the splitting test.

Values from these two tests upon the tensile strength ought to be dependent on the dimension of the actual specimen. This is because the fracture within the tests starts at a specific point and propagates from this point through the specimen.

One of the very first analysis by means of the FCM was an analysis of the dimensional dependency of bending test specimens upon the tensile strength. This analysis is reported in Hillerborg, Modéer, Petersson [17].

To elucidate these early results the structure in Fig 4.1.7(1) was analyzed.

The σ-w curve was varied within a wide range of appearances, all with the same area between the curve and the coordinate axes. The four analysed cases are shown in Fig 1.

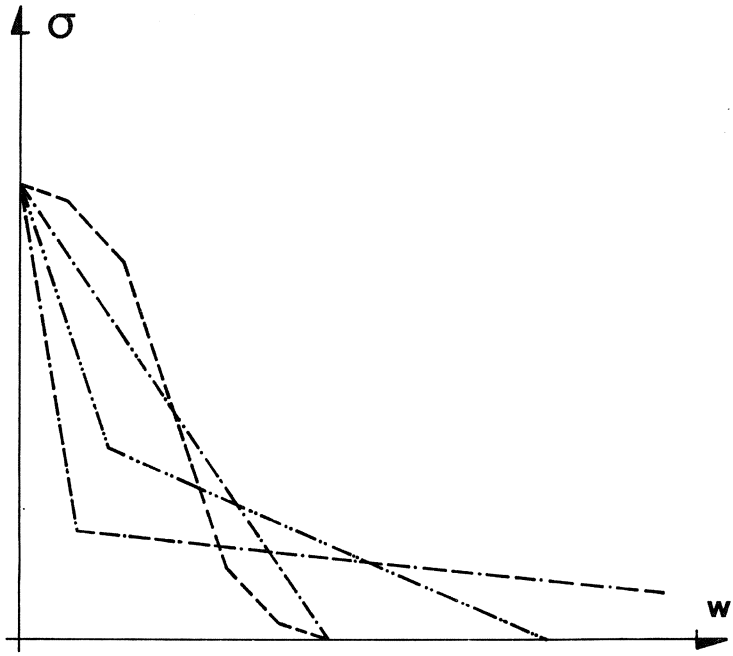

Fig 1. Different choises for the σ-w curve.

The results of the FEM analyses are shown in Fig 2. The continuous line is from the early analyses [17] , the other lines are from the different choises for the σ-w curve.

Under the heading "4.1.5 Choise of σ-w curve" it is concluded that the initial slope of the descending curve is very important to the final result. This is confirmed by the results shown in Fig 2.

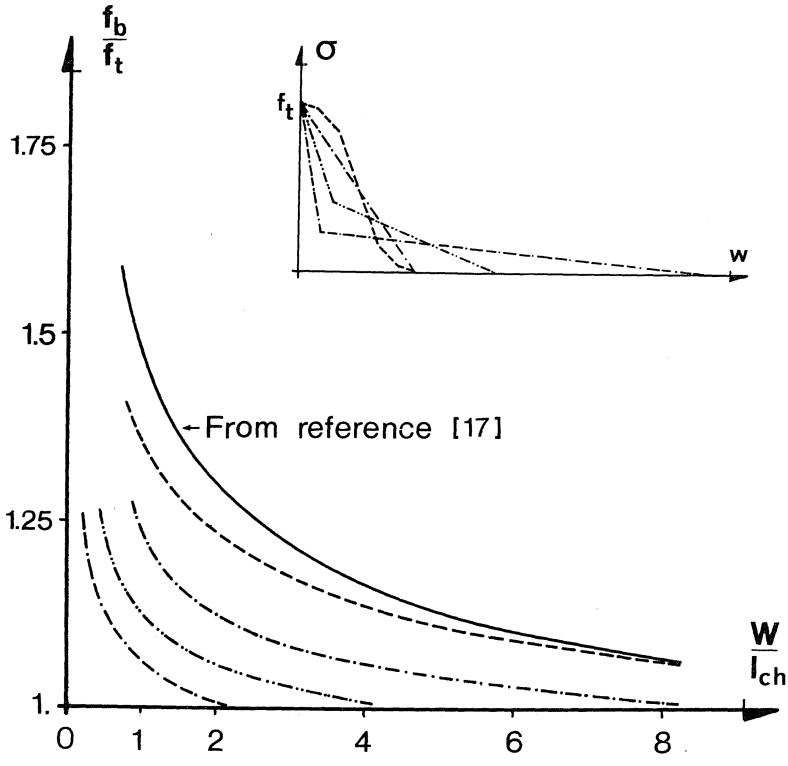

Fig 2. Bending strength over tensile strength versus beam depth over the characteristic length.

As seen, the early result differs from the later one with the same descending σ-w curve-approximation, i.e. the straight line. The differense is presumably due to an unsuitable element mesh in the early analyses.

In spite of the obvious uncertainty when choosing a suitable σ-w curve, it may be concluded that results from the bending test are strongly dependent upon the specimen dimensions.

4.2.3 Splitting strength

If a cylinder, cube or beam is loaded in compression along two opposite generators as indicated in Fig 1, the vertical plane between the line loads is subjected to a horizontal splitting tension.

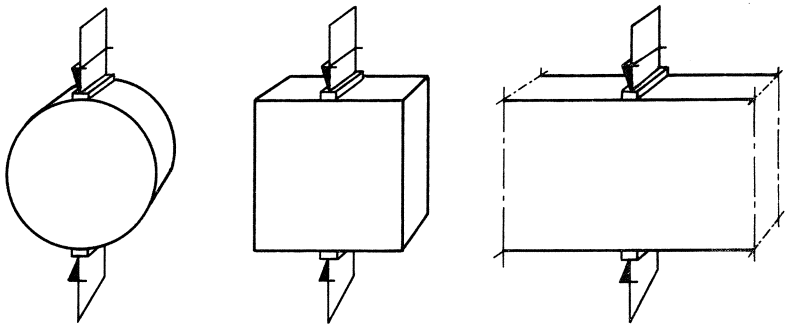

Fig 1. Specimen used in the splitting test.

Different states of elastic stress distributions are reached, dependent upon the shape of the specimen and the packing between the specimen and the loading platens. The horisontal tension for different geometries is shown in Fig 2. The figure originates from Schleeh [34].

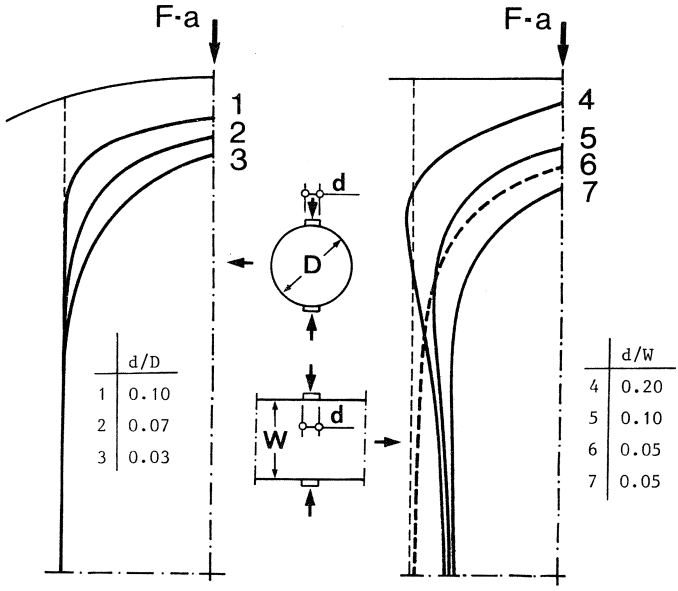

Fig 2. Stress distribution normal to the loading axis in the splitting test. Specimens 4, 5, and 6 are beams; specimen number 7 is a cube (According to Schleeh).

This figure indicates that the cylinder specimen is the less questionable, the value of the maximum stress being approximately:

$$\sigma \approx 0.64 \frac{P}{DL} \qquad \ldots.(1)$$

where P is the load at fracture, D the diameter of the cylinder and L the length of the generator which the load is subjected (which is the same as the length of the cylinder).

In addition to this horizontal elastic tensile stress there is a vertical elastic compressive stress. The distribution of these stresses for the cylinder and the beam is shown in Fig 3. The cube stresses may be estimated from the beam stresses; the figure originates from Schleeh [34].

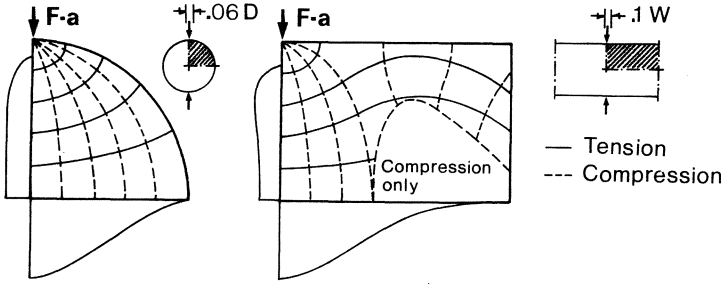

Fig 3. Stress distribution for a cylinder and a beam in the splitting test.

Again the state of stress of the cylinder is the less questionable.

Concrete materials have a remarkable two-dimensional failure envelope, see Fig 4.

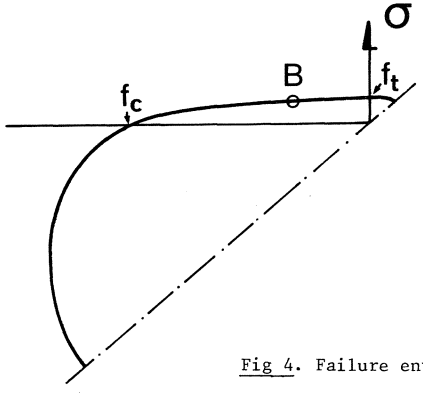

Fig 4. Failure envelope for concrete under plane stress.

As the compressive stress at the center of a cylinder specimen is about three times the tensile stress, the point B in Fig 4 may be the point of failure. This indicates that the tensile stress of fracture is approximately 0.8 f_t.

Thus, the splitting test seems to be somewhat controversial, even if the material is considered to be perfectly elastic. But, as we know, it is not.

Among all the papers regarding the splitting test upon concrete specimens, only very few deal with the assumption that the material is not pure elastic. About this matter, Mitchell [26] says: "Perhaps the biggest assumption in the theoretical development is that the elastic hypothesis holds true until failure". His words are so very right.

In order to elucidate some of these latter problems, a FEM analysis was carried out using the FCM. As there are so many questions about the test, the simplest specimen from the analytical point of view was chosen, i.e. the cube. The load strips were 1/10 of the cube side; the element mesh is shown in Fig 5.

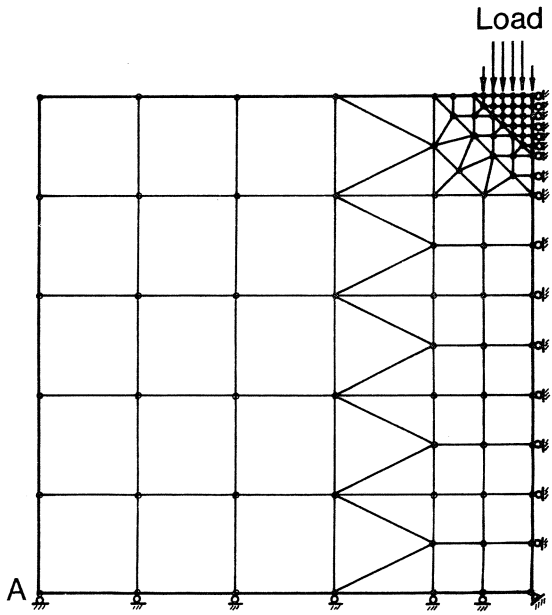

Fig 5. Element mesh for the studied case.

As a control of the element mesh, the elastic stress distribution was studied. The horizontal tensile stress along the vertical midsection of the cube is shown in Fig 6; the continous line represents the theoretical distribution and the points represent the FEM results.

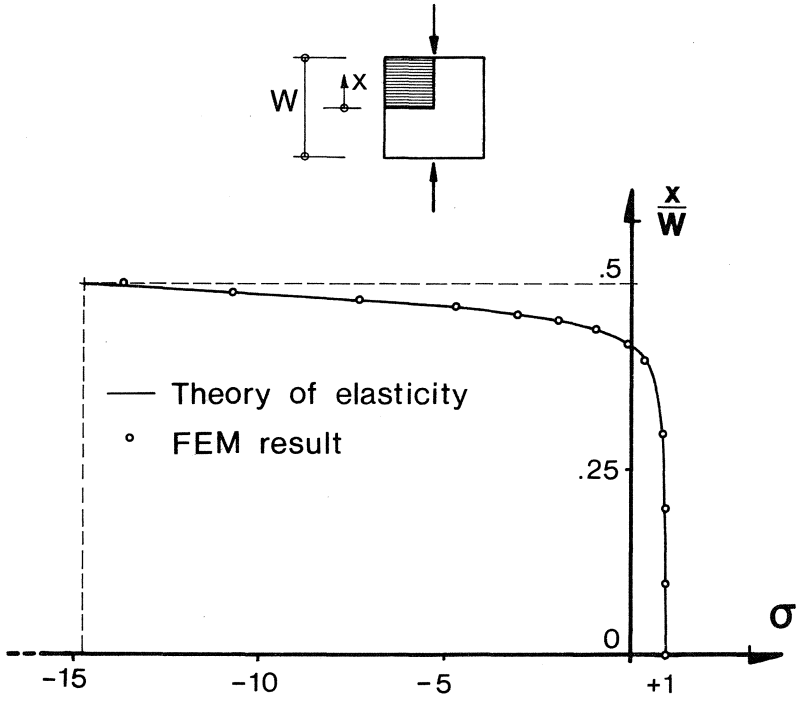

Fig 6. Control of the element mesh of Fig 5.

The fracture criterion chosen was the major principle stress criterion, i.e. a crack starts developing when the stress reaches the maximal tensile strength f_t. The σ-ε and σ-w curves were approximated as straight lines; the result of the analyses is shown in Fig 7.

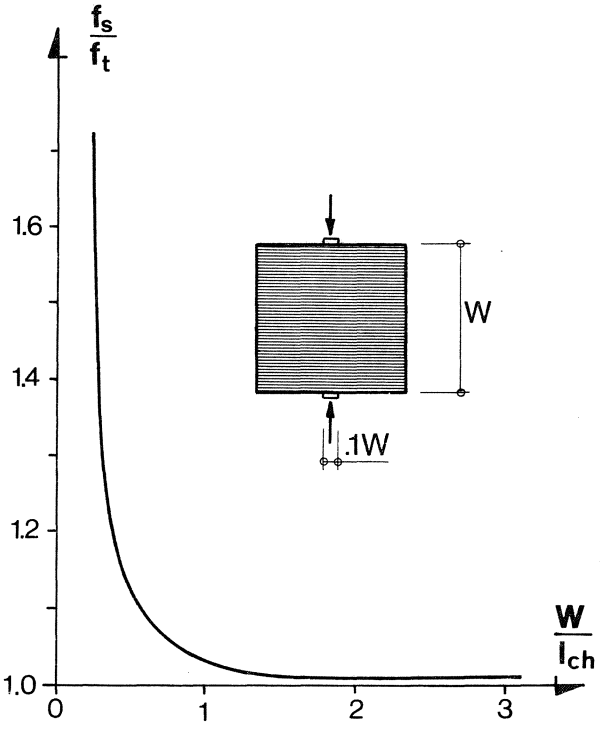

Fig 7. Splitting strength over tensile strength versus cube side over the characteristic length.

During the analyses just one fictitious crack, that along the vertical mid section, was considered. When $W/\ell_{ch} < 1$ this is not correct because the tensile stress at the point A in Fig 5 is now bigger than f_t. If this had been considered, a different result would have been obtained.

Fig 7 does not represent any exact result. But it indicates that the splitting test may be strongly dependent upon the specimen dimensions, especially when $W/\ell_{ch} < 1$. This ought to be considered when any standard method of testing by means of the splitting test is formulated.

5. TESTS

5.1 TEST METHODS

5.1.1 Fracture energy

By definition, see 1.2.5, may the strain energy release rate for half a crack be written,

$$-\frac{\partial Q}{\partial a} = G \qquad \ldots.(1)$$

where Q is the strain energy and a half the crack length as shown in Fig 1.2.1(2). G may thus be called the strain energy release rate per unit crack extension.

When $-\partial Q/\partial a = G_c$ the crack is metastable and its subsequent behaviour depends upon how $-\partial Q/\partial a$ changes when the crack increases in size. If it increases the crack will accelerate because the strain energy release is then bigger than that sufficient to create new surface areas. If it decreases the crack is stable because external work must be done to keep the crack moving.

This elastic stability criterion is better described as the rate of $-\partial Q/\partial a$, i.e. $-\partial^2 Q/\partial a^2$.

If $-\partial^2 Q/\partial a^2 > 0$	the crack is unstable	
If $-\partial^2 Q/\partial a^2 = 0$	the crack is metastable	....(3)
If $-\partial^2 Q/\partial a^2 < 0$	the crack is stable	

The metastable condition, Eq (3), is the critical one; by combining Eq:s (1), (3) and 1.2.5(2), a general elastic stability criterion may be expressed as,

$$-\frac{\partial^2 Q}{\partial a^2} = \frac{\partial}{\partial a}\left(-\frac{\partial Q}{\partial a}\right) = \frac{\partial}{\partial a}(G) = \frac{\partial}{\partial a}\left(\frac{K_I^2}{E}\right) = \frac{2K_I}{E}\,\frac{\partial}{\partial a}(K_I)$$

As $2K_I/E > 0$, the condition of the crack is determined from the term $\partial K_I/\partial a$. Eq (3) may thus be written

If $\partial K_I/\partial a > 0$	the crack is unstable	
If $\partial K_I/\partial a = 0$	the crack is metastable	....(4)
If $\partial K_I/\partial a < 0$	the crack is stable	

It is in this manner possible to formulate stability criteria for any crack figuration. First the stress intensity factor as a function of the crack length for a fixed displacement under the load must be found. Then the metastable condition of Eq (4) is found by setting $\partial K_I/\partial a = 0$

For the three-point bend specimen of Fig 4.2.1(1), these calculations are performed in Appendix F. The results are shown in Fig 1 below. The notation is the same as in Fig 4.2.1(1) except the symbol k which expresses the stiffness of the testing machine and E which is the ordinary Young´s modulus. The stiffness k is assumed to be constant, and the testing machine has of necessity a constant deformation velocity.

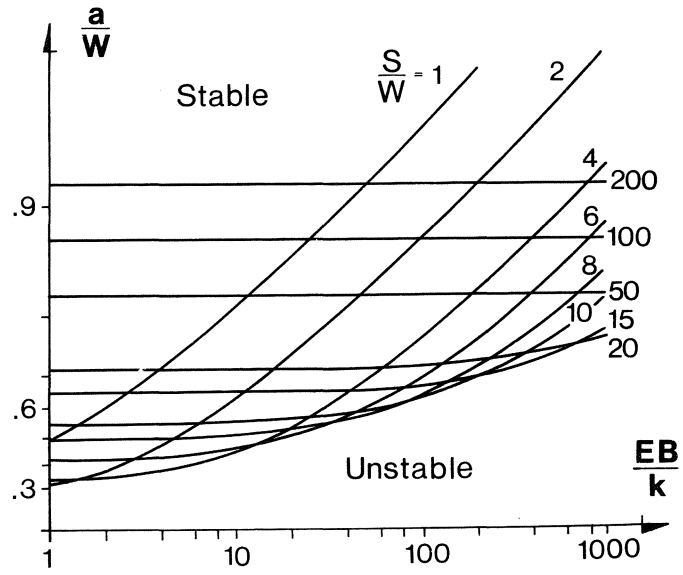

Fig 1. Metastable conditions for a notched specimen in three-point bending. Poissons ratio is assumed to be 0.2.

Each curve in Fig 1 represents the metastable condition, below each curve is the unstable region and above the stable region. The curves are valid for linear elastic materials; if W/ℓ_{ch} is small there is a divergence on the safe side, if W/ℓ_{ch} is big the agreement is almost perfect.

It is thus possible to get stable crack growth in concrete materials, which is a very useful finding. Since the loads at the beginning and at the end of such a stable three-point bend test are zero, the area under the force-displacement curve of the test-machine between these two conditions must equal the energy consumed in producing new fracture surfaces.

Assuming that the energy consumed in other non-elastic deformations is neglegible, G_c may be obtained by dividing the area under the force-displacement curve by the area over which the crack front passes. If the width of the pre-manufactured crack is of the same order as the particle phase of the actual composite, this assumption is fair and the G_c-value obtained may be regarded as a good value of the fracture energy.

A typical force-displacement curve of mortar is shown in Fig 2. The curve is considered to be stable if the test may be stopped at any point of the curve.

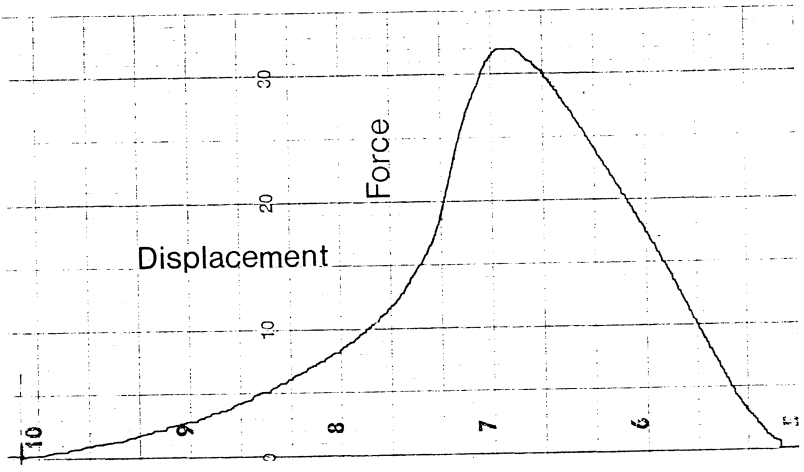

Fig 2. A typical force displacement curve from the testing machine for a mortar specimen broken in a stable manner.

The basic test method is shown in Fig 4.2.1(1). The specimen is laid on roller bearings to eliminate uniting horizontal forces. These rollers must be almost frictionless and may not cause any crushing at their contact with the specimen. The latter is also consistent for the applied force. The rollers may also permit some movement perpendicular to their axes because the concrete members are often not perfectly plane.

One way to eliminate some of these problems is to use loading equivalent to that shown in Fig 3. This way of doing the test is also much simpler to perform than that in Fig 4.2.1(1).

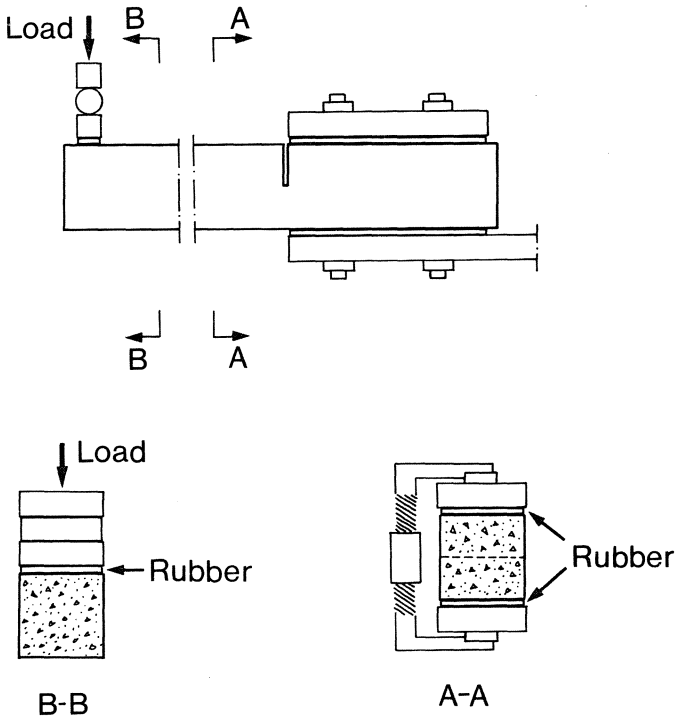

Fig 3. Cantilever beam for measurement of G_c.

Besides the external force there is gravititional force. This force accomplishes approximately the work,

$$M \delta/2 + m \delta \qquad \ldots.(5)$$

where M is the mass of the cantilever, m the mass of the loading point arrangement, and δ the deflection at the end of the cantilever. As m is often small, this contribution may be neglected.

The total energy requirement may be illustrated as shown in Fig 4.

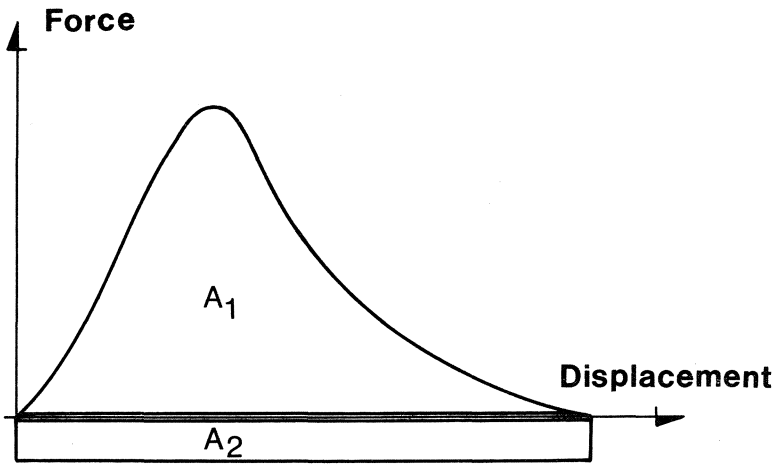

Fig 4. Total energy requirement.

A_1 is the area under the force-displacement curve of the testing-machine and A_2 the gravititional addition. The G_c-value is thus obtained as:

$$G_c = \frac{A_1 + A_2}{B(W-a)} \qquad \ldots.(6)$$

Observe that the area of the crack is not the real area of the fracture surface. It is instead a representative value for the actual material, which demands a number of tests and that the final G_c-value is calculated as an average.

If the gravititional effect is to be diminished, the simplest way may be to arrange the test as shown in Fig 5. This has not yet been tried but may be relevant when the specimen is big.

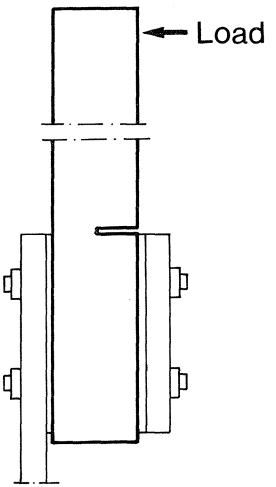

Fig 5. Arrangement for diminishing of the gravititional effekt upon the G_c-test.

5.1.2 Tensile strength

The tensile strength was primary obtained in direct tension tests by means of specimens as shown in Fig 1.

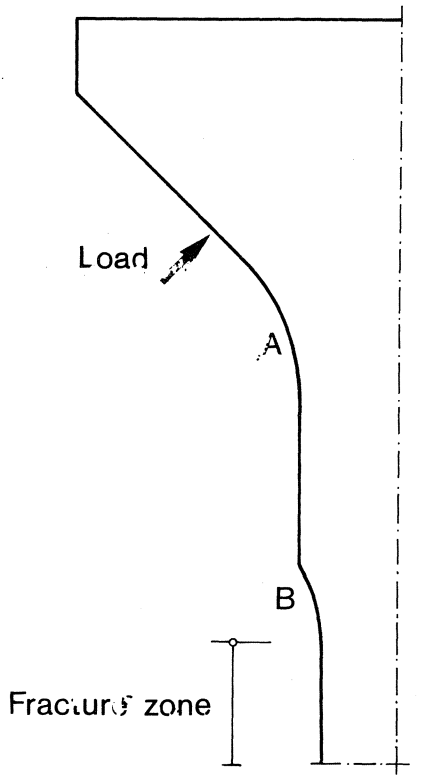

Fig 1. Specimen for direct tension test.

The specimen is designed from FEM analyses. The first curve inwards, at point A in Fig 1, produces a uniaxial tensile field. The second curve inwards, at point B in Fig 1, gives the location of the fracture to be within the tensile field. All specimens were broken within the fracture zone in Fig 1.

The specimens were gripped by means of steel yokes, as shown in Fig 2.

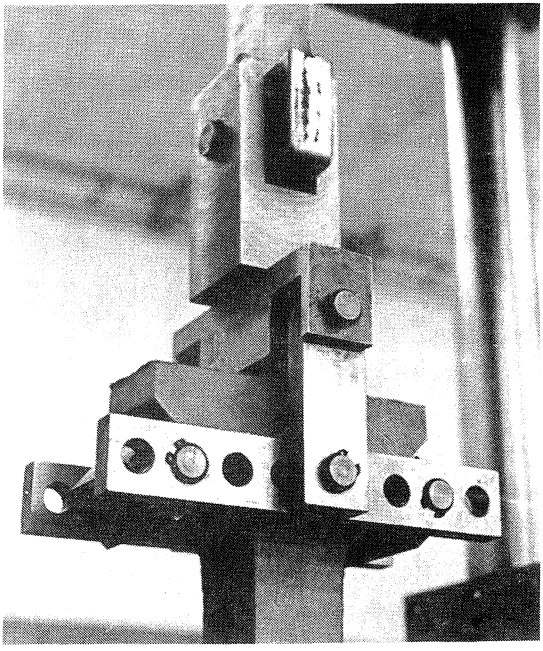

Fig 2. Gripping arrangement for direct tension test.

When the test was performed, the specimens were carefully mounted. The small eccentricity left was taken care of by the yokes; this was controlled by strain measurements within the fracture zone by means of inductive displacement transduction.

5.1.3 Splitting strength

When testing the splitting strength both cylinder and cube specimens were used, see 4.2.3. The cylinders were used for smaller specimens, i.e. when the diameter was $\leq$ 0.1 m, and the cubes for bigger specimens. This division was done for practical reasons; the cylinders were manufactured in moulds of different tubes, the cubes in moulds manufactured of plywood.

The width of the loading strips was 1/10 of the cylinder diameter or the cube side. The strips were manufactured of hardened fiberboards of the type "masonite".

The type of fracture for concrete and mortar was of the central failure type as described in 4.2.3. The type of fracture for paste was different, as there was a gouging out of the cylinders along with the central failure, Fig 1.

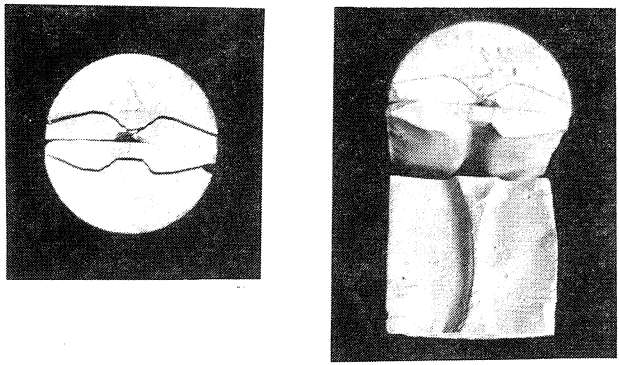

Fig 1. Gouging out of paste specimen.

These failures were along the photoelastic fringe lines of a point-loaded disk, Mitchell [26] , by which the isochromatic lines may be interpreted as loci of constant intensity of maximum shearing stress. This phenomenon may be explained by the Coulomb-mohr criterion of failure, see 1.3.1.

The Coulomb-Mohr diagram representing tension, compression and shear stress with failure envelope is shown in Fig 2.

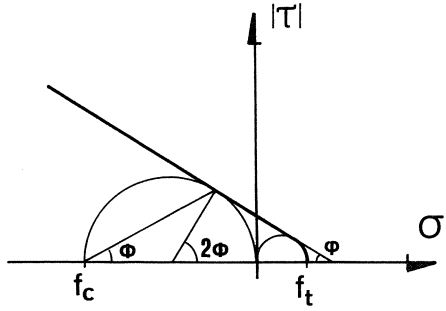

Fig 2. Coulomb-Mohr failure envelope.

As described in "1.3.2 Failure angle hypothesis" the slip angle is Φ,

$$\Phi = 45 - \varphi/2 \qquad \ldots.(1)$$

where φ is the angle of friction, see Fig 2.

The slope of the failure envelope has a physical significance. When the envelope becomes parallel with the σ_N-axis then $\Phi = 45°$ and the failure will be a maximum shear failure. The apex of the envelope is where pure cleavage failure takes place and $\Phi = 0°$, i.e. the rupture is in the direction normal to the maximum tensile stress. The transitional part, when $0° < \Phi < 45°$, is indicative of an ordinary obliquely inclined shear fracture.

The shear failure appearance of the splitting test for paste thus indicates a decreased slope of the failure envelope compared with that of concrete and mortar. This is somewhat contradictory to the results of Alexander [2], see Fig 4.1.9(5). This, furthermore, confirms the fact that the splitting test is dubious.

5.1.4 Modulus of elasticity

The modulus of elasticity, i.e. the Youngs modulus, in Hooke´s definition does not apply to concrete materials. To define a static modulus therefore seems problematic; is it to be defined at compression or tension, after one or ten loading-cycles, with fast or slow loading velocities, at a load of 1/4 or 1/2 of the load at fracture and so on ....? It is obvious that a static modulus of elasticity for concrete materials is not a real material constant.

The dynamic modulus of elasticity is, however, a real material constant (if the material is not fractured by shrinkage). It is an expression for a modulus without any load, i.e. for a material that is not fractured.

In the thesis a dividing up of the material behaviour into one σ-ε and one σ-w curve has been discussed. The σ-ε curve in this classification applies to an unfractured material. For that reason a dynamic modulus of elasticity is more logical than a sort of statical modulus in fracture mechanical analyses.

The method of measurement of the dynamic modulus of elasticity is found in the literature, e.g. Vinkeloe [41]. The method is also described in Appendix G.

5.2 TEST RESULTS

5.2.1 Test material

The concrete and mortar used was of the strain-line aggregate type discussed under the heading "2.3 Aggregate particles".

The aggregates were crushed rock materials of a type that is not reactive. The cement was standard Portland cement.

The water to cement ratio by weight of the concrete and the mortar was 0.5 and of the paste 0.35. This made the material easy to work.

All specimens were cured in water with an admixture of lime during the hardening process. The hardening time was seven days, after which half of the cement had hardened. The latter conclusion was drawn from measurements of the non-evaporable water content of the paste.

The test material was all the time prevented from drying in order to avoid shrinkage. This made the experiments rather splashy!

The notches of the precracked specimens for the G_c-measurements must be manufactured with some caution. The width of the notches must not be too big and the material in front of them must be representative of the actual material.

A notch may be manufactured by a saw-blade just before testing or by a non-adhesive film already at the casting time. Three different cases may be discerned as shown in Fig 1.

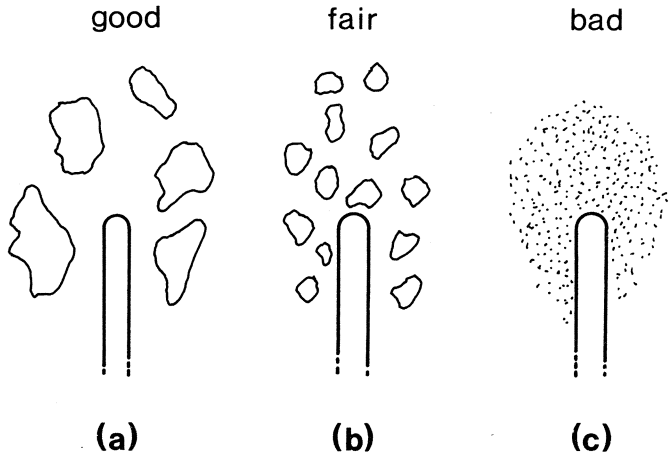

Fig 1. A notch compared with the particle phase in a two-phase material.

In Fig 1 a the notch width is smaller than the mean particle size and the mean free distance between the particles, in Fig 1 b it is approximately the same, and in Fig 1 c it is much bigger.

The sawed notch is superior to the film notch in one essential respect, the particle distribution in front of the notch tip is not disturbed. A number of tests thus guarantee an average behaviour.

For concrete and mortar a sawed notch according to Fig 1 a and b is conceivable, for paste the saw brings about a notch like that in Fig 1 c. In this latter case the notch tip is no representative crack tip, instead it is a type of beam and a stable crack growth is difficult to attain. A film notch must therefore be used.

The particle disturbance in the paste specimens is of course limited to a small area in front of the notch tip. Thus, if the material over which the crack front must pass is very big compared to this disturbed area, the measured fault is insignificant.

Notches in concrete and mortar specimens were manufactured with a 2 mm thick diamond saw-blade. The notches in paste specimens were manufactured with a 50 μm thick nonadhesive plastic film.

Another problem is the loading velocity. To choose proper loading velocities is an impossible balancing between dynamic loading and creep influence.

The guiding rules therefore were:

if failure occurs less than about ten seconds after the load is attained, the test is considered to be dynamic;

the creep during the first five minutes is considered to be a part of the statical deformation.

The loading velocities chosen are seen in Table 1.

Test	Loading velocity
Fracture energy	0.2
Splitting strength	0.5
Tensile strength	0.5

Table 1. Loading velocities. Units in mm/min.

5.2.2 Fracture energy

The specimen sizes were chosen by means of Fig 5.1.1(1) and tests, as shown in Table 1:

	S	B	W	a/W
Paste	0.440	0.010	0.050	0.6
Mortar	0.640	0.050	0.050	0.5
Concrete	0.8	0.100	0.100	0.5

Table 1. Specimen sizes. Units in meters.

The specimen dimensions and the machine stiffness 5000 MN/m indicate that only the paste specimen ought to be stable according to Fig 5.1.1(1). This is mentioned in "5.1.1 Fracture energy".

The tests on paste and mortar were carried out as shown in Fig 5.1.1(3); the concrete specimens were tested as shown in Fig 4.2.1(1). If the cantilever method is to be used on concrete, the arrangement must be done as shown in Fig 5.1.1(5). The reported G_c-values for concrete are therefore not quite correct; they are too high.

	Number of specimens	Median mean	Arithmetic mean	Standard deviation	95% confidence interval
Paste	7	9.3	9.0	1.5	1.4
Mortar	12	59.5	60.9	6.7	4.3
Concrete	11	108	114	25.6	17

Table 2. G_c-values. Units in N/m.

In the tables to come is "Number of specimens" denoted n, "Median mean" of a as $\tilde{a}$, "Arithmetic mean" of a as $\bar{a}$, "Standard deviation" as s, and "95% confidence interval" as 95% c.i.

Among the concrete specimens reported in the Table 1 was one with an apparently high G_c-value, 297 N/m. As this value is almost twice the value beneath, 153 N/m, this specimen was considered to be unrepresentative.

Typical force-displacement curves from the testing machine are shown in Fig 1. The figure shows mortar and paste curves. The curve for concrete is similar to the mortar curve.

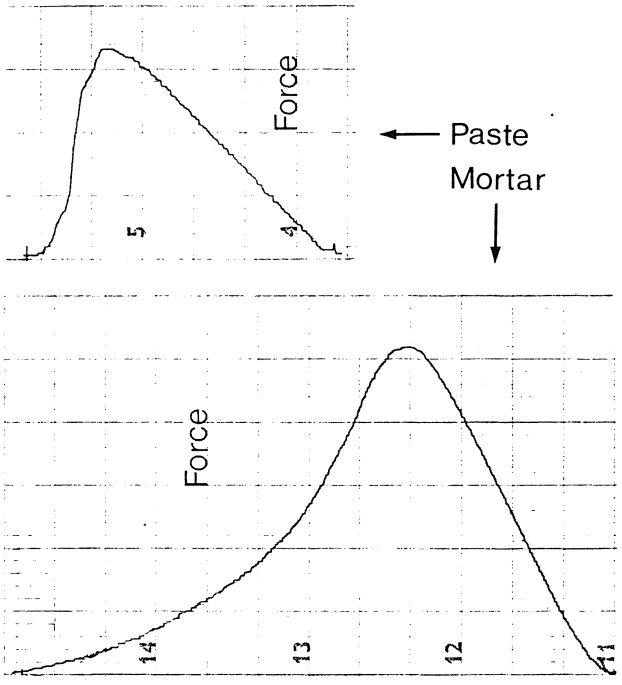

Fig 1. Typical force-displacement curves from the testing machine for paste and mortar.

The interface between the aggregates and the paste has properties of its own. These properties, of course, depend upon the surface texture of the aggregates. If the aggregate surface is smooth the bonds between paste and aggregate are chemical and if it is rough they are both chemical and mechanical.

G_c-values of the interface were obtained from specimens as shown in Fig 2.

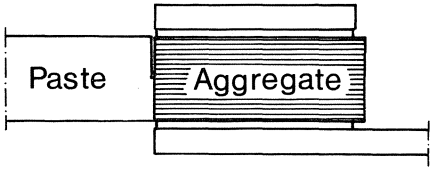

Fig 2. Cantilever method for paste-aggregate interface.

Both smooth and rough aggregate surfaces were examined. The smooth surface was obtained by a diamond saw-blade, the rough surface by breaking a precracked specimen (with a sawed notch) in three-point bending. The notch made when casting the stone and the paste together was then obtained by means of a very thin plastic film (~ 10 μm).

The stones used were natural rock (granite) of the non-reactive sort.

It was found that the bond to the smooth surface was so weak that an arrangement like that in Fig 5.1.1(5) presumably must be used. The specimens with rough surface stones, however, were easy to examine as shown in Fig 2. The paste-cantilever was $0.20 * 0.05 * 0.05$ m^3.

The results of the measurements are shown in Table 3. The number of specimens was from the beginning twelwe, but 50 per cent of them were lost in unstable crack propagation. This is natural as the strength is proportional to the roughness of the stone surface (which varied rather widely). The uncertainty is also expressed by the high confidence interval limits.

n	$\tilde{G}_c$	$\bar{G}_c$	s	95% c.i.
6	16.4	17.0	4.0	4.2

Table 3. G_c values for the interface between natural rough rock material and cement paste. Units in N/m.

The G_c-values of the interface between mortar and stone was tested in the same manner as the paste-stone interface, the results are evident from Table 4.

n	$\tilde{G}_c$	$\bar{G}_c$	s	95% c.i.
6	[illegible]	18.3	4.0	4.2

Table 4. G_c-values for the interface between natural rough rock material and mortar. Units in N/m.

The difference between these results and those of Table 3 is negligible. The variation in the W/c-ratio presumably does not have any significant influence; however, in a concrete the difference is most likely more pronounced. Around coarse aggregates the mortar is separated and air-pockets are formed, resulting in a smaller G_c-value between coarse aggregates and mortar than between fine aggregates and paste.

A characteristic force-displacement curve from the interface measurements is shown in Fig 3. The figure is characteristic for both aggregate-paste and aggregate-mortar.

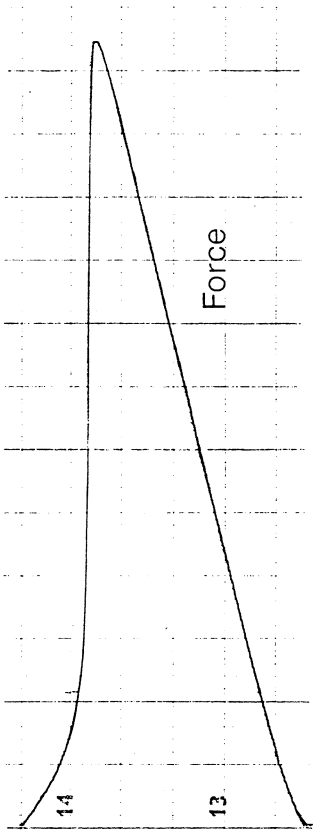

Fig 3. Typical force-displacement curve from the testing machine for interface tests.

The G_c-value of the interface, when the adhesive capacity is at its maximum, is thus almost twice that of the paste. This difference is amazing but not quite inexplicable.

The surface energy of the tobermorite gel is 0.5 N/m, Brunauer et al [9c], and of the calcium hydroxide 1 N/m, Idorn et al [20]. As most of the interface consists of calcium hydroxide, see 2.2, the relation found between G_c-paste and G_c-interface is not too strange. It also indicates that the formation of microcracks at the interface is comparable to that in the paste.

G_c-values are useful not only for calculation purposes but also as a characterizing material property. An example of the latter is demonstrated below.

For different purposes, often to improve the frost resistance, air-entraining agents are used to increase the capillary pore system, see 2.2. These agents do of course influence the properties of concrete; in order to elucidate their effect on G_c, mortar specimens with different amounts of agents were tested. The mortar was the same as that shown in Table 2; the different amounts of agents versus the resulting air contents of the mortar are shown in Fig 4.

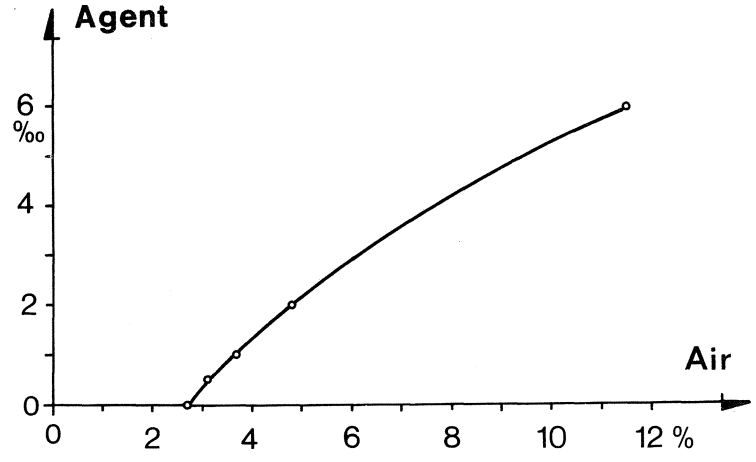

Fig 4. ‰ air-entraining agent of the cement weigth versus the resulting air content. The curve is valid for the mortar from Table 2.

The results of these tests are somewhat astonishing, they are presented in Table 5 and demonstrated in Fig 5.

‰ agent	% air	n	$\tilde{G}_c$	$\bar{G}_c$	s	95% c.i.
0	2.7	12	59.5	60.9	6.7	4.3
0.5	3.1	6	36.3	36.7	2.3	2.4
1	3.7	6	32.7	33.1	1.8	1.9
2	4.8	6	31.4	31.4	2.3	2.4
6	11.5	6	25.1	26.4	2.6	2.7

Table 5. Fracture energies for mortar specimens with different amounts of air content. Units in N/m.

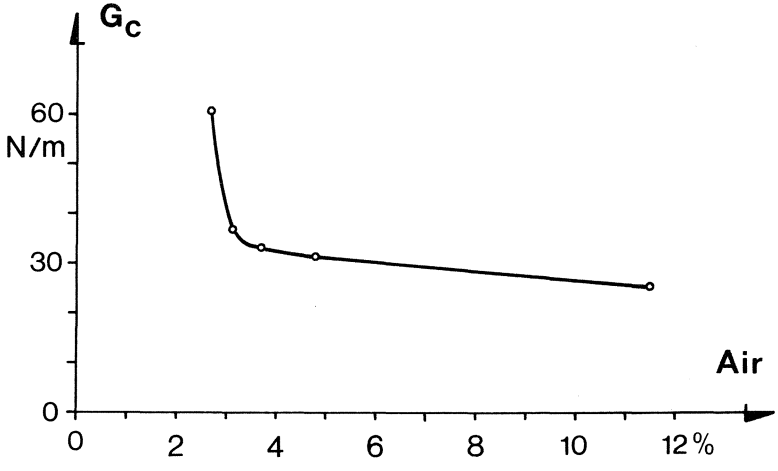

Fig 5. Fracture energy versus air content for a mortar as that of Table 2.

The effect of the air-entraining agents on the G_c-value is significant and unequivocal. One reason for this may be that the tensides of the agent very soon have an influence on the most critical part, the interface, of the mortar structure. If so, the concrete with its coarce aggregates and enclosed bad interfaces might not be so sensitive. This conclusion of course also applies for plain paste.

5.2.3 Tensile strength

The specimen dimensions chosen are shown in Fig 1. Observe the somewhat different specimen for the interface strength test.

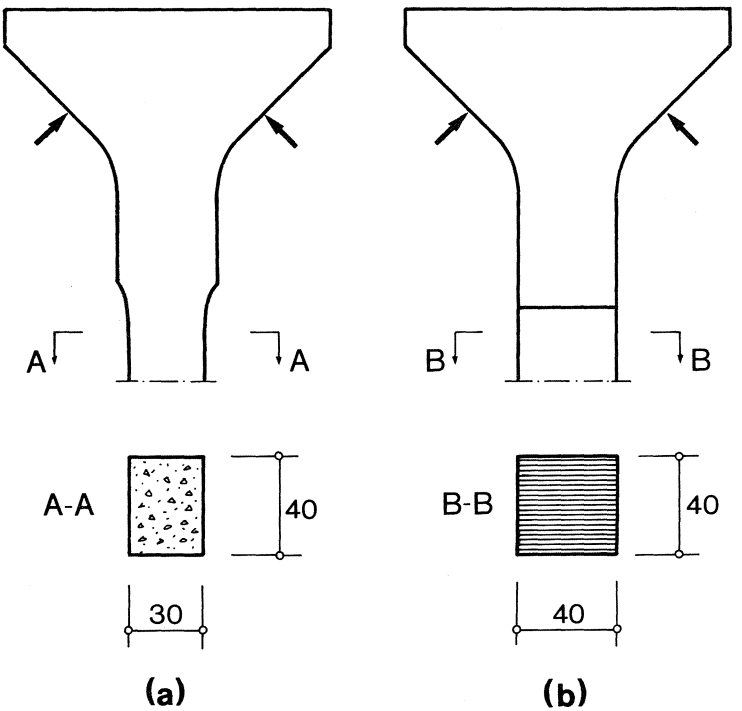

Fig 1. Direct tensile test specimens. Dimensions in mm.

The waist was not necessary for the interface specimens as the interface was weaker than the paste though the surface of the stones was rough (manufactured by three-point bending, like the G_C-specimens of section 5.2.2). The results of the tests are evident from Table 1.

	n	$\tilde{f}_t$	$\bar{f}_t$	s	95% c.i.
Paste	8	5.5	5.5	1.0	0.9
Mortar	7	3.5	3.4	0.4	0.3
Interface paste-agg.	12	1.4	1.5	0.3	0.2

Table 1. Direct tensile strengths. Units in MN/m^2.

No concrete specimens were tested because of the limitations of the testing equipment, i.e. its dimensions.

5.2.4 Splitting strength

The splitting strength was obtained for mortar and paste specimens of different dimensions. When using cylinders the diameter-length ratio were always 1. The results from the tests on mortar are shown in Table 1. The splitting strength is calculated by means of Eq 4.2.3(1).

Diameter (m)	n	$\tilde{f}_s$	$\bar{f}_s$	s	95% c.i.
0.025	12	2.9	3.0	0.2	0.1
0.050	12	3.0	3.0	0.1	0.1
Cube side (m)					
0.200	6	3.4	3.4	0.4	0.4
0.250	6	3.3	3.3	0.2	0.2

Table 1. Splitting strength for paste (cylinder) and mortar (cube). Units in MN/m^2.

As Eq 4.2.3(1) is valid for cylindrical specimens, the values for the cubes ought to be corrected. A correction factor of 0.75 may be found from Fig 4.2.3(2), yielding,

Diameter (m)	n	$\tilde{f}_s$	$\bar{f}_s$	s	95% c.i.
0.200	6	2.6	2.6	0.4	0.4
0.250	6	2.5	2.5	0.4	0.2

Table 2. Corrected splitting strength values for the cube specimens of table 1. Units in MN/m^2.

The characteristic length of mortar is about 0.15 m, see section 5.2.6. Two different groups, each with two different specimen dimensions, may thus, according to Fig 4.2.3(7), be found in Table 1 and 2. Either the specimen is so big that the dimensional dependency is not pronounced or it is so small that the apparent strength in tension is considerably increased. In the latter case the specimen may fall in compression as the compressive stress at the loading points is very high, see Fig 4.2.3(3). This is also indicated by the uniform failure stress for the small specimens.

As mentioned, paste specimens of different dimensions were also examined. The results of these tests are evident from Table 3 and Fig 1.

Diameter (m)	n	$\tilde{f}_s$	$\bar{f}_s$	s	95% c.i.
0.010	8	5.8	5.4	1.2	1.0
0.015	12	4.8	4.9	0.8	0.5
0.020	12	4.2	4.3	1.0	0.6
0.025	12	4.0	4.2	0.8	0.5
0.050	12	4.2	4.1	0.5	0.3

Table 3. Splitting strength for paste specimens of different dimensions. Units in MN/m^2.

A significant dimensional dependency as predicted by the FCM is evident. However, by reason of the different failure modes (see section 5.1.3), no direct comparison between these experimental results and Fig 4.2.3(7) ought to be made.

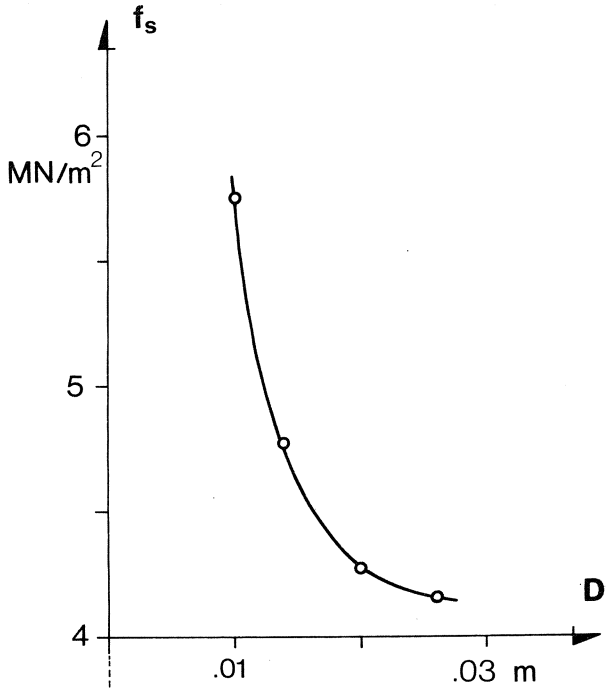

Fig 1. Splitting strength versus paste cylinder dimensions.

As discussed under section 5.2.2, an air-entraining agent should decrease the G_c-value of paste to some extent. If that hypothesis is correct the characteristic length ought to be shorter, see section 5.2.6, and the dimensional dependency, for the same dimension, less pronounced.

To examine these ideas, two different amounts of air-entraining agents were used upon the same specimens as those in Table 3. The results of these tests are shown in Table 4 and Fig 2.

Diameter	Air %	Agent ‰	n	$\tilde{f}_s$	$\bar{f}_s$	s	95% c.i.
0.010	2	2	12	6.2	6.0	1.1	0.7
0.025	2	2	11	4.9	5.0	0.4	0.3
0.050	2	2	12	4.2	4.3	0.4	0.3
0.010	4.7	6	10	4.5	4.4	0.7	0.5
0.025	4.7	6	12	4.3	4.3	0.3	0.2
0.050	4.7	6	12	4.2	4.1	0.5	0.3

Table 4. Splitting strength versus paste cylinder dimensions and different air contents. Units in m and MN/m^2.

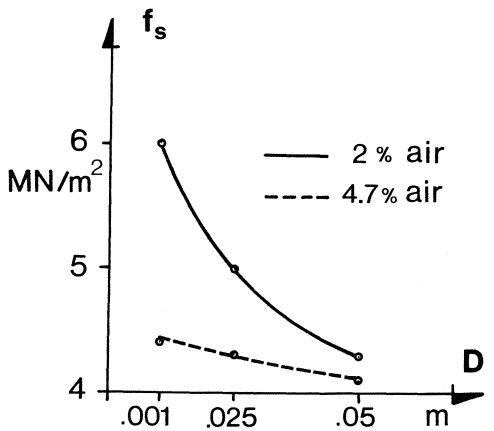

Fig 2. Splitting strength versus cylinder diameter and air content for paste specimens.

Thus the results confirm the discussion under section 5.2.2 regarding the air-entraining agent.

5.2.5 Modulus of elasticity

The dynamic modulus of elasticity was obtained for paste and mortar; the results are shown in Table 1.

	n	$\bar{E}$	$\tilde{E}$	s	95% c.i.
Paste	11	21700	21600	780	520
Mortar	12	29300	29200	800	510

Table 1. Dynamic moduluses of concrete materials. Units in MN/m^2.

According to Herman et al [15] these values are about 6% higher than the initial tangent static modulus in compression.

5.2.6 Characteristic length

From the experimentally found values on G_c, f_t and E, it is possible to calculate the characteristic length ℓ_{ch} which according to Eq 4.2.1(7) is,

$$\ell_{ch} = \left(\frac{K_{Ic}}{f_t}\right)^2 \qquad \ldots.(1)$$

Together with Eq 1.2.5(3) this yields,

$$\ell_{ch} = \frac{G_c E}{f_t^2} \qquad \ldots.(2)$$

which is used in Table 1.

	G_c	E	f_t	ℓ_{ch}
Paste	9.3	21600	5.5	0.007
Mortar	59.5	29200	3.5	0.142
Concrete	108	29200	3.5	0.257

Table 1. Properties of concrete materials. Units in N/m, MN/m^2, and m.

The paste and mortar of this Table are described under "5.2.1 Test material". The characteristic length of concrete is somewhat uncertain even if the magnitude presumably is correct. Its G_c-value is based on a slightly incorrect measurement, see under 5.2.2, and its E-value and f_t-value are assumed to be the same as those of the mortar.

The ℓ_{ch}-values of Table 1 may be used on the FCM results regarding fracture toughness, bending strength and splitting strength. These results are summarized in Fig 1:

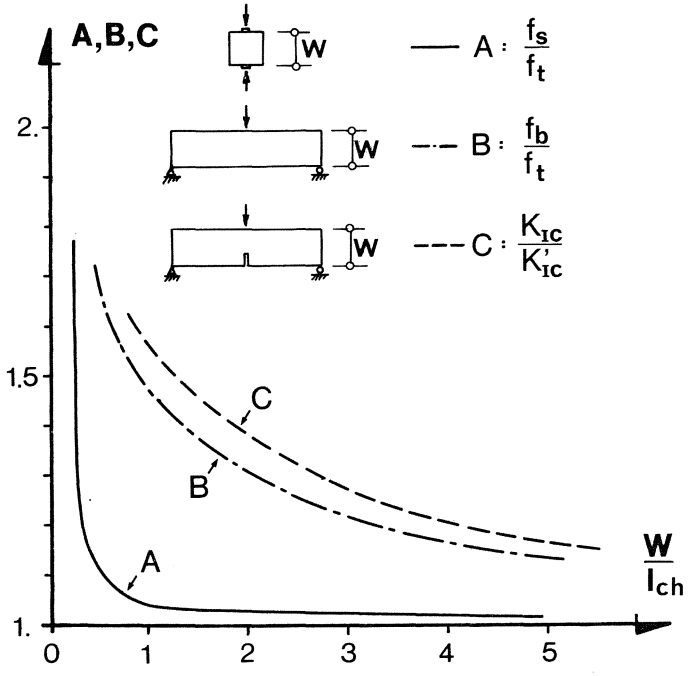

Fig 1. Dimensional dependency for different properties of concrete materials.

The specimen dimensions should thus be much bigger than the usual laboratory sizes when testing the fracture toughness and the tensile strength. If they are too small the measured values are just values of the apparent fracture toughness, the bending strength, and the splitting strength (even this is dubious) for the actual material and specimen dimension, nothing else.

Appendix A

The binominal series of the expression $(a + b)^n$ is,

$$(a+b)^n = a^n + n\,a^{n-1}b + \frac{n(n-1)}{2!}\,a^{n-2}b^2 + \frac{n(n-1)(n-2)}{3!}\,a^{n-3}b^3 + \ldots + \binom{n}{k}a^{n-k}b^k + \ldots$$

This expression can, if $b^2 < a^2$, be written:

$$(a+b)^n = a^n\left[1 + n\left(\frac{b}{a}\right) + \frac{n(n-1)}{2!}\left(\frac{b}{a}\right)^2 + \frac{n(n-1)(n-2)}{3!}\left(\frac{b}{a}\right)^3 + \ldots + \binom{n}{k}\left(\frac{b}{a}\right)^k + \ldots\right]$$

The equation that is to be expanded in this way is:

$$\sigma_2 = \frac{\sigma}{\sqrt{1 - \left(\frac{a}{a+r}\right)^2}}$$

With $n = -\frac{1}{2}$, $a = 1$, and $b = -\left(\frac{a}{a+r}\right)^2$ we get:

$$\sigma_2 = \sigma\left[1 + \frac{1}{2}\left(\frac{a}{a+r}\right)^2 + \frac{3}{8}\left(\frac{a}{a+r}\right)^4 + \frac{5}{16}\left(\frac{a}{a+r}\right)^6 + \ldots + \binom{1/2}{k}\left(\frac{a}{a+r}\right)^{2k} + \ldots\right]$$

Appendix B

According to Fagerlund [13], the free mean distance between aggregate particles or air pores in concrete systems can be found by means of Eq (1).

$$v_p\left(1+\tfrac{1}{2}\bar{d}\alpha_p+\tfrac{1}{2}\bar{d}^2\alpha_p\frac{[u]_1}{[u]_2}+\tfrac{1}{6}\bar{d}^3\alpha_p\frac{[u]_0}{[u]_2}\right)=1 \qquad \ldots.(1)$$

where $\bar{d}$ = free mean distance between the particles
v_p = volume fraction of the particles
α_p = specific surface of the particle
$[u]_k$ = k:th statistical moment of the diameter distribution of the particle

If s_p is the total surface of the particles, the specific surface α_p is defined by Eq (2):

$$\alpha_p = \frac{s_p}{v_p} \qquad \ldots.(2)$$

If F(u) is the relative frequency distribution function of the particles, u_0 the minimum, and u_1 the maximum particle diameter, the k:th statistical moment $[u]_k$ is defined by Eq (3):

$$[u]_k = \int_{u_0}^{u_1} u^k F(u)\, du \qquad \ldots.(3)$$

If we now have a rectangular size distribution, i.e. if F(u) = constant, and if $u_0 \ll u_1$, Eq (1) becomes:

$$v_p\left[1+4\frac{\bar{d}}{u_1}+6\left(\frac{\bar{d}}{u_1}\right)^2+4\left(\frac{\bar{d}}{u_1}\right)^3\right]=1 \qquad \ldots.(4)$$

Concrete

The particle phase of concrete is aggregates bigger than 4 mm in diameter. A model gradation curve with a rectangular size distribution is shown in Fig. 2.3(2). The maximum particle size is 32 mm, a usual value for concrete, and the mean particle size is 12 mm.

An ordinary aggregate content is 70 per cent by volume. Of this amount about 40 per cent by volume is coarse aggregates, yielding a $\bar{d}$-value by means of Eq (1) as:

$$0.4\left[1+4\frac{\bar{d}}{32}+6\left(\frac{\bar{d}}{32}\right)^2+4\left(\frac{d}{32}\right)^3\right]=1$$

$\Rightarrow \bar{d} = 8.3$ mm.

Mortar

The particle phase of mortar is sand equal to or less than 4 mm in diameter. A model gradation curve with a rectangular size distribution is shown in Fig. 2.3(2). The minimum particle size is 0.125 mm, which is an acceptable value of u_0, and the mean particle size is 0.70 mm.

An ordinary aggregate content of mortar is 50 per cent by volume, yielding a $\bar{d}$-value by mean of Eq 1 as,

$$0.5 \left[1 + 4\frac{\bar{d}}{4} + 6\left(\frac{\bar{d}}{4}\right)^2 + 4\left(\frac{\bar{d}}{4}\right)^3 \right] = 1$$

$$\Rightarrow \bar{d} = 0.76 \text{ mm}.$$

Cement paste

The particle phase of cement paste is the unhydrated cement particles. The free mean distance between these particles varies therefore in a significiant way as the hydration increases; $\bar{d}$ attains its smallest value at the fictitious moment when the hydration is about to begin.

A gradation curve for ordinary Portland cement is shown in Fig 1 [11]. The mean particle size is 0.022 mm.

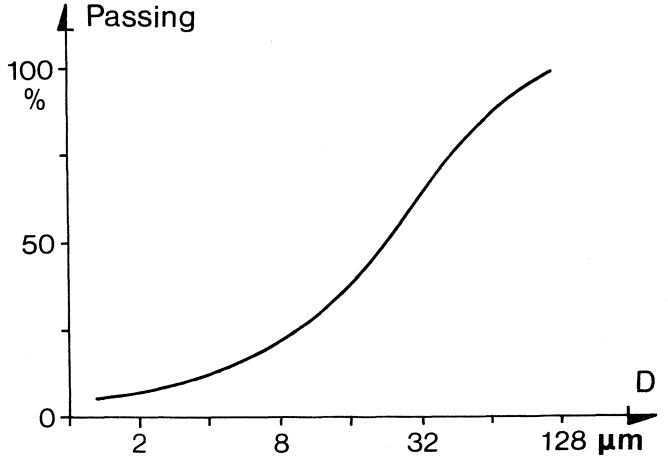

Fig 1. Mean particle size of ordinary Portland cement.

A model gradation curve with a rectangular size distribution, on the basis of Fig 1, has a maximum particle size of 0.128 mm. The cement content of an unhydrated paste with vct = 0.5 is 0.64 per cent by volume, yielding a $\bar{d}$-value by means of Eq 1 as:

$$0.64 \left[1 + 4\frac{\bar{d}}{0.128} + 6\left(\frac{\bar{d}}{0.128}\right)^2 + 4\left(\frac{\bar{d}}{0.128}\right)^3 \right] = 1$$

$$\Rightarrow \underline{\bar{d} = 0.015 \text{ mm}.}$$

This $\bar{d}$-value, however, is fictitious because as soon as the cement particles are mixed with water, an amorphous layer of calcium silicate hydrates is established at the surface of the particles. Then the hydration continues in two directions; into the particle, which results in an increase of the amorphous calcium silicate hydrate layer; and out from the particle when the calcium silicate hydrate ions diffuse through the amorphous layer and crystallize at the surface as tobermorite.

First, this crystallization is located between closely situated cement particles. This tobermorite gets a high density and forms a framework of crystallized stable gel.

When the hydration continues, the vacant space in this framework is filled up, partly or completely, by a low density tobermorite. This low density gel is metastable as every reduction of the distance between the crystals increase its stability.

Finally, this framework hypothesis, Ishai [21], indicates that $\bar{d}$ may vary between 0.015 and 0.037 mm, if the particles are stabilized at their original location.

Summary

The mean diameter of the coarse aggregates is 12 mm and the $\bar{d}$-value between them is 8.3 mm.

The mean diameter of the fine aggregates is 0.70 mm and the $\bar{d}$-value 0.76 mm.

The maximum mean diameter of the cement particles is 0.022 mm and the minimum $\bar{d}$-value 0.015 mm. When the hydration is almost complete, $\bar{d}$ is 0.037 mm. These values are hypothetical only.

Appendix C

According to Broberg [9a], in the case of a linear elastic solid (the brittle case) the fracture criterion $J = J_c$ is almost exactly identical with the Griffith criterion $G = G_c$. It is therefore possible to use the path-independent Rice-intergral J [31], see Eq 1, when calculating G_c-values for quasi-brittle solids such as concrete.

$$J = \int_{\Gamma} (W\, dy - \vec{T} \frac{\partial \vec{u}}{\partial x}\, ds) \qquad \ldots.(1)$$

Here, Γ is a curve which surrounds the crack tip in a counter clockwise direction, W is the strain energy, $\vec{T}$ is the traction vector on Γ according to an outward unit vector n normal to the curve, $\vec{u}$ is the displacement vector, and s the arc length of Γ. The direction of the x-axis is parallel to the crack-plane.

In concrete materials we have a case like that shown in Fig 1.

When using Eq 1 in this case, note that it is path-independent, i.e. it applies for any contour Γ surrounding the crack tip and not passing through the microcracked zone.

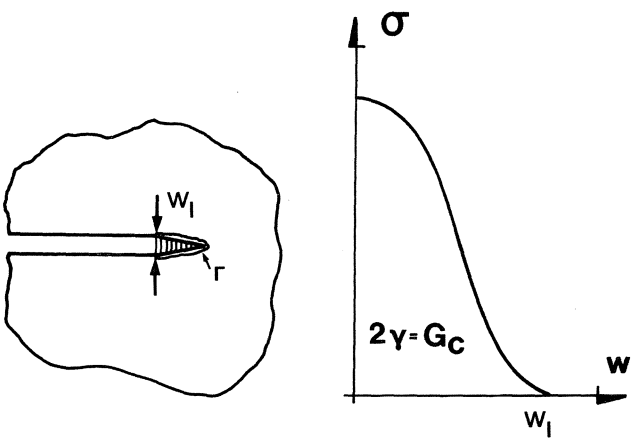

Fig 1. Essentials when calculating J_c.

A convenient choise of Γ is shown in Fig 1. Since dy = 0 for this choise of Γ , we get:

$$G_c = -\int_\Gamma T_i \frac{\partial u_i}{\partial x}\, ds = -\int_\Gamma \sigma(w)\, \frac{\partial w}{\partial x}\, dx = \int_{-w_{\ell/2}}^{0} \sigma(w)\, dw + \int_0^{w_{\ell/2}} \sigma(w)\, dw$$

$$\Rightarrow G_c = \int_0^{w_\ell} \sigma(w)\, dw$$

Appendix D

For a mode I crack, the basic equation of the force method is:

$$[w] = [w]_e + [w]_i$$

This equation can be written:

$$\begin{aligned} w_1 &= k_1 Q - k_{11}F_1 - k_{12}F_2 - \ldots - k_{1n}F_n \\ w_2 &= k_2 Q - k_{21}F_1 - k_{22}F_2 - \ldots - k_{2n}F_n \\ &\vdots \\ w_n &= k_n Q - k_{n1}F_1 - k_{n2}F_2 - \ldots - k_{nn}F_n \end{aligned} \qquad \ldots.(1)$$

where w_j = fictitious crack width at node j

k_j = flexibility at node j for external forces

Q = external force

k_{ij} = flexibility at node i for force at node j

F_j = force at node j

and the nodes i and j are located within the fictitious crack.

Condition 1 (see 4.1.2), if the σ-w curve is approximated as a straight line, can be written

$$\sigma_j = \sigma_F \left(1 - \frac{w_j}{w_\ell}\right)$$

of which the notation is shown in Fig 1.

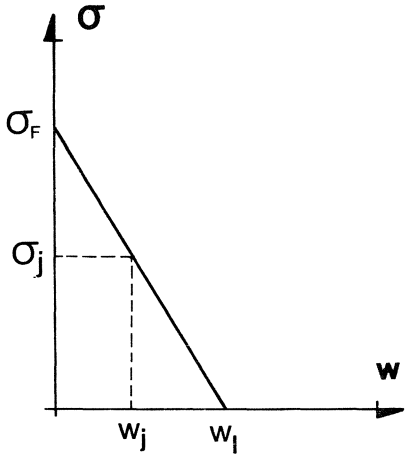

Fig 1. Approximation of the σ-w curve.

Instead of the stress σ_j, the force F_j may be used, yielding:

$$F_j = Q_F \left(1 - \frac{w_j}{w_\ell}\right) \qquad \ldots.(2)$$

Condition 2 (see 4.1.2) can be written:

$$\sigma_F = CQ - C_1F_1 - C_2F_2 - \ldots.- C_nF_n \qquad \ldots.(3)$$

where C = proportional factor for external force
C_j = proportional factor for force at node j

and the other notations as before.

The simple example of Fig 2 may elucidate the method (the example was prepared by the author in 1975).

Beam depth = .6 m

Beam width = .6 m

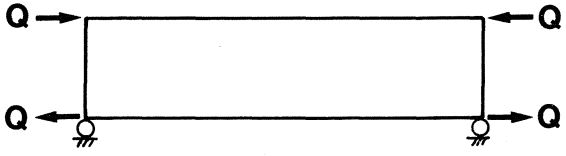

Fig 2. Beam under bending moment.

The analyses were performed by means of the FCM, the material properties of the beam being

$$f_t = 1 \text{ MN/m}^2$$
$$E = 30\,000 \text{ MN/m}^2$$
$$\nu = 0.2$$
$$G_c = 5 \text{ N/m}$$

If the σ-w curve is approximated as shown in Fig 1, w_ℓ is found as follows:

$$w_\ell = \frac{2G_c}{f_t} = 10 * 10^{-6} \text{ m}$$

If there are 13 nodes within the width, all at the same distance from each other, the fracture force Q_F may be found as follows:

$$Q_F = f_t * (\text{beam depth}) * (\text{beam width}) / (13-1)$$

$$\Rightarrow Q_F = 0.03 \text{ MN}$$

Crack length 0 m

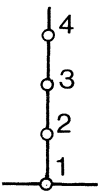

Fig 3. Node figuration for crack length 0 m.

$$Q = 0.011 \Rightarrow \sigma_1 = 0.21 \quad \text{(by means of FEM)}$$

$$\because Q_F^o = 0.011/0.21 = \underline{0.052 \text{ MN}}$$

Crack length 0.05 m

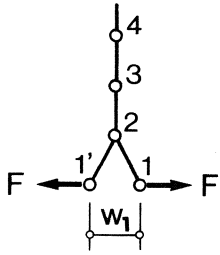

Fig 4. Node figuration for crack length 0.05 m.

Equation (1), (2) and (3) yield:

$$\begin{cases} w_1 = k_1 Q - k_{11} F_1 \\ F_1 = Q_F (1 - w_1/w_\ell)/2 \\ \sigma_F = CQ - C_1 F_1 \end{cases}$$

$Q = 0.011 \Rightarrow w_1 = 1.42$ and $\sigma_2 = 0.26$ (by means of FEM)

$\Rightarrow k_1 = 1.42/0.011 = 129$ and $C = 0.26/0.011 = 23.6$

$F_1 = 0.01 \Rightarrow w_1 = 4.96$ and $\sigma_1 = 0.36$ (by means of FEM)

$\because k_{11} = 4.96/0.01 = 496$ and $C_1 = 0.36/0.01 = 36.0$

Thus

$$\begin{cases} w_1 = 129Q - 496\ F_1 \\ F_1 = 0.03(1-w_1/10)/2 \\ 1 = 23.6\ Q - 36.0\ F_1 \end{cases} \Rightarrow \begin{cases} w_1 = 1.69\ 10^{-6} & \text{m} \\ F_1 = 0.012 & \text{MN} \\ Q = 0.060 & \text{MN} \end{cases}$$

Q_F^o has thus increased by

$$\left[\frac{0.060}{0.052} - 1\right] 100 = \underline{15 \text{ per cent}}$$

Crack length 0.10 m

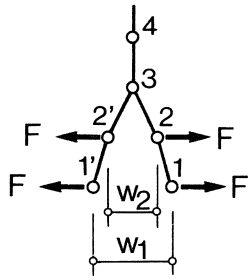

Fig 5. Node figuration for crack length 0.10 m.

Equations (1), (2) and (3) yield

$$\begin{cases} w_1 = k_1 Q - k_{11} F_1 - k_{12} F_2 \\ w_2 = k_2 Q - k_{21} F_1 - k_{22} F_2 \\ F_1 = Q_F (1 - w_1/w_\ell)/2 \\ F_2 = Q_F (1 - w_2/w_\ell) \\ \sigma_F = CQ - C_1 F_1 - C_2 F_2 \end{cases}$$

$$Q = 0.01 \Rightarrow \begin{cases} w_1 = 2.92 \\ w_2 = 1.99 \\ \sigma_3 = 0.33 \end{cases} \Rightarrow \begin{cases} k_1 = 2.92/0.011 = 265 \\ k_2 = 1.99/0.011 = 199 \\ C = 0.33/0.011 = 30.0 \end{cases}$$

$$F_1 = 0.01 \Rightarrow \begin{cases} w_1 = 6.60 \\ w_2 = 2.18 \\ \sigma_1 = 0.30 \end{cases} \Rightarrow \begin{cases} k_{11} = 6.6/0.01 = 660 \\ k_{21} = 2.18/0.01 = 218 \\ C_1 = 0.30/0.01 = 30.0 \end{cases}$$

$$F_2 = 0.01 \Rightarrow \begin{cases} w_1 = 2.18 \\ w_2 = 2.88 \\ \sigma_2 = 0.26 \end{cases} \Rightarrow \begin{cases} k_{22} = 2.88/0.01 = 288 \\ k_{12} = 2.18/0.01 = 218 \\ C_2 = 0.26/0.01 = 26.0 \end{cases}$$

Thus

$$\begin{cases} w_1 = 265\ Q - 660\ F_1 - 218\ F_2 \\ w_2 = 181\ Q - 218\ F_1 - 288\ F_2 \\ F_1 = 0.03(1 - w_1/10)/2 \\ F_2 = 0.03(1 - w_2/10) \\ 1 = 30\ Q - 30\ F_1 - 26\ F_2 \end{cases}$$

This system of equations may also be written

$$\begin{cases} 1\,w_1 + 0\,w_2 + 660\,F_1 + 218\,F_1 - 265\,Q = 0 \\ 0\,w_1 + 1\,w_2 + 218\,F_1 + 288\,F_2 - 181\,Q = 0 \\ 0.0015\,w_1 + 0\,w_2 + F_1 + 0\,F_2 + 0\,Q = 0.015 \\ 0\,w_1 + 0.003\,w_2 + 0\,F_1 + 1\,F_2 + 0\,Q = 0.03 \\ 0\,w_1 + 0\,w_2 - 30\,F_1 - 26\,F_2 + 30\,Q = 1 \end{cases}$$

or, as matrices

$$\begin{bmatrix} 1 & 0 & 660 & 218 & -265 \\ 0 & 1 & 218 & 288 & -181 \\ 0.0015 & 0 & 1 & 0 & 0 \\ 0 & 0.003 & 0 & 1 & 0 \\ 0 & 0 & -30 & -26 & 30 \end{bmatrix} * \begin{bmatrix} w_1 \\ w_2 \\ F_1 \\ F_2 \\ Q \end{bmatrix} = \begin{bmatrix} 0 \\ 0 \\ 0.015 \\ 0.03 \\ 1 \end{bmatrix} \quad \ldots.(4)$$

If A*B = C, then B = A^{-1}*C. Thus

$$\begin{cases} w_1 = 7.75\ 10^{-6} & \text{m} \\ w_2 = 2.41\ 10^{-6} & \text{m} \\ F_1 = 0.003 & \text{MN} \\ F_2 = 0.020 & \text{MN} \\ Q = 0.055 & \text{MN} \end{cases}$$

Q_F^o has thus increased by

$$15 + \left(\frac{0.055}{0.052} - 1\right) * 100 = \underline{21 \text{ per cent}}$$

By identifying the coefficients of Eq (4), we get

$$\begin{bmatrix} 1 & 0 & k_{11} & k_{12} & -k_1 \\ 0 & 1 & k_{21} & k_{22} & -k_2 \\ \frac{Q_F}{2w_\ell} & 0 & 1 & 0 & 0 \\ 0 & \frac{Q_F}{w_\ell} & 0 & 1 & 0 \\ 0 & 0 & -C_1 & -C_2 & C \end{bmatrix} * \begin{bmatrix} w_1 \\ w_2 \\ F_1 \\ F_2 \\ Q \end{bmatrix} = \begin{bmatrix} 0 \\ 0 \\ \frac{Q_F}{2} \\ Q_F \\ \sigma_F \end{bmatrix}$$

which can easily be enlarged for longer cracks. It is also easy to change material properties and specimen dimensions.

Appendix E

A simple example may elucidate the element method. (The example shows the method only.) Consider the case in Fig 1.

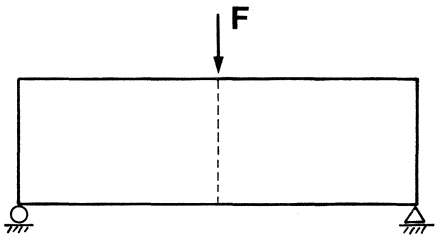

Fig 1. Studied loadcase.

Suppose that f_t = 3.0 MN/m^2 and G_c = 50 N/m

Crack length 0 m

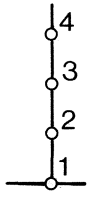

Fig 2. Node figuration for crack length 0 m.

$$F = 1 \Rightarrow \sigma_1 = 0.05$$

where σ_1 is the maximum principal stress at the node 1.

This yields

$$F_0 = 3/0.05 = \underline{60 \text{ MN}}$$

This load yields σ_2 = 2.9 MN/m^2, σ_3 = 2.8 MN/m^2, and so on, all stresses approximately perpendicular to the supposed crack path.

Crack length 0.001 m

When F = 60 MN the stress at node 1 reaches the maximal tensile strength f_t. An FCM element must be introduced at this node.

The new node, called 1', is placed very close to 1, e.g. at a distance of 10^{-6} m. In this way the stiffness of the original structure is hardly disturbed. We get

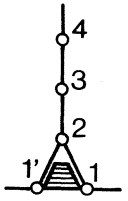

Fig 3. Node figuration for crack length 0.001 m.

The modulus M of the FCM element is found in a similar way as an ordinary Young's modulus.

$$M = -\frac{\ell\, f_t}{w_\ell} \qquad \ldots.(1)$$

where ℓ is the length of the FCM element and f_t and w_ℓ as before.

As $f_t = 3$ MN/m^2 and $G_c = 60\ 10^{-6}$ MN/m, we get w_ℓ as follows (if the σ-w curve is approximated as a straight line between f_t and w_ℓ):

$$w_\ell = \frac{2\, G_c}{f_t} = \frac{2\ 60\ 10^{-6}}{3} = 40\ 10^{-6}\ \text{m}$$

From Eq (1) M is now found as follows:

$$M = -\frac{10^{-6}\ 3}{40\ 10^{-6}} = -\ 0.075\ \text{MN/m}^2$$

The area of the FCM element is the beam width * half the distance to node 2. It is often convenient to choose the beam width as 1; the FCM element areas are then equal to the distances between the nodes.

A FEM analysis of this new structure is performed with F = 1 MN which yields $\sigma_2 = 0.01$ and $\sigma_3 = 0.007$ MN/m^2. The stress in the FCM element is - 0.001 MN/m^2

As F_0 = 60 MN gave σ_2 = 2.9 MN/m^2 we get

F_1 = (3.0-2.9)/0.01 = 10 MN/m^2 ⇒ F = F_0 + F_1 = 60 + 10 = 70 MN

This load yields σ_2 = 2.9 + 10 0.01 = 3.0 MN/m^2, σ_3 = 2.8 + 10 0.007 = = 2.87 MN/m^2 and the stress in the FCM element = 3.0 + 10 (-0.001) = = 2.99 MN/m^2

Crack length 0.002 m

When F = 70 MN the stress at node 2 reaches the strength f_t. An FCM element is introduced at the node.

The new node 2' is placed at a distance of 10^{-6}m from 2. We get

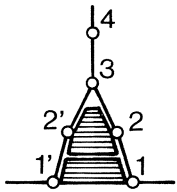

Fig 4. Node figuration for crack length 0.002 m.

The M-value is the same, - 0.075 MN/m^2, but the area is twice that of the first FCM element.

A FEM analysis of this new structure is performed with F = 1 MN which yields σ_3= 0.04 MN/m^2 and the stress in the FCM elements as - 0.009 in the first and - 0.003 MN/m^2, in the second.

As F_0 + F_1 = 70 MN gave σ_3 = 2.87 MN/m^2 we get

F_2 = (3.00-2.87)/0.04 = 3.25 MN ⇒ F_0 + F_2 + F_3 = 70 + 3.25 = 73.25 MN

This load yields σ_3 = 2.87 + 3.25 0.04 = 3.00 MN/m^2 and the stress in the FCM elements are 2.99 + 3.25 (-0.009) = 2.96 and 3.0 + 3.25 (-0.003) = = 2.99 MN/m^2.

The analysis is then carried out in the same manner. When an FCM element stress reaches zero again, the element is removed, the structure is finally cracked.

These routines are carried out on a computer. However, when the crack path is unknown or when the material is multiphased, these automatic routines tend to be complicated and stepwise analyses as shown in the example are therefore more easy to grasp.

Appendix F

The elastic stability criterion below originates in the main from Bergquist [6] .

Consider a specimen such as in Fig 4.2.1(1).

The stress intensity factor K_I for this body is of the same type as Eq 1.2.3(4) and may be found in any modern engineering handbook.

$$K_I = \sigma\sqrt{\pi a}\ F(a/W) = \frac{FS}{4}\frac{6}{BW^2}\sqrt{\pi a}\ F(a/W) \qquad ....(1)$$

The calibration function F may be obtained in several ways; normally it is written in the form,

$$F(a/W) = \Sigma c_i (a/W)^i \quad (i = 0,1,...,4) \qquad ....(2)$$

where c is a constant.

The deflection δ_a under the point load is, according to Broberg [9b] ,

$$\delta_a = \delta_0 + B\int_0^a \frac{\partial G(F,a')}{\partial F}\,da' \qquad ....(3)$$

where δ_0 is the deflection when no crack is present and G, as usual, is the strain energy release rate.

According to engineering handbooks δ_0 is,

$$\delta_0 = \frac{F\ S^3}{4\ E\ B\ W^3}\left[1 + 3(1+\nu)\frac{W^2}{S^2}\right] \qquad ....(4)$$

where E = Young´s modulus
ν = Poisson´ratio

For plane strain conditions G is equal to, (compare Eq 1.2.5(2)),

$$G = \frac{K_I^2\ (1-\nu^2)}{E} \qquad ....(5)$$

If now Eq (1) is combined with Eq (5),

$$G = \frac{9}{4}\frac{F^2S^2}{B^2W^4}\pi a\ F^2(a/W)*\frac{(1-\nu^2)}{E} \qquad ....(6)$$

The second half of the right side of Eq (3), the deflection contribution due to the crack, combined with Eq (6), yields:

$$\frac{9\pi}{2} \frac{F\ S^2(1-\nu^2)}{E\ B\ W^2} \int_0^a \frac{a'}{W^2} F^2(a'/W)\ da' \qquad ....(7)$$

If this integral is written as

$$H(a/W) = \int_0^{a/W} x\ F^2(x)\ dx \qquad ....(8)$$

Eq (3), combined with Eq:s (4) and (7), is equal to,

$$\delta_a = \frac{1}{4} \frac{F\ S^2}{E\ B\ W^2} \left\{ \frac{S}{W} \left[1 + 3(1+\nu) \frac{W^2}{S^2} \right] + 18\pi(1-\nu^2)\ H(a/W) \right\}$$

If S/W = I and a/W = J, the equation above becomes,

$$\delta_a = \frac{F}{EB} \frac{I^2}{4} \left\{ I \left[1 + 3(1+\nu)/I^2 \right] + 18\pi(1-\nu^2)\ H(J) \right\}$$

or written in a short way,

$$\delta_a = \frac{F}{E\ B}\ f(I, J) \qquad ....(9)$$

This equation yields,

$$F = \frac{\delta_a\ E\ B}{f(I,J)} \qquad ....(10)$$

Eq (10) together with Eq (1) now yields:

$$K_I = \frac{3\sqrt{\pi}}{2} \frac{\delta_a\ E}{\sqrt{S}} \sqrt{I^3}\ \sqrt{J}\ \frac{F\ (J)}{f(I,J)} \qquad ....(11)$$

In an ordinary testing machine the load is applied to the beam by means of a spring of the stiffness k, Fig 1.

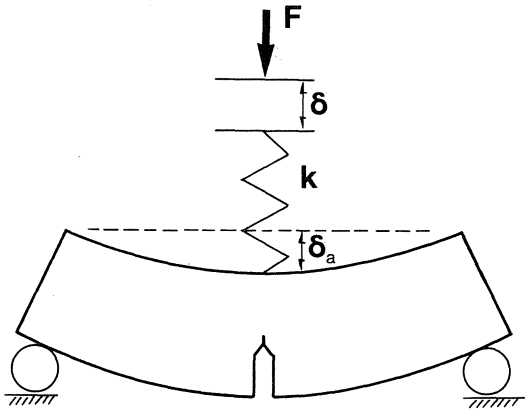

Fig 1. Spring loaded three point bend specimen.

The compression δ of the spring is by definition:

$$\delta - \delta_a = \frac{F}{k} \qquad \ldots.(12)$$

Eq (10) together with Eq (12) yields:

$$\delta_a = \frac{\delta}{1 + \frac{E\ B}{f(I,J)\,k}} \qquad \ldots.(13)$$

Together with Eq (11) this yields,

$$K_I = \frac{3\sqrt{\pi}}{2} \frac{\delta}{1 + \frac{E\ B}{f(I,J)\,k}} \frac{E}{\sqrt{S}} \sqrt{I^3}\sqrt{J}\,\frac{F(J)}{f(I,J)} \qquad \ldots.(14)$$

If now the non-dimensional quantity $K_{I\delta}$

$$K_{I\delta} = \frac{K_I \sqrt{S}}{E\ \delta} \qquad \ldots.(15)$$

is introduced, we get,

$$K_{I\delta} = \frac{3\sqrt{\pi}}{2} \frac{\sqrt{I^3}\sqrt{J}\ F(J)}{f(I,J) + \frac{E\ B}{k}} \qquad \ldots.(16)$$

The function T(J) is now introduced,

$$T(J) = \sqrt{J}\ F(J) \qquad \ldots.(17)$$

Eq:s (9) and (17) together with Eq (16) yield,

$$K_{I\delta} = \frac{3\sqrt{\pi}}{2} \frac{T(J)}{\frac{\sqrt{I}^3}{4}\left[1+3(1+\nu)/I^2\right] + \frac{18\pi}{4}\sqrt{I}\,(1-\nu^2)\,H(J) + \frac{E\,B}{k\sqrt{I^3}}} \qquad \ldots.(18)$$

The denominator of this expression may be written as:

$$\frac{1}{4}\,18\pi\,\sqrt{I}\,(1-\nu^2)\left[\frac{I}{18\pi(1-\nu^2)} + \frac{3(1+\nu)}{18\pi(1-\nu^2)}\,\frac{1}{I} + H(J) + \frac{4}{18\pi(1-\nu^2)}\,\frac{1}{I^2}\frac{E\,B}{k}\right] \qquad \ldots.(19)$$

If now

$$C_1 = \frac{3\sqrt{\pi}}{2}\,\frac{4}{18\pi\,\sqrt{I}\,(1-\nu^2)} \qquad \ldots.(20)$$

and

$$C = \frac{I}{18\pi(1-\nu^2)} + \frac{3(1+\nu)}{18\pi(1-\nu^2)}\,\frac{1}{I} + \frac{4}{18\pi(1-\nu^2)}\,\frac{1}{I^2}\frac{E\,B}{k} \qquad \ldots.(21)$$

the equation (18) becomes,

$$K_{I\delta} = C_1\,\frac{T(J)}{H(J) + C} \qquad \ldots.(22)$$

The limit between unstable and stable crack extension is now found from:

$$\frac{\partial K_{I\delta}}{\partial(J)} = 0 \qquad \ldots.(23)$$

which yields,

$$C = \frac{T(J)}{T'(J)}\,H'(J) - H(J) \qquad \ldots.(24)$$

The C-value of Eq (21) as a function of E B/k when I and ν are fixed becomes a straight line with stability and unstability on each side of the line. Instead of the C-value, the relation J = J(C) [a/W=a/W (C)] from Eq (24) is used, yielding Fig 2.

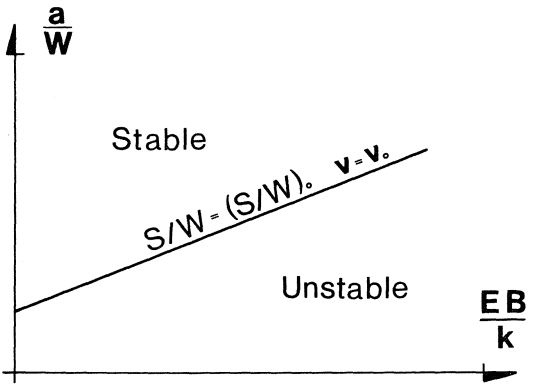

Fig 2. a/W versus EB/k for fixed S/W and ν.

Fig 2 represents an elastic stable crack propagation criterion for three-point bend specimens with a precracked section as shown in Fig 1.

Appendix G

The principle of measuring the dynamic modulus of elasticity is shown in Fig 1.

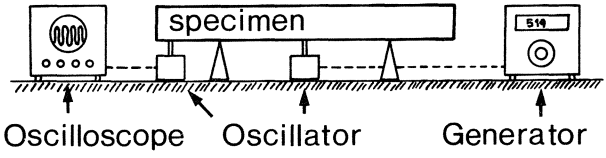

Fig 1. Principle of measuring E_{dyn}.

Between the dynamic modulus of elasticity and the natural frequency of a beam, not subjected to external forces causing forced oscillation, there is a connection as expressed in Eq (1),

$$E_d = \frac{f^2\ M\ S^3\ T}{C^2\ I} \qquad \ldots.(1)$$

where E_d is the dynamic modulus of elasticity, f is the resonance frequency, M is the mass of the beam, S is the length of the beam, T is a correction factor depending on the dimensions and the Poisson´s ratio of the actual specimen, C is a constant depending on the mode of oscillation, and I is the moment of inertia for the beam.

The constant C in Eq (1) is found from Fig 2.

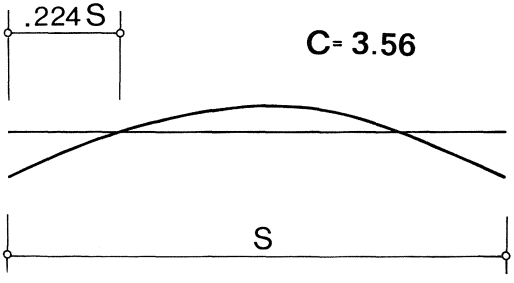

Fig 2. C for the first mode of oscillation.

The value of the correction factor T is found by means of the radius of gyration K (which is equal to $\sqrt{I/A}$ where I is the moment of inertia and A is the cross- sectional area) divided by the length S. If the Poisson's ratio ν is equal to 1/6, T is found from Table 1.

K/S	T	K/S	T
0.00	1.00	0.09	1.60
0.01	1.01	0.10	1.73
0.02	1.03	0.12	2.03
0.03	1.07	0.14	2.36
0.04	1.13	0.16	2.73
0.05	1.20	0.18	3.14
0.06	1.28	0.70	3.58
0.07	1.38	0.75	4.78
0.08	1.48	0.80	6.07

Table 1. Correction factor T.

If $\nu \neq 1/6$, T may be obtained from Eq (2),

$$T' = T \left[\frac{1 + (0.26\,\nu + 3.22\,\nu^2)\ K/S}{1 + 0.1328\ K/S} \right] \qquad \ldots.(2)$$

where T' is the corrected value and T the value from Table 1.

Appendix H

General

This thesis is an attempt, or maybe another attempt, to adapt the fracture mechanics approach to failure analyses of concrete materials.

The fracture mechanics concept entered the consciousness of material researchers, especially metal researchers, in the late 1940´s. After that the modern theory of fracture mechanics has been developed. This theory is as a logical consequence especially fit to metals. It is not until the last 10 - 15 years these ideas have entered also the consciousness of concrete researchers.

One of the first articles found on the subject *Concrete Cracking* is "A study of the failure of concrete under combined compressive stresses" from 1928 by Richardt, Brandtzaeg, and Brown [32] .

After that start nothing of real importance happened until the 1950´s. Then, among others, Blakey and Beresford 1955 published "Strain distribution in concrete beams" [7] . They show the interesting figure below,

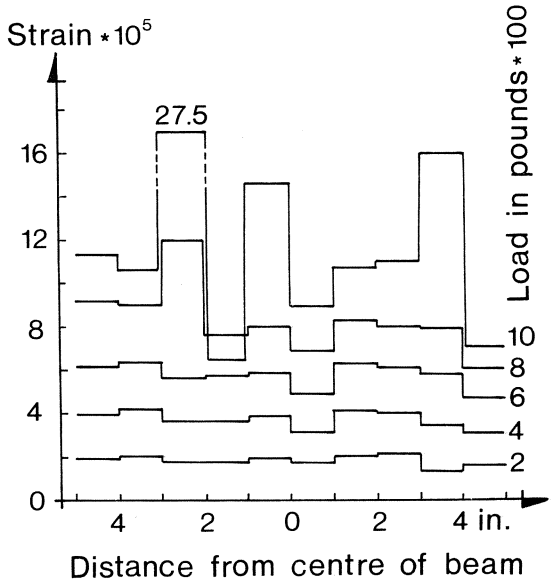

Fig 1. Strain distribution on the underside of the beam under three-point loading.

and make the following conclusions,

"1. Microcracks develop in unreinforced concrete beams at loads measurably below the maximum that the units will carry.
2. Until these cracks develop the tensile stress-strain relationship is effectively linear and the modulus of elasticity is equal to the modulus determined from the sonic vibration test.
3. When beams are submitted to third point loading, the strain over the extreme tension face in the middle section of the beam is uniform until the microcracks develop. In the beams tested there is no evidence that the so-called Seewald effect was important.
4. Until microcracks develop, both stress and strain distributions are linear over the cross-section of a beam."

In 1957 Blakey published "The cracking or fracture of concrete" [8] where he reviews the previous work.

The first "modern" article on the subject is "Crack propagation and the fracture of concrete" from 1961 by Kaplan [23] . He states,

"Further research is necessary, particularly in regard to the question of slow growth prior to fast fracture. The results of this investigation nevertheless indicate that the Griffith concept of a critical strain-energy-release rate being a condition for rapid propagation and consequent fracture, is applicable to concrete. The critical strain-energy-release rate may be ascertained by suitable analytical and experimental procedures and it is possible that the fracture strength of concrete containing cracks may thereby be predicted."

A very interesting article from that period is "Fracture of plain concrete" from 1963 by Glucklich [14] . He says,

"1. The stress determining property in concrete for all types of loads is G_c, the critical strain-energy release rate.
2. In the concrete, the strain-energy is transformed almost entirely to surface energy, but the new surfaces are much larger in area than the effective fracture surface.
3. The increase of the microcracked zone and the heterogeneity of the material contribute to the relatively high G_c value in concrete.
4. The basic difference between tensile and compressive fracture is that in the former, the "driving force" (i.e. the rate of strain-energy release) increases with crack length, whereas in the latter, it is a constant value.
5. In tension, the first crack to grow is the fatal crack. However, preceding its fast growth is a stage of slow growth that is responsible for the slight curvature of the stress-strain curve.
6. In compression, fracture is preceded by a process of progressive cracking that is beneficial inasmuch as it provides an alternative to fracture. Compressive strength is thus much higher than tensile strength, and the stress-strain relationship has a greater curvature."

In 1965 there was a conference held in London called "The structure of concrete and its behaviour under load" [2] . The proceedings of this conference are very illustrative and most interesting to read. They review in an outstanding way the previous work.

Another review that is interesting is "Fracture of Concrete" from 1969 by Moavenzadeh and Kuguel [26a].

From 1969 is also "Fracture Mechanism in Concrete: How much do we know?" by Popovics [29]. His article is very informative and includes a very big reference list.

Popovics concludes,

> "Various measurements indicate that the failure of concrete under load takes place through progressive internal cracking. This cracking starts at about 30% of the ultimate load at the interface between mortar and coarse aggregate. Cracks through the mortar begin to noticeably increase at about 70 to 90% of the ultimate load. The conspicuous disintegration of a strength specimen is only the last stage of the process. This process is essentially independent of the type of loading. The cracking is caused by tensile stress concentrations, which develop under loading at the tips of the existing "flaws" in the material. Thus, when an increase in flaws reduces the area under maximum stress by say 1%, the resulting decrease of strength, as a percentage, is much more.
>
> Of the available failure hypotheses, the Griffith criterion seems to be the most suitable for concrete because it provides at least a qualitatively correct picture of the crack propagation in concrete. The most serious difficulty with the numerical application of the Griffith criterion is the elusiveness of the E, γ, etc. values. Weibull's calculations, as well as the other statistical methods, predict properly that large specimens will be weaker and the scatter of their measured strength will be less. However, quantitatively, there are discrepencies between the calculated and the experimental values. Therefore, these statistical flaw theories, as well as the Griffith criterion, can be considered to be only marginally successful for concrete."

A very modern review is a special issue on fracture of Cement and Concrete Research, No. 4, from 1973. This issue reviews literature on work in the field from the very beginning. The reference list is enormous.

One of the latest, and therefore maybe the most interesting work, is, "Mechanism of fracture and failure of concrete as a composite material" from 1975 by Tanigawa and Kosaka [39] . Their reference list is very interesting and there is even a table that shows previous studies on fracture and failure of concrete. The table is classified into,

1. Direct method a. Observation by microscopy b. Observation by X-ray
2. Indirect method a. Observation by ultrasonic pulse velocity b. Observation by crack noise c. Observation by stress-strain curve
3. Model analyses a. Model with one aggregate b. Model with regularly arranged aggregates c. Model with randomly arranged aggregates.

Under each heading is a number of investigators listed.

Analytical

One of the first really important fracture analysis of concrete is done by Carino, Nilson, and Slate in 1974. Their work is presented in "The behaviour of a model of plain concrete subject to compression-tension and tension-tension biaxial stresses" [10] . This work is in fact the background material of the actual thesis.

Other pioneer works are "Analysis of some nonlinear fracture phenomena by the finite element method" from 1973 by Andersson [3] and "Application of the finite element method to problems in linear and nonlinear fracture mechanics" from 1974 by Aamodt [1] .

Interesting works in the field are also "Partially cracked finite elements" from 1971 by Bell and Elms [5] , "Sprödbrudsteoretisk bestemmelse af revnelängder i betonkonstruktioner med elementmetoden" from 1971 by Rostam and Byskov [33] (only in danish), and "Some applications of plastic analysis to plain and reinforced concrete" from 1977 by Jensen [22] .

On the microfracture of concrete is "Some aspects of the micromechanics of concrete" from 1973 by Stroeven [37] an outstanding contribution.

Experimental

The number of experimental investigations are overwhelming. Most of them are listed in the literature mentioned in this Appendix under the heading General.

Most work is concerned with measurements of the fracture toughness K_{Ic}. All these values, with very few excepts, are done on small specimens and may thus just be apparent.

One of the few investigations on the fracture toughness dependency on specimen depth is that by Higgins and Bailey [16] . They reported a variation of the apparent fracture toughness for cement paste versus specimen width W in three-point bending, as shown in Fig 2.

It is always possible to fit these values to the analytical results by the FCM reported in this thesis as ℓ_{ch} must be guessed. The fit is almost perfect if ℓ_{ch} is assumed in a modest way.

Another paper that casts doubt on laboratory scale K_c measurements of paste is that by Watson [43] . Here is said "...suggests that the value of fracture surface energy, γ_f, derived from laboratory scale K_c measurements will generally be too low (provided, of course, that such a derivation is valid for this type of material)".

Walsh [42] calls attention to the need to consider the absolute size of the specimens in the design of fracture tests.

The only fracture toughness measurements originating from large concrete specimens are those of Entov and Yagust [12] . Values on K_{Ic} ranging from 1.1 to 2.3 $MN/m^{3/2}$ are reported (the values normally reported are 0.5 - 1.0 $MN/m^{3/2}$) indicating that K_{Ic} according to the calculated values by means of Eq 1.2.5(3) and as shown by the FCM may be reasonable.

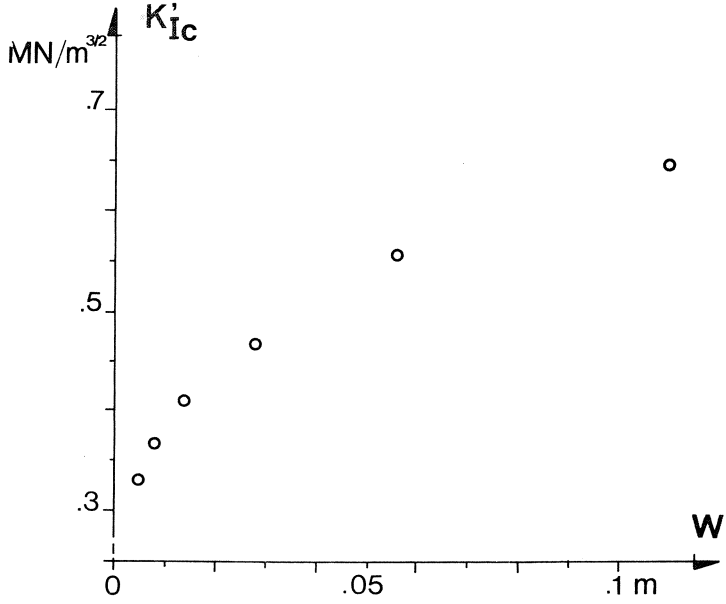

Fig 2. Apparent fracture toughness versus specimen depth [16] .

Another matter that has been indirectly investigated is the influence of the beam depth on the bending strength. Mayer [25] has reviewed these investigations and shows the following curve, including more than 1200 experiments from seven different researches. The curve is discussed further on in [17] .

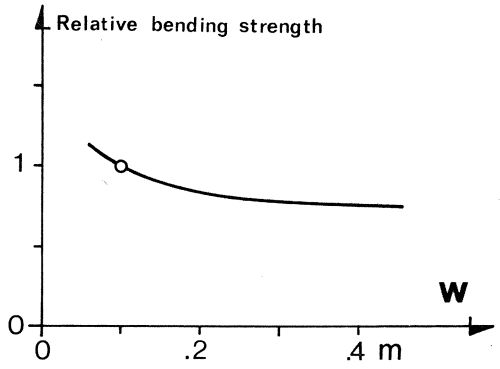

Fig 3. Test results of bending strength versus beam depth summarized by Mayer [25].

It is possible to fit these values to the results of the FCM-calculations in an almost perfect manner.

Appendix I

1. Aamodt, B., "Application of the Finite Element Method to Problems in Linear and Nonlinear Fracture Mechanics", Report 74-1, Division of Structural Mechanics, University of Trondheim, Norway, June, 1974.

2. Alexander, K.M., discussion of "Properties of Concrete under Complex states of Stress", Proceedings of the International Conference on The Structure of Concrete, Brooks, A.E., Newman, K., ed, Cement and Concrete Association, London, 1968, p. 294.

3. Andersson, H., "Analysis of some Non-linear Fracture Phenomena by the Finite Element Method", thesis presented to the University of Lund, at Lund, Sweden, in 1973, in partial fulfillment of the requirements for the degree of Doctor of Technology.

4. Barenblatt, G.I., The Mathematical Theory of Equilibrium Cracks in Brittle Fracture, Institute of Mechanics, Moscow State University, Moscow, USSR, 1973.

5. Bell, J.C., Elms, D.G., "Partially Cracked Finite Elements", Journal of The Structural Division, ASCE, ST 7, July, 1971, pp. 2041-2045.

6. Bergquist, H., "Stability Criteria for a Cracked Specimen", Cerac Report No. 403:2, Schweiz, 1976.

7. Blakey, F.A., Beresford, T.D., "Strain Distribution in Concrete Beams", Civil Engineering and Public Works Review, Vol. 50, No. 586, 1955, pp. 415-417.

8. Blakey, F.A., "The Cracking or Fracture of Concrete", Civil Engineering and Public Works Review, Vol. 52, No. 615, September, 1957, pp. 1000-1003.

9a. Broberg, K.B., "Crack-growth Criteria and Non-linear Fracture Mechanics", Journal of the Mechanics and Physics of Solids, Vol. 19, 1971, pp. 407-418.

9b. Broberg, K.B., "On Stable Crack Growth", Journal of the Mechanics and Physics of Solids, Vol. 23, 1975, pp. 215-237.

9c. Brunauer, S., Kantro, D.L., Weise, C.H., "Paste Hydration of Beta-Dicalcium Silicates, Tricalcium Silicate, and Alite", Proceedings of the Symposium on Structure of Portland Cement Paste and Concrete, Highway Research Board, Washington, D.C., 1966, pp. 309-327.

10. Carino, N.J., Nilsson, A.H., Slate, F.O., "The Behaviour of a Model of Plain Concrete Subject to Compression-Tension and Tension-Tension Biaxial Stresses, Report 357, Department of Structural Engineering, Cornell University, Ithaca, N.Y., 1974.

11. CTO, Aalborg Portland, "Portland Cement", Informative paper,(in Danish only), Aalborg Portland, Aalborg, Denmark, 1973.

12. Entow, V.M., Yagust, V.I., "Experimental Investigation of Laws Governing Quasi-Static Development of Macrocracks in Concrete", Mekhanika Tverdogo Tela, Vol. 10, No. 4, 1975, pp. 93-103.

13. Fagerlund, G., "Equations for calculating the mean free distance between aggregate particles or air-pores in concrete", CBI Research 8:77, Swedish Cement and Concrete Research Institute at the Institute of Technology, Stockholm, Sweden, 1977.

14. Glucklich, J., "Fracture of Plain Concrete", Journal of the Engineering Mechanics Division, ASCE, EM 6, December, 1963, pp. 127-137.

15. Hermann, V., Weber, I.W., Wesche, K., "The Dynamic Modulus of Elasticity as an Equivalent for the Initial Tangent Modulus at Static Testing", Report, Building Research Institute, T.U., Aachen, later than 1972.

16. Higgins, D.D., Bailey, I.E., "Fracture Measurements on Cement Paste", Journal of Materials Science, Vol. 11, No. 11, November, 1976, pp. 1995-2003.

17. Hillerborg, A., Modéer, M., Petersson, P.E., "Analysis of Crack Formation and Crack Growth in Concrete by means of Fracture Mechanics and Finite Elements", Cement and Concrete Research, Vol. 6, No. 6, 1976, pp. 773-782.

18. Hillerborg, A., "A Model for Fracture Analysis", Report TVBM-3005, Division of Building Materials, University of Lund, Sweden 1978.

19. Hillerborg, A., "The Physical Properties of Cement Paste", Building Materials FK I, Division of Building Materials, University of Lund, Sweden, 1979.

20. Idorn, G.M., et. al., "Morphology of Calcium Hydroxide in Cement Paste", Proceedings of the Symposium on Structure of Portland Cement Paste and Concrete, Highway Research Board, Washington, D.C., 1966, pp. 154-174.

21. Ishai, O., "The time-dependent deformational behaviour of cement paste, mortar and concrete", Proceedings of the International Conference on the Structure of Concrete, Brooks, A.E., Newman, K., ed., Cement and Concrete Association, London, 1968, pp. 345-348.

22. Jensen, B.C., "Some Applications of Plastic Analysis to Plain and Reinforced Concrete", Report No. 123, Institute of Building Design, Technical University of Denmark, 1977.

23. Kaplan, M.F., "Crack Propagation and the Fracture of Concrete", Journal of the American Concrete Institute, Title No. 58-28, November, 1961, pp. 591-610.

24. Kinnunen, S., Nylander, H., Tolf, P., "Punching Shear Strength of Concrete Slabs with Highstrength Reinforcement. Appropriate Arrangement of Shear Reinforcement", presented at the August 21-23, 1978, 10th Nordic Concrete Research Congress, held at Saltsjöbaden, Sweden.

25. Mayer, H., "Die Berechnung von Durchbiegung von Stahlbetongbauteilen", Deutscher Ausschluss für Stahlbeton, heft 194, W. Ernst & Sohn, Berlin, 1967.

26. Mitchell, N.B.Jr., "The Indirect Tension Test for Concrete", Materials Research & Standards, No. 1, October, 1961, pp. 780-788.

26a Moavenzadeh, F., Kuguel, R., "Fracture of Concrete", Journal of Materials, Vol. 4, No. 3, September 1969, pp. 497-519.

27. Nilsson, L.O., "Moisture Problems at Concrete Floors", Report TVBM-3002, Division of Building Materials, University of Lund, Sweden, 1977.

28. Paul, B., "Macroscopic Criterion for Plastic Flow and Brittle Fracture", in Fracture, Liebowitz, H., ed., Vol. II, Academic Press, New York, N.Y., 1968, pp. 315-489.

29. Popovics, S., "Fracture Mechanism in Concrete: How much do we know?", Journal of the Engineering Mechanics Division, ASCE, EM 3, June, 1969, pp. 531-544.

30. Powers, T.C., Brownyard, T.L., "Studies of the Physical Properties of Hardened Portland Cement Paste", Journal of the American Concrete Institute, April, 1947, p. 977.

31. Rice, J.R., "Mathematical Analysis in the Mechanics of Fracture", in Fracture, Liebowitz, H., ed., Vol. II, Academic Press, New York, N.Y., 1968, pp. 192-314.

32. Richardt, F.E., Brandtzaeg, A., Brown, R.L., "A Study of the Failure of Concrete under Combined Compressive Stresses", Bulletin No. 185, University of Illinois. 1928.

33. Rostam, S., Byskov, E., "Sprödbrudsteoretisk bestemmelse af revnelängder i betongkonstruktioner med elementmetoden", Internal Report Nr I 15, (in Danish only), Structural Research Laboratory, Technical University of Denmark, 1971.

34. Schleeh, W., "Zur Ermittlung der Spaltzugfestigkeit des Betons", Beton, No. 2, 1978, pp. 57-62.

35. Sidenbladh, T., "The Aggregate Influence upon the Failure Mechanism of Concrete", (in Swedish only), CBI Research 3:74, Swedish Cement and Concrete Research Institute at the Swedish Institute of Technology, Stockholm, Sweden, 1974.

36. Srawley, J.E., "Plane Strain Fracture Toughness", in Fracture, Liebowitz, H., ed., Vol IV, Academic Press, New York, N.Y., 1969, pp. 45-70.

37. Stroeven, P., "Some aspects of the micromechanics of concrete", thesis presented to the University of Delft, at Delft, in 1973, in partial fulfillment of the requirements for the degree of Doctor of Technology.

38. Taylor, A.M., Broms, B.B., "Shear Bond Strength Between Coarse Aggregate and Cement Paste or Mortar", Journal of the American Concrete Institute, August, 1964, pp. 939-956.

39. Tanigawa, Y., Kosaka, Y., "Mechanism of Fracture and Failure of Concrete as a Composite Material", Memoirs of the Faculty of Engineering, No. 2, 1975, Nagoya University, Vol. 27, pp. 208-263.

40. Verbeck, G., "Pore Structure", Significance of Tests and Properties of Concrete and Concrete-making Materials, ASTM Special Technical Publication No. 169-A, Baltimore, Md., April, 1966, pp. 212-213.

41. Vinkeloe, R., "Prüfverfahren zur Ermittlung des dynamischen Elastizitätsmoduls von Betonprismen", Tonindustrie Zeitung, Heft 10, 86, 1962, pp. 272-276.

42. Walch, P.F., discussion of "Measuring the Fracture Toughness of Cement Paste and Mortar", by Brown, I.H., Magazine of Concrete Research, Vol. 24, No. 81, December 1972, pp. 220-221.

43. Watson, K.L., "The Estimation of Fracture Surface Energy as a Measure of the "Toughness" of Hardened Cement Paste", Cement and Concrete Research, Vol. 8, No. 5, September, 1978, pp. 651-656.

44. Zienkiewiez, O.C., The Finite Element Method, 3rd ed. Mc Graw-Hill, London, 1977.

The references listed above are all refered to in the text. Another reference that must be mentioned, is

Hernelind, J., Pärletun, L.G., "EUFEMI - a Finite Element Computer Program for Solid Mechanics and Heat Conduction", Report TMHL-3006, Division of Solid Mechanics, University of Lund, Sweden, 1976.

The program described in this report, EUFEMI, has been used in all FEM-analyses presented in this thesis.

Appendix J

This list contains all principle notations appearing in more than one place in the thesis.

a = crack length

B = width

c = cohesion intercept

D = diameter

E = modulus of elasticity

F = force

FCM = Fictitious Crack Model

FEM = Finite Element Method

f_b = bending strength

f_c = uniaxial compressive strength

f_s = splitting strength

f_t = uniaxial tensile strength

G = strain energy release rate

G_c = critical strain energy release rate or fracture energy

K = stress intensity factor

K_{Ic} = fracture toughness

K_{Ic}^{i} = apparent fracture toughness

L = error to the left

ℓ_{ch} = characteristic length

M = modulus for the σ-w curve

P = load at fracture

Q = strain energy per unit thickness

R = error to the right

r = coordinate in front of a crack tip

S = length

W = depth

w = fictitious crack width

w/C = water to cement ratio (by weight)

w_ℓ = limiting fictitious crack width

γ = surface energy

δ = deformation (length)

ε = strain

σ = stress

σ_F = fracture stress

σ_N = normal stress

τ = shear stress

ν = Poisson´s ratio

ϕ = angle of friction

Φ = angle of failure

I = modus I; opening mode

II = modus II; shear mode

III = modus III; antiplane strain

Appendix K

To convert	To	Divide by
millimeters (mm)	inches (in.)	25.40
centimeters (cm)	inches (in.)	2.540
meters (m)	inches (in.)	0.0254
meters (m)	feet (ft)	0.305
meters (m)	yards (yd)	0.91
square centimeters (cm^2)	square inches (sq in.)	6.45
square meters (m^2)	square feet (sq ft)	0.093
square meters (m^2)	square yards (sq yd)	0.836
square meters (m^2)	acres (acre)	4,047.
cubic centimeters (cm^3)	cubic inches (cu in.)	16.4
cubic meters (m^3)	cubic feet (cu ft)	0.028
cubic meters (m^3)	cubic yards (cu yd)	0.765
kilograms (kg)	pounds (lb)	0.453
kilograms (kg)	tons (ton)	907.2
newtons (N)	one pound force (lbf)	4.45
newtons (N)	one kilogram force (kgf)	9.81
newtons per square meter (N/m^2)	pounds per square foot (psf)	47.9
kilonewtons per square meter (kN/m^2)	pounds per square inch (psi)	6.9
cubic meters (m^3)	gallon (gal)	0.0038
cubic meters (m^3)	acre-feet (acre-ft)	1,233.
pascals (Pa)	newtons per square meter (N/m^2)	1.00

SIGMA·TRYCK
TLTH · Lund